POLITECNICO DI MILANO

Facoltà di Ingegneria dei Sistemi

Corso di Laurea Magistrale in Ingegneria Biomedica

Tesi di Laurea Magistrale

Engineering and Characterization of a Silk-based Organic Artificial Retina

Relatore: Prof. Ing. Andrea Aliverti

Correlatore: Dott.ssa Maria Rosa Antognazza

Tesi di Laurea Magistrale di:

Daniele Carbone

Matricola 770766

Anno Accademico 2014/2015

Contents

3 Methods and Materials

4 Device Characterization

5 Validation and Conclusions

Introduzione

E' stato stimato nel 1997 che più di otto milioni di persone soffrono di cecità causata da patologie degenerative della retina, come la Retinite Pigmentosa (RP) e la Degenerazione Maculare senile (AMD). Tali patologie non sono attualmente curabili tramite chirurgia o trattamenti genetici. Un approccio valido sembra essere la sostituzione del tessuto degenerato con una retina artificiale. In letteratura è stato studiato un dispositivo che consiste generalmente in una telecamera che acquisisce immagini sul mondo esterno, e che ne invia una versione codificata ad un elettrostimolatore impiantato. Gli svantaggi di questo tipo di dispositivo, tuttavia, sono molteplici. In questo lavoro di tesi, realizzato presso l'Istituto Italiano di Tecnologia (IIT) unitamente al Politecnico di Milano, viene analizzata la possibilità di creare una retina artificiale basata su tecnologia organica che possa superare le limitazioni caratteristiche della controparte basata su Silicio. Nei fotorivelatori organici, i materiali fotoattivi sono liquidi a temperatura ambiente e devono essere depositati su un substrato solido. Questo grado di libertà aggiuntivo sulla scelta del substrato permette di utilizzare materiali flessibili, trasparenti nel range visivo, e con una elevata biocompatibilità. In particolare, il substrato scelto per questa retina artificiale organica è un film sottile di seta Bombyx-Mori. Nel presente lavoro viene descritto accuratamente il processo di fabbricazione di tale dispositivo, il quale viene successivamente caratterizzato da un punto di vista ottico, meccanico, strutturale, chimico/fisico ed elettrico. La validazione viene realizzata con un impianto in occhi di ratti RCS (Royal College of Surgeons). I Potenziali Evocati Visivi (VEP) vengono misurati prima su ratti ciechi e su ratti sani, al fine di stabilire una linea di base comparativa, e successivamente su ratti impiantati. Infine, si analizza tramite test psicofisici l'attitudine comportamentale del ratto impiantato rispetto a quella del ratto cieco o sano.

Abstract

It was estimated in 1997 that more than eight million people were legally blind from retinal degeneration, like Retinite Pigmentosa (RP) and Age-Related Macular Degeneration (AMD). These pathologies are not currently treatable with surgery or genetic cures. A valid approach seems to be the replacement of the degenerated tissue with an artificial retina. A device was studied in literature, consisting of a videocamera acquiring images of the external world, and in their codified transmission towards an implanted electrical stimulator. The disadvantages of such a device, however, are numerous. In this thesis work, realized at the Istituto Italiano di Tecnologia (IIT) jointly with Politecnico di Milano, the possibility to create an organic-based artificial retina capable of overcoming the Silicon-based one limitations. In organic photodetectors, the photoactive materials are liquids at ambient temperature and they must be deposed on top of a solid substrate. This additional degree of freedom about the substrate choice allows the use of flexible materials, transparent in the optical range, and with high biocompatibility. In particular, the substrate chosen for this artificial retina is a Bombyx-Mori silk thin film. The fabrication process of the aforementioned device is accurately described in this thesis work. Also, the artificial retina is characterized from an optical, mechanical, structural, chemical/physical, and electrical point of view. The validation is realized through the implantation in eyes of RCS (Royal College of Surgeons) rats. Evoked Visual Potentials (VEP) are firstly measured in blind rats and healthy rats, in order to establish a comparative baseline, and then in implanted rats. Finally, the behavioural aptitude of the implanted rat with respect to the blind or the healthy one is analyzed through psychophysical tests.

Sommario

L'Organizzazione Mondiale della Sanità (OMS) definisce la cecità come una acuità visiva inferiore a 1/20 o una riduzione del campo visivo inferiore a dieci gradi, con l'occhio migliore e la miglior correzione possibile. E' stato stimato nel 1997 che più di otto milioni di persone soffrono di cecità causata da malattie degenerative della retina, come la Retinite Pigmentosa (RP) e la Degenerazione Maculare senile (AMD). Una ulteriore stima da parte della OMS afferma che solo il 29% delle persone diagnosticate con cecità grave possiede un lavoro redditizio, generando così un forte impatto anche sull'economia. La grande diffusione di queste patologie e la loro natura debilitante sia dal punto di vista fisico che psicologico genera l'esigenza di trovare soluzioni e terapie efficaci. Retinite Pigmentosa e Degenerazione Maculare Senile non sono attualmente curabili tramite chirurgia o trattamenti genetici, e l'unica strada percorribile sembra essere l'impianto di una retina artificiale che sostituisca la funzionalità della retina degenerata. Ciò è vero soltanto per casi di cecità retinica, cioè tutte le strutture dal nervo ottico in poi devono essere sane per rendere valido l'approccio. La applicazione di una retina artificiale è giustificata dalle scoperte del fisiologo boemo Johanne Purkinje, che nel 1819 condusse il primo studio scientifico documentato sui fosfeni. Il concetto di fosfene era già noto dai tempi della Antica Grecia, la parola stessa ha infatti una etimologia greca (φῶσ - φαινω) che significa "mostrare luce". Un fosfene può essere definito come la sensazione visiva di un punto luminoso generata dalla stimolazione puntuale di una porzione di retina. Inoltre, il primo studio sulla manifestazione di fosfeni generata dalla stimolazione elettrica della corteccia visiva fu condotto dal neurologo tedesco Otfrid Foerster nel 1929. La retina artificiale prende forma a partire da queste basi, ed oggi consiste in una telecamera che acquisisce immagini sul mondo esterno, e che ne invia una versione codificata ad un elettrostimolatore impiantato. In tutti i vari risultati discussi in letteratura, lo stimolatore è un dispositivo elettronico basato su Silicio e spesso ricoperto da materiali polimerici al fine di migliorare la biocompatibilità e la stabilità dell'impianto. Gli svantaggi di questo tipo di dispositivo sono molteplici. Per prima cosa, lo stimolatore impiantato possiede una struttura fisica ingombrante e rigida che rende difficile il processo di impianto, oltre a generare un accoppiamento non ideale con il fundus oculi. Inoltre, lo stimolatore impiantato riceve le informazioni visive e l'energia per il suo funzionamento attraverso un sistema di telemetria che consiste in una bobina esterna ed una bobina impiantata. Tale sistema, misto al funzionamento intrinseco dello stimolatore, genera un forte rilascio di calore ai tessuti e può causare necrosi e degenerazioni. Anche la biocompatibilità del dispositivo non è ottimizzata, poichè la necessità di rivestire l'elettronica con ulteriori materiali aumenta le dimensioni dell'impianto. Ulteriormente, il segnale visivo è ottenuto tramite una stimolazione basata su un flusso di elettroni, mentre l'organismo utilizza come suo veicolo preferenziale un flusso di ioni. Infine, la stimolazione stessa ha una natura discreta, basata sul numero di elettrodi nello stimolatore. Un aumento di elettrodi, e quindi di acuità visiva, è necessariamente legato ad un aumento di spessore del dispositivo, poichè ogni elettrodo ha bisogno di una pista elettrica e l'unico modo di utilizzarne molti è quello di metterne in pila le piste conduttive.

In questo lavoro di tesi, realizzato presso l'Istituto Italiano di Tecnologia (IIT) unitamente al Politecnico di Milano, viene analizzata la possibilità di creare una retina artificiale basata su tecnologia organica che possa superare le limitazioni precedentemente elencate. Il concetto di retina artificiale organica si basa sugli studi moderni di elettronica organica e di fotorivelatori organici. In questo tipo di dispositivi i materiali fotoattivi sono liquidi a temperatura ambiente, e devono essere depositati su un substrato solido attraverso particolari tecniche di deposizione. Questo grado di libertà aggiuntivo sulla scelta del substrato permette di utilizzare materiali flessibili, trasparenti nel range visivo, e con una elevata biocompatibilità. Il substrato della retina artificiale studiata in questa tesi è basato su un particolare film di seta Bombyx-Mori. La seta è un materiale largamente studiato in letteratura, dalle eccellenti proprietà meccaniche e dalla elevata biocompatibilità nei confronti di impianti in-vivo. Il fotorivelatore organico a base di seta che viene discusso di seguito possiede una struttura ibrida: da una parte, il suo anodo consiste nella deposizione del polimero conduttore PEDOT:PSS, un ottimo accettore di lacune, mentra dall'altra il suo catodo consiste nell'umor vitreo dell'occhio. Come polimero fotoattivo è stato scelto il blend P3HT/PCBM, ben noto ai costruttori di celle solari organiche, grazie al suo picco di assorbimento centrato attorno ai 530 nm (il verde, il colore per cui l'occhio umano ha la più elevata acuità visiva) ed alle sue ottime performance. Un dispositivo di questo tipo presenta notevoli vantaggi rispetto al caso inorganico. La natura flessibile del substrato di seta, nonchè la sua biocompatibilità, rende ottimali le condizioni di impianto e di stabilità. I segnali ionici prodotti dai fotorivelatori organici, frutto delle reazioni di ossido-riduzione tipiche dei materiali organici, sono benvisti dalle strutture biologiche e generano una riduzione nei fenomeni di fatica cellulare. E' importante poi notare che il dispositivo non genera calore, poichè l'energia

necessaria al suo funzionamento proviene direttamente dai fotoni incidenti. Infine, per sua natura intrinseca, il polimero fotoattivo funziona come un elettrostimolatore continuo invece che discreto, non esistendo degli elettrodi fisici. Questa caratteristica non limita la risoluzione spaziale del dispostivo che, a questo punto, è dettata solo dalle strutture nervose della retina (che devono essere sane). L'unica controindicazione è in realtà una limitazione dei fotorivelatori organici, e cioè delle efficienze quantiche inferiori a quelle delle loro controparti inorganiche. Tale limitazione tuttavia è dovuta a problemi tecnologici che potrebbero essere risolti con il progredire delle conoscenze nel settore dell'elettronica organica.
Il presente lavoro di tesi descrive nel dettaglio il processo di fabbricazione della retina artificiale organica, la quale viene successivamente caratterizzata dal punto di vista ottico, meccanico, fisico-chimico, strutturale ed elettrico. La validazione consiste nell'impianto di tali retine artificiali in occhi di ratti RCS (Royal College of Surgeons), delle cavie che ereditano geneticamente una degenerazione retinica. I potenziali evocati visivi nella corteccia del ratto vengono acquisiti prima e dopo l'impianto della retina artificiale, e forniscono un metodo di giudizio oggettivo. Uno studio psicofisico sugli animali impiantati, invece, fornisce delle evidenze comportamentali su ratti che non presentano danni fisici o psicologici a seguito del processo di anestesia e di impianto.

Il presente lavoro di tesi viene strutturato come segue:

Il **Capitolo 1** revisiona i concetti di base sulla retina e sulle patologie degenerative della retina, AMD e RP. I principi fondamentali della stimolazione elettrica della retina vengono successivamente discussi. Segue una profonda analisi dello stato dell'arte, mirata alla contestualizzazione del lavoro. Infine, viene discussa la dimostrazione di fattibilità che giustifica l'implementazione di tale approccio;

Nel **Capitolo 2** vengono passate in rassegna le basi di Bioelettronica Organica. In particolare viene analizzata la differenza tra fotorivelatori organici ed inorganici. Concetti importanti come l'eccitone, le bande HOMO e LUMO, e le bulk heterojunction vengono presentati e discussi. Due materiali importanti per questo studio, il PEDOT:PSS ed il blend P3HT/PCBM sono esaminati. Vengono infine presentati i diagrammi energetici ed il modello generale della retina artificiale organica;

Nel **Capitolo 3** viene revisionata tutta la strumentazione sperimentale ed i metodi utilizzati per la fabbricazione e la caratterizzazione della retina artificiale;

Il **Capitolo 4** consiste nella analisi del processo di fabbricazione, e nella caratterizzazione completa del dispositivo. In particolare, viene presentato il processo di fabbricazione del film di seta e viene discussa la scelta di una fra tre sue possibili varianti. Successivamente, viene esaminata la deposizione dei materiali polimerici attraverso le tecniche di spin coating e spray coating. La caratterizzazione viene effettuata da un punto di vista ottico, meccanico, chimico/fisico, strutturale ed elettrico. Infine, uno studio di degradazione quantifica l'effetto debilitante che ha la permanenza del dispositivo in una soluzione salina (come l'umor vitreo);

Il **Capitolo 5** presenta la validazione del dispositivo, la quale consiste nel suo impianto in occhi di ratti RCS. I Potenziali Evocati Visivi (VEP) ed i test psicofisici dimostrano l'efficacia della retina artificiale organica realizzata in questo lavoro di tesi. Vengono infine discusse le conclusioni ed i potenziali sviluppi futuri.

Summary

The World Health Organization (WHO) defines blindness as a visual acuity less than 1/20 or a visual field loss to less than 10 degrees, with the better eye and best possible correction. It was estimated in 1997 that more than eight million people were legally blind from retinal degeneration, like Retinite Pigmentosa (RP) and Age-Related Macular Degeneration (AMD). An additional statistics from WHO states that only the 29% of severely visually impaired persons are gainfully employed, thus generating a big impact also on the economy. The great diffusion of these pathologies and their debilitating nature both physically and psychologically generates the necessity to find concrete solutions and therapies. Retinite Pigmentosa and Age-Related Macular Degeneration are not currently treatable with surgery or genetic cures, and the only possible path seems to be the implantation of an artificial retina which is able to replace the lost functionality of the degenerated retina. That is true only in case of retinal degeneration blindness, the approach is valid onlu if every physiological structure from the optical nerve upwards is healthy. The application of an artificial retina is justified by the discoveries of the Bohemian physiologist Johanne Purkinje, which in 1819 led the first documented scientific study on phosphenes. The concept of phospene was already known at the time of Ancient Greece, in fact the word has a greek etymology (φῶσ - φαινω) meaning "to show light". A phosphene can be defined as the visual sensation of a light spot generated by the punctual stimulation of a retina portion. Furthermore, the first study about a phosphene manifestation generated by the visual cortex electrical stimulation was carried out by the German neurologist Otfrid Foerster in 1929. The artificial retina shapes starting from these premises, and today it consists of a videocamera acquiring images of the external world, and in their codified transmission towards an implanted electrical stimulator. In almost every work present in literature, the stimulator is a silicon-based electronic device often coated with polymeric materials in order to enhance the implant biocompatibility and stability. This device has many disadvantages. Firstly, the implanted stimulator has a bulky and rigid physical structure which makes the implantation process very difficult, rather than generating a non-ideal coupling with fundus oculi. Moreover, the implanted stimulator receives visual information and the energy needed for its working through a telemetry system consisting of an external coil and an implanted coil. Such a system, together with the intrinsic stimulator functioning, generates a high heat release to tissues and it can cause necrosis and degenerations. Also, the biocompatibility of the device is not optimized, because the need to coat the electronics with additional materials increases the implant size. Furthermore, the visual signal is achieved through a stimulation based on an electron flux, while the organism uses an ion flux as its preferential vehicle. Finally, the stimulation itself has a discrete nature, based on the number of electrodes in the stimulator. An increase of electrodes, and therefore an increase of visual acuity, is necessarily linked to an increase in thickness for the device, since every electrode needs its electric track and the only way to use lots of electrodes is to stockpile their conductive tracks.

In this thesis work, realized at the Istituto Italiano di Tecnologia (IIT) jointly with Politecnico di Milano, the possibility to create an organic-based artificial retina capable of overcoming the aforementioned limitations is analyzed. The concept of organic artificial retina is based on modern studies of organic electronics and organic photodetectors. In these devices the photoactive materials are liquids at ambient temperature, and they must be deposed on top of a solid substrate using particular deposition techniques. This additional degree of freedom about the substrate choice allows the use of flexible materials, transparent in the optical range, and with high biocompatibility. The substrate of the artificial retina studied in this thesis is based on a particular silk film from Bombyx-Mori. Silk is a widely studied material in literature. It has remarkable mechanical properties and a good in-vivo biocompatibility. The silk-based organic photodetector discussed below has a hybrid structure: on the one hand, its anode consists of the PEDOT:PSS conductive polymer deposition, a good hole acceptor, and on the other hand its cathode consists of the vitreous humor in the eye. The P3HT/PCBM blend was chosen as photoactive polymer, well known to solar cells manufacturers, thanks to its absorption peak centered around 530 nm (the green, a color for which the human eye has the highest visual acuity) and to its good performance. A device like that has remarkable advantages with respect to the inorganic one. The flexible nature of the silk substrate, in addition to its biocompatibility, makes optimal the implantation conditions and the stability. The ionic signals produced by organic photodetectors, caused by the typical redox reactions for organic materials, are well-suited for the coupling with biological structures and they generate a lowering of cellular fatigue phenomena. It is important to notice that the device does not generate heat, since the energy needed for its functioning comes directly from incident photons. Finally, for its intrinsic nature, the photoactive polymer works as a continuous electrical stimulator, rather than being discrete, since it has no physical electrodes. This feature does not limit the spatial resolution of the device which is limited now only by the nervous structures

inside the retina (they have to be healthy). The only drawback is a limitation of organic photodetectors, that is a lower quantum efficiency with respect to inorganic devices. However, such limitation is due to technical issue that may be overcome with the knowledge progression in the organic electronics field.
The present thesis work describes in details the fabrication process of the organic artificial retina, which is then characterized from an optical, mechanical, physical/chemical, structural and electrical point of view. The validation consists of the implantation of these retinas in the eye of RCS (Royal College of Surgeons) rats, test animals which genetically inherit a retinal degeneration. Evoked potentials in the visual cortex of the rat are acquired before and after the device implantation, and they provide an objective yardstick. The psychophysical study of implanted animals, instead, provides behavioural evidences about rats without physical or psychological traumas due to implantation and anesthesia processes.

The present thesis work is structured as follows:

The **Chapter 1** reviews basic concepts about the retina and retinal diseases like AMD and RP. The main principles behind the electrical stimulation of the retina are discussed. Then, a deep state of the art analysis is performed in order to contextualize the work. Finally, it is discussed a demonstration of feasibility for the organic artificial retina application;

In **Chapter 2** the Organic Bioelectronics fundamentals are reviewed. In particular, the difference between inorganic and organic photodetector is analyzed. Important concepts like excitons, HOMO and LUMO levels, and bulk heterojunctions are presented and discussed. Two important materials for this study, PEDOT:PSS and the P3HT/PCBM blend, are examined. Finally it is presented the general model for the organic artificial retina and its energy diagram;

In **Chapter 3** all the experimental tools and techniques used for the fabrication and the characterization of the organic artificial retina are reviewed;

Chapter 4 consists of the fabrication process analysis, and in the complete characterization for the device. In particular, it is presented the silk film fabrication process and the reasons behind the choice of one over three different alternatives. Then, the deposition of polymeric materials through spin coating and spray coating is discussed. The characterization is performed under an optical, mechanical, chemical/physical, structural and electrical point of view. Finally, a degradation study quantifies the weakening effect that the permanence in a saline solution (like the vitreous humor) applies on the device;

Chapter 5 presents the device validation, consisting of its implantation into RCS rats. Visual Evoked Potentials (VEP) and psychophysical tests demonstrate the effectivenes of the organic artificial retina realized in this work. Conclusions and future developments are finally discussed.

Chapter 1

The Artificial Retina

1.1 Physiopathology of the Retina

The retina is a complex and layered tissue responsible for the transduction of visible photons into electrical signals. Signals resulting from the transduction mechanism get processed through several layers of cells inside the retina, and they reach the visual cortex through the optical nerves and the thalamus.

The present work is focused on the physical mechanisms behind the vision process which happens in the retinal layer, without considering the further elaboration in the visual cortex. An introductive overview of the retinal tissue is given in paragraph 1.1.1. Then, the main pathologies that can benefit from an artificial retina implant, Age-related Macular Degeneration (AMD) and Retinitis Pigmentosa (RP) are briefly discussed.

1.1.1 The Retinal Tissue

The retina is approximately a 0,5 mm thick tissue and it lays on the posterior wall of the eye. It includes both the light-sensitive neurons and the neural circuits responsible for a preliminary stage of the image processing. The retina is divided into eight different layers:

1. The Pigment Epithelium: it is a monocellular layer containing melanin, which absorbs the light before a backward beam can be reflected. It also acts as a blood supply for the retina, synthesizes light-sensitive pigments, phagocytes and recycles the upper portion of cones and secures the retina in a stable position applying a suction force;

2. The Layer of Rod and Cones: it contains cones, used for daylight vision or photopic vision, and rods used for nighttime vision or scotopic vision. This layer is further divided into outer segment layer, containing the light-sensitive pigments (rhodopsin for rods and color pigments for cones), and inner segment layer which holds the cytoplasm and cellular organelles. The central portion of the retina, called fovea, is made of a dense package of green and red cones and it is responsible for the maximum visual acuity. In details, the fovea has a diameter of 1,2-1,4 mm and is surrounded by the macula, which has a diameter of around 6 mm;

3. The External Limiting Membrane: this layer connects rods and cones cell bodies to their photosensitive processes. It also contains processes of Müller cells;

4. The Outer Nuclear Layer: it contains the cell bodies of rods and cones;

5. The Outer Plexiform Layer: it consists of every place of interaction between receptors, bipolar cells and horizontal cells. Axonal processes of rods and cones, processes of horizontal cells and dendrites of bipolar cells lie in this layer;

6. The Inner Nuclear Layer: it includes cell bodies of bipolar cells, amacrine cells and horizontal cells;

7. The Inner Plexiform Layer: it contains the places of synaptic interaction between bipolar cells, amacrine cells and ganglion cells;

8. The Layer of Ganglion cells: it contains the cell bodies of the ganglion cells;

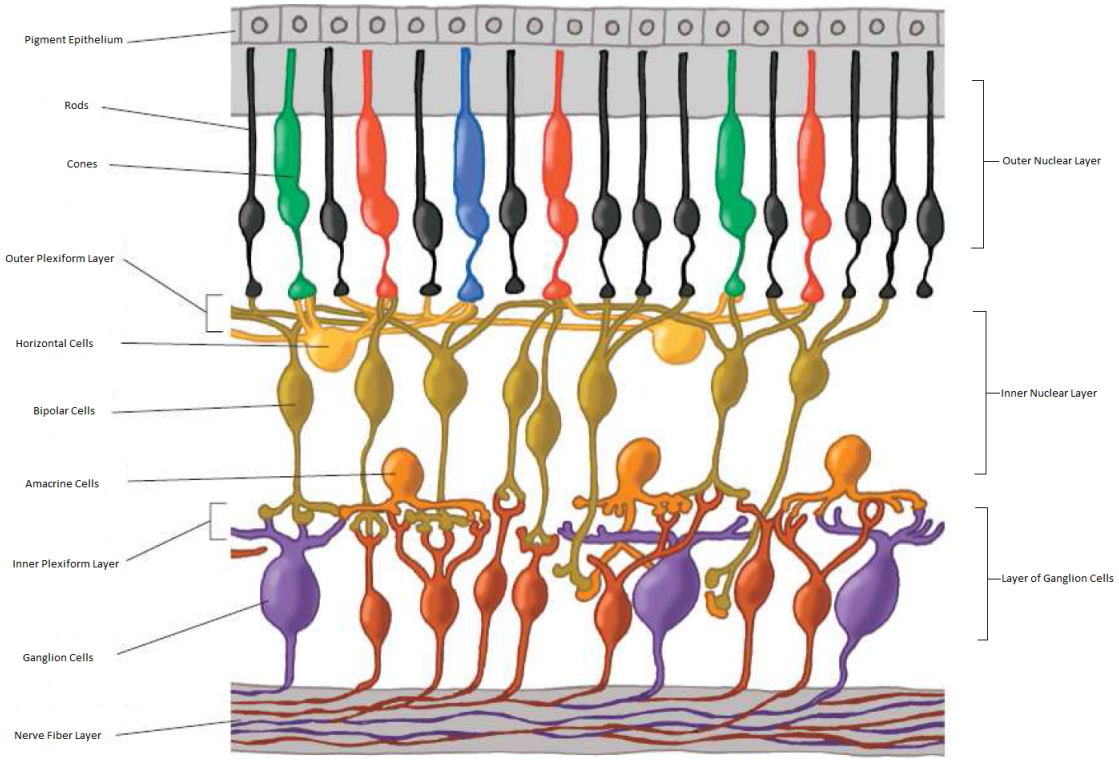

Figure 1: The cross section of a retina

The outer segments of photoreceptors are filled with pigments capable of absorbing ligth. They are arranged in a stack of discs generated by the infolding of the plasma membrane, and the outer segment is continuously renewed (a cone substitutes 3 new discs per hour). This infolding greatly increases the light-sensitive surface area and therefore the amount of absorbed photons. In rod cells the visual pigment is called rhodopsin and it consists of the union of opsin, a membrane protein, and retinal which is the light absorbing part. In absence of light there are two ionic currents in a photoreceptor, one is a sodium current internally flowing through cGMP channels (cyclic guanosine 3-5 monophosphate) situated on the outer segment, and the other is a current of k^+ions flowing through potassium selective channels. The k^+current tends to hyperpolarize the receptors towards the potassium resting potential (about -70 mV), meanwhile the sodium current tends to depolarize the receptor. Active transport mechanism allows the maintenance of a steady state in the photoreceptor. In darkness conditions there is a high cytoplasmic concentration of cGMP channels, so the receptor is always depolarized to about -40 mV due to the Na^+dark current. Light absorption from pigments generates a morphological change to retinal, from 11-cis-retinal to 11-trans-retinal, and therefore a series of chemical reactions leading to the production of cGMP phosphodiesterase and to the following hydrolysis of cGMP channels. This chain reaction is a high gain process, since a single photon can lead to the hydrolysis of 10^5molecules of cGMP per second. The closure of cGMP channels stops the dark current and generates the hyperpolarization of the cell, which is the signal resulting from the phototransduction mechanism.

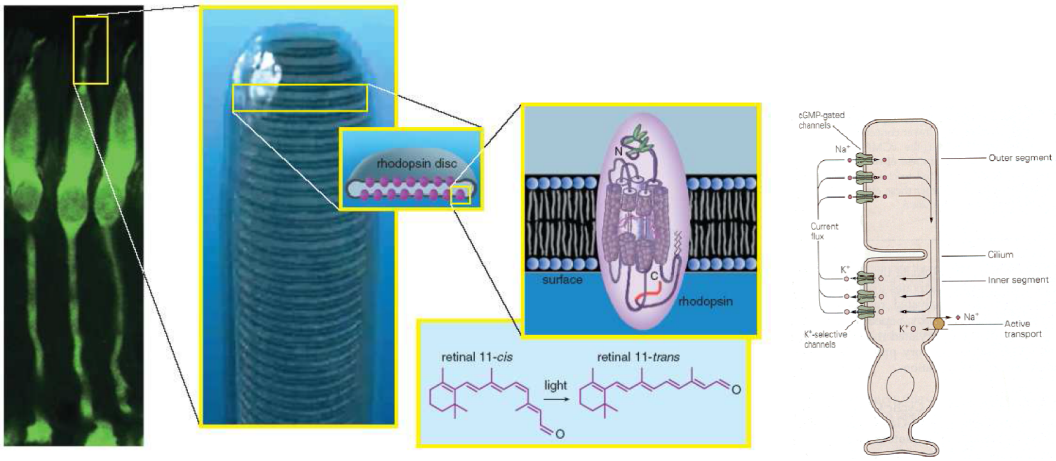

Figure 2: The structure of a photoreceptor

The electrical signal resulting from the phototransduction process undergoes several further processing. In the outer plexiform layer happens the "lateral inibition" phenomenon mediated by the horizontal cells. When a light beam strikes a photoreceptor, it generates an electrical signal which excites the corresponding bipolar cells and inhibits the neighboring ones at the same time. This kind of processing is needed to achieve a sharp contrast between a bright point and his surrounding. Every horizontal cell receives inputs from several photoreceptors and therefore it has a wide receptive field.

Getting deeper into the processing we find the bipolar cells which are divided into two main types: one kind responds to the excitation and the other to the inhibition. We distinguish bipolar cells in on-center and off-center, respectively. On-center bipolar cells react to hyperpolarization of photoreceptors by depolarizing themselves, inhibiting surrounding cells and allowing the contrast between bright images and dark backgrounds. Off-center bipolar cells react to the inhibition of photoreceptors, allowing the contrast between dark images and bright backgrounds. This kind of double behaviour is useful to keep a certain invariance to lighting with positive or negative contrast. The processing in the inner plexiform layer is far more complex and it generates various types of integration, modulation and convergence of the visual signal. What is important to notice is that the segregation between on-center and off-center information is kept separated and carried throughout the whole processing path, even in the visual cortex. On-center bipolar cells establish connections with on-center ganglion cells and the same happens for off-center cells. These observations bring to the conclusion that the retinal tissue is not only responsible for the phototransduction of light into electrical charge but also for a very first stage of the visual processing. This is one of the reasons why the retina can be considered as an actual part of the central nervous system.

1.1.2 Age-related Macular Degeneration and Retinitis Pigmentosa

The World Health Organization defines blindness as a visual acuity less than 20/400 (6/120) or a visual field loss to less than 10 degrees, with the better eye and best possible correction. There are two kind of blindness, one derives from damages to the optical pathway and the other results from damages to the neural pathway. Among the leading causes of blindness we find cataract, glaucoma, AMD, diabetic retinopathy, trachoma and A-vitamine deficiency. Even though the major cause of blindess is cataract, in this work we are not interested in optical pathway damages but only in the neural one. The artificial retina approach to blindness therapy usually adresses two main neural pathway pathologies, AMD (Age-related Macular Degeneration) and RP (Retinitis Pigmentosa). According to World Health Organization in 1997 more than eight million people were legally blind from retinal degeneration and it was estimated that only 29% of severely visually impaired persons are gainfully employed, thus generating a big impact also on the economy [3]. Degenerative pathologies like AMD and RP are so common and meaningful that is born the necessity to find concrete solutions and therapies.

AMD is more prevalent than RP and it consists of the presence of abnormal blood vessels under the retina, the leak of blood and fluid, general degeneration of the tissue and scarring. This slow degeneration ends in the photoreceptor cell death and therefore in the severe loss of visual acuity and in a distorted central vision. RP has a minor incidence, about 1 per 4000 live births [4], but his symptoms may appear earlier in life and are generally more severe than the AMD ones. RP is a retinal dystrophy consisting of a photoreceptor degeneration

and a reduction of the visual field, the latter being directed either from the outside inward or from the center outward. This visual fields loss can generate the sensation of light flashes and a distorted center vision, and in his end-stage the degeneration can be induced also to the foveal ganglion cells. Both AMD and RP are not currently treatable with surgery and genetic cures are very difficult to achieve due to mutation in over 30 different retinal genes, to the autosomal-dominant and autosomal-recessive nature of the pathologies, to X-linking, and to non-familial etiology [5]. Moreover, about 60% of RP cases still have no known genetic cause [6]. The idea of an artificial retina approach was born from the evidence of healthy retinal neurons in postmortem analyses of patients with AMD and RP. Aside from end-stage cases with advanced degeneration, the presence of well functioning bipolar cells or ganglion cells gives the possibility to electrically stimulate those cells with an implanted device.

1.2 Electrical Stimulation of the Retina

It is known since the time of the Ancient Greece that a light spot sensation can be artificially created with a mechanical pressure upon the eye, or experiencing long periods of time in the darkness (also known as "Prisoner's Cinema"), or taking hallucinogen drugs. This artificial light spot takes the name of "Phosphene", a Greek word meaning " to show light". The first documented scientific study on phosphenes was led by the Bohemian physiologist Johanne Purkinje in 1819, and the first discovery of phosphenes induced by electrical stimulation of the visual cortex was carried out by the German neurologist Otfrid Foerster in 1929. The concept of an artificial vision device was firstly introduced by Tassiker in 1956 [7], and later by Brindley and Lewin in 1968 [8]. The latter work can be considered as the demonstration of feasibility of sight restoration through the application of an electrical stimulation device. An extract from their article states: "An array of radio receivers, connected to electrodes in contact with the occipital pole of the right cerebral hemisphere, has been implanted into a 52-year-old blind patient. By giving appropriate radio signals, the patient can be caused to experience sensations of light ('phosphenes') in the left half of the visual field. The sensation caused by stimulation through a single electrode is commonly a single very small spot of white light at a constant position in the visual field; but for some electrodes it is two or several such spots, or a small cloud". Furthermore, about the features of the phosphenes: " The phosphenes produced by stimulation through electrodes 2*4 mm apart can be easily distinguished. By stimulation through several electrodes simultaneously, the patient can be caused to see predictable simple patterns"... "During voluntary eye movements, the phosphenes move with the eyes. During vestibular reflexes eye movements they remain fixed in space"... " Phosphenes ordinarily cease immediately when stimulation ceases but after strong stimulation they sometimes persist for up to 2 min". Finally: " Our findings strongly suggest that will be possible, by improving our prototype, to make a useful prosthesis".

These findings work as a premise to an artificial retina device. The idea behind a device like that is to artificially stimulate bipolar cells and/or ganglion cells through an implanted electric stimulator which replaces the function of photoreceptors. It is important to highlight that the artificial retina replaces the function of photoreceptors and not only physically the photoreceptors, because the implant site does not necessarily has to be on top of the photoreceptors layer. Depending on the position of the device we distinguish epiretinal, subretinal and suprachoroidal implants:

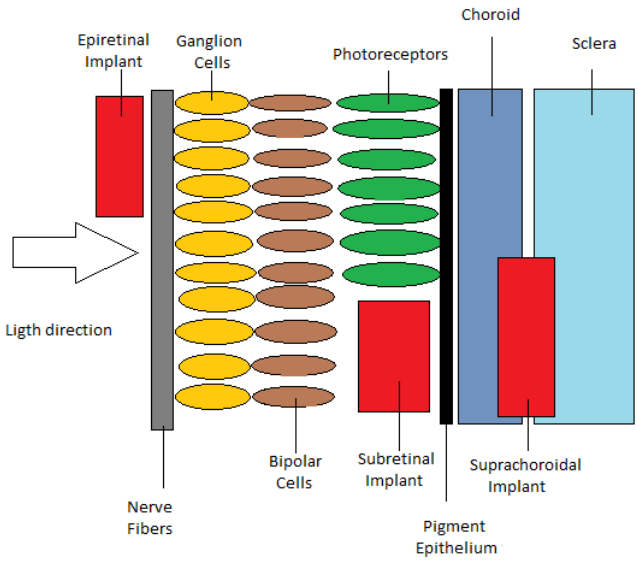

Figure 3: Epiretinal, Subretinal and Suprachoroidal implants

- Epiretinal implant: in this approach the artificial retina is placed in front of the layer of ganglion cells and the surgery does not involve the retinal detachment. The position of the device, however, does not match the position of the retina and, therefore, the output signal must take into account the physiologic processing in the intermediate levels;

- Subretinal implant: in this configuration the implant site is between the pigment epithelium and the layer of photoreceptors. It is a particularly invasive approach because it requires the detachment of retina and it may occlude the retinal vasculature. The advantage of this implant is that the artificial stimulation is very similar to the physiologic one;
- Suprachoroidal implant: the device is positioned between the choroid and the sclera. The advantages of this approach are that the stimulation is applied in a site very close to the natural one, and that retinal detachment risk and vascular damages are minimized. The surgery is relatively simply and the device can be positioned in a very stable way. The disadvantage is that the implant stimulates directly on the resistive barrier of the pigment epithelium, with a resistance 5-15 fold higher than the retina [5]. This leads to a reducion in spatial resolution and to heat release on the tissues.

The basic goals of an artificial retina are the achievement of face-recognition skills, the ability to read a text, and the autonomy in movements. The specifics of a device like that strongly depends on the pathology and on the features of the diseased visual system. Stimulation thresholds are in fact very variable, both interspecies and intraspecies, and they depend also on the type of the implant (epiretinal, subretinal, suprachoroidal). The position of the electrode is another important parameter, specifically the threshold grows linearly with the distance between electrode and stimulation site. Thresholds can be studied both in vivo and in vitro (with explanted retinas) with particular interest in peak values and in the shape of the stimulus signal. Figure 4 shows various results about in vivo and in vitro thresholds:

Stimulating Electrode Position	Recording Method	Electrical Threshold	Reference
Epiretinal, blind human acute	Perception	600 nC (average)	Humayun, 1996 and 1999
Epiretinal, isolated rabbit retina	Microelectrode recording retinal ganglion cell	< 2 nC	Grummet, 2000
Subretinal, isolated chick retina	Microelectrode recording retinal ganglion cell	0.4–0.9 nC	Stett, 2000
Epiretinal stim, cat in vivo	Cortical recording	14 nC	Hesse, 2000
Subretinal, cat in vivo	Cortical recording	50 nC	Zrenner, 2004
Transchoroidal, normal and retinal degenerate rat	Superior colliculus	7.2 nC (normal retina) 12.9 nC (degenerate retina)	Tano, 2004
Epi- and subretinal in rabbit	Retinal ganglion cell	10 nC	Shyu, 2000
Epiretinal, blind human acute	Perception	300–500 nC	Rizzo, 2003
Epiretinal, blind human chronic	Perception	28–900 nC	Humayun, 2003

Figure 4: Stimulation thresholds for retina, Weiland and Humayun [9]

Epiretinal and subretinal implants show similar results, and generally a degenerated retina requires a higher level of stimulation (from 1-10 nC to 30-50 nC). The working range of an artificial retina has an upper bound, limited by the safety of the stimulation, and a lower bound determined by the thresholds. In order to understand how the device should properly stimulate the tissues, we must exploit the principles of Electrochemistry (an exhaustive treatise can be found in [11]). Electrodes can be considered as electron-ion transducers and they work with redox reactions. The electrochemical reaction unbalances the equilibrium towards oxidation or reduction depending on the direction (sign) of the stimulation current. Unbalanced redox reactions imply a release of reactants in the electrolyte or a stockpile of reactants on the electrode surface. Being a safe stimulation of the retina an important requirement of the design, there are a couple of requirement to fulfill. A first aspect of safety consists in delivering an amount of charge that does not generate significant quantities of potentially harmful reactants, like H_2or O_2 on the electrode surface [9]. Platinum electrodes are well known in literature and widely used in these kind of applications because they can safely deliver up to 0,35 mC/cm^2 [10]. Another aspect of safety is about the damage produced on tissues, a factor limited by the balance of the net charge delivered. For this purpose the ideal waveform of the stimulating signal is a charge-balanced biphasic signal, as depicted in Figure 5:

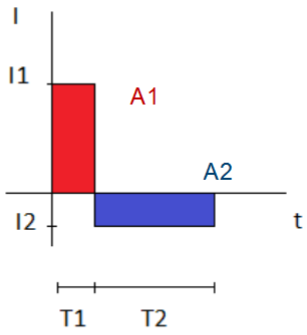

$$Q=\int_0^T I(t)dt = A1 + A2 = I1 * T1 + I2 * T2$$

Figure 5: Example of the stimulation signal waveform

The stimulation signal has a null net-charge when the biphasic signal has matching areas for both positive and negative waves. From a dimensional point of view, in fact, the area subtended by the curve in a current-time characteristic corresponds to a charge. Matching areas imply an equal rate between oxidation and reduction, hence generating a dynamical equilibrium which guarantees a safe stimulation most of the time. A last precaution must be followed even when charge-balance is achieved, that is charge density limitation. The dimension of the electrode is inversely proportional to the charge density, therefore small electrodes are potentially harmful because they deliver high values of charge density. A compromise must be chosen between the dimension of the electrode and the spatial resolution of the device, since small electrodes enhance the spatial resolution but are less safe (and viceversa). According to these specifics and to the thresholds studies an artificial retina should be able to safely deliver at least 100 nC, that is twice the amount of the average estimated threshold. Given that $Q = \int_0^T I(t)dt$ we can achieve 100 nC with 100 μA and 1ms for example, or use any combination provided that the stimulation time is not less than 1 ms because a longer pulse reaches deeper positions of the retina.

The geometry of the electrode pattern is another important feature. Depending on the pathology it could be preferable to choose a space-variant stimulation. For instane, in RP we want to stimulate the periphery of the retina rather than the macula because of the peripheral degeneration, while in AMD we want a higher density of electrodes in the macula. The amount of electrodes per cm^2can be optimized by designing the patterning in a non-square grid, like an hexagonal packing or some other fitting geometry. The hexagonal patterning in particular can deploy 1000 electrodes each with a 100 μm diameter [9], while a square patterning can deploy the same number of electrodes but their sizes must be reduced to 93 μm. The optimization of the number of electrodes does not correspond to the maximization of the electrodes per cm^2because we have to deal with the resolution of the system. Using more electrodes than needed, hence delivering more signal than the central nervous system can perceive as different, only generates useless heat release, an increase of thickness of the device (because the conducting lines needs to be layered), a waste of materials and a general increase of design complexity. Several studies on in vivo and in vitro retinas show that a reasonable number of electrodes is about 1000, providing at least 1000 pixels needed to fulfill necessary tasks as face-recognition and reading.

1.3 The State of the Art

The artificial retina can be classified as active device, when it is powered by an external source, or as a passive device when it is powered by the incident light. In 1.3.1 it is discussed the working principle of the device, i.e. the inorganic approach that has been widely studied in literature. Then, in 1.3.2 the artificial retina state of the art is reviewed. Finally, some primary considerations are made about the organic approach, the main focus of this thesis.

1.3.1 Working Principles of the Device

The general model of an artificial retina consists of a videocamera, a pair of coils and an implanted stimulator, as depicted in Figure 6:

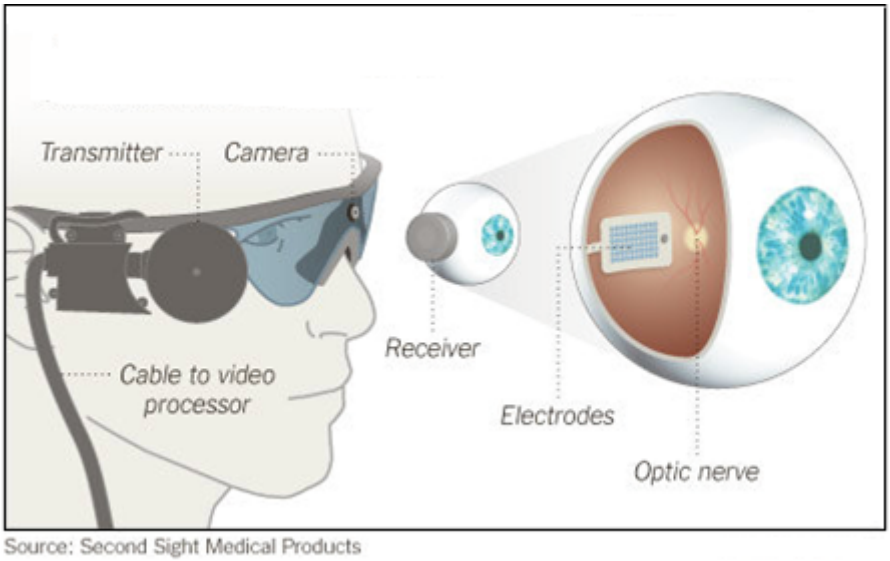

Figure 6: General model of an artificial retina

The videocamera is a CCD camera which transduces photons into electrical signals, and the image is processed by an external processor. The camera and the video processor are mounted on top of a pair of glasses, together with an external coil that communicates with an implanted coil. The processed image is sent to the internal receiver through an electromagnetic induction and the internal stimulator uses this signal in order to recreate the visual pattern acquired from the videocamera. The external signal processing generally consists of a PWM (Pulse-Width-Modulation) encoding, an ASK (Amplitude-Shift-Keying) modulation and an amplification. The internal electronic cannot be powered by a battery because of heat release problems, integration issues and above all because of the consequences that the reimplantation of a new battery involves. Therefore the internal signal processing has to recover both the information and the power supply from the induced signal. This feature leads to a further problem which is the encoding of the analogic signal. If the videocamera acquires the image of a white piece of paper for a long time, and if we decide to codify the white as a 0 and the black as a 1, the internal electronic has to recover the power supply from a long chain of 0 (representing a white pixel). Since the recovery of the power supply is generally achieved by an operation of arithmetic mean, in the case of a persistent white image the device stops to be powered. A solution to this problem is the PWM encoding, the very first step of the external signal processing. For example we can codify the information into a duty cycle using the following rule:

- A 0 is codified with a duty cycle equal to 50%;
- A 1 is codified either with a duty cycle equal to 40% or 60%;

Of course this is not the only solution to the problem of the signal encoding, indeed every design can have his own codification. Implementing this solution leads to a signal oscillating between 0 and 1 with a duty cycle

of 50%, if the videocamera acquires a persistent white image, and the power supply recovery can be normally accomplished with the average signal.

A second step of elaboration has to be the ASK modulation of the signal, because of the nature of the induction principle (Faraday-Lenz law of induction). Only a time-variant electromagnetic field can induce an electromotive force into a conductor, hence our signal must be modulated in amplitude before it reaches the transmitter coil. Furthermore, we have to consider that the carrier frequency dictates the bandwidth of the transferred image, but the higher is the frequency, the greater is the heat release. So, there is a trade off between spatial resolution and damage to tissues. The ASK modulation can be achieved using a class E amplifier (power amplifier) with a carrier frequency from 1 to 10 MHz. External and internal coils should be as close as possible, about 2-3 cm, in order to maximize the magnetic flux linkage.

As far as the internal processing is concerned, the first operation is the power recovery and it can be achieved with a rectification and a peak stretcher circuitry (diode bridge and low pass filter), and the extraction of the average signal. The demodulation of the signal can be obtained with an ASK demodulator, an analogic circuit which receives as input the signal from the secondary coil and gives as output the PWM digital signal. At this point, the digital signal undergoes several processing like the clock and data recovery, the synchronization, and the current control which drives the stimulator. Without a further inspection into these operations, already reported in literature [12], the most important thing to notice is the huge amount of calculations and operations managed by the implanted control unit, leading to a potentially harmful heat release to the tissues due to the working electronic.

The last part of the chain in the artificial retina is the stimulator. It receives the processed signal from the secondary coil as input, and it applies a proportional electrical current in output. We already discussed the features of the electrical stimulation of the retina, and the differences between epiretinal, subretinal and suprachoroidal implants in section 1.2, hence it remains to discuss only the practical implementation of the stimulator. In a real scenario the stimulator is a package of electrodes integrated into a microsystem, usually embedded in a flexible substrate and coated with some hermetic material in order to block infiltrations of water or ions. The stimulator must be protected from the aggressive physiological environment for 10 years at least, but the coating cannot reach the stimulation sites because the electrical feedthrough must be guaranteed in these spots (usually called “vias”). There are a lot of ongoing challenges in the engineering of hermetic coatings, like the creation of pinhole free coatings, the realization of thin devices, the integration of the electronic, the flexibility and the biocompatibility. Several solutions were adopted in literature, mainly focused on polymeric coatings, ceramic and also some metallic one. In details, polymeric coatings like polyimide, parylene and polyurethanes are the most popular in literature because of their cheapness, flexibility, biocompatibility and easy manufacturing. Polyimide in particular has ben extensively studied also in the case of electrical stimulation of the retina and it has been proven to be biocompatible both in vitro and in vivo [13]. The only downside to polymeric coating is their high vapor penetration coefficient. Ceramic and glass coatings like silicon nitride, silicon carbide, polycristalline diamond can solve this problem but their processing is not as cheap as the polymeric one.

Another approach that has been studied in literature is the packaging of an electronic module with integrated circuits and off-chip components like capacitors and resistors. The electronics is embedded into a shell and the physical gap between packaging and circuits is filled with an inert gas or vacuum. The main downsides to this approach are the sizes of the device and the complexity of the implantation process.

In literature a lot of effort was put into the development of pillar-shaped electrode arrays in order to create a better interface between stimulator and targeting cell layers, since planar devices do not manage to minimize the distance between them. Koo et al. realized a pyramid shaped 8x8 electrode matrix based on silicon which can penetrate the inner limiting membrane, stimulating the degenerated retinal tissue more effectively [14]. Kim et al. realized instead a pillar shaped electrode array based on polyimide and tested it with a suprachoroidal implant in a rabbit eye [15].

1.3.2 Review of the literature

We want now to discuss the main results obtained in literature regarding the fabrication, the engineering and the validation of an artificial retina. The results are briefly analyzed underlining the unique features they bring to the literature, more than providing an exhaustive description of every approach (which can be found reading the references).

We already mentioned the work of Liu et al. Their work provides a very detailed technical description about the electronic design behind an artificial retina, and their approach follows very closely the general model we discussed before.

Stieglitz et al. realized an epiretinal prosthesis based on a polyimide thin and flexible substrate with monolithically integrated electrode arrays and printed circuit boards [16]. They used a hybrid assembling technique and flexible multilayer encapsulation using parylene and silicone rubber. The stimulator had 24 integrated electrodes. The device works as described in paragraph 1.3.1, using a transceiver with inductive coupling in order to transmit energy and data to a coil with an integrated electronic circuitry. Their validation consisted firstly in the implantation of an inactive device, in order to explore histological and electrophysiological behavior, proving the long-term compatibility of the electrodes and the stability of the implant. They also led in-vivo experiments in cats, proving with optical imaging of the visual cortex an increased activity after a wireless stimulation of the prosthesis, and exploring the spatial selectivity varying the stimulation sites.

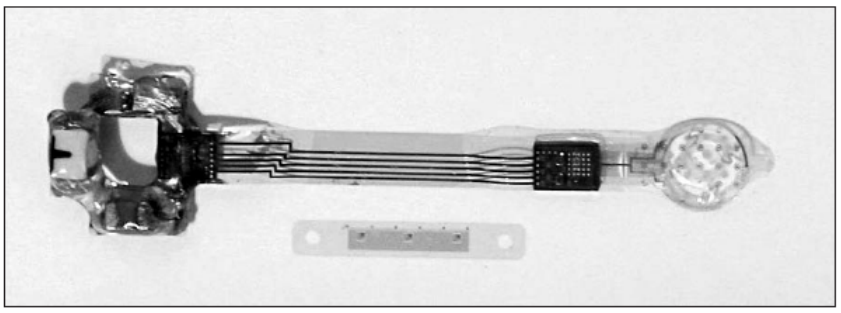

Figure 7: Epiretinal implant from Stieglitz et al [16].

The Boston Retinal Implant Prosthesis is a subretinal device that lies almost entirely outside the eye in order to minimize biocompatibility issues [17]. It follows the main model we discussed in paragraph 1.3.1. The external part of the implant is encapsulated in a titanium shell and has 15 stimulating channels, while the internal implant is encapsulated in polyimide. The device is still being improved, the current goal is to reach 200 stimulation channels, better hermetic features and a more efficient power management.

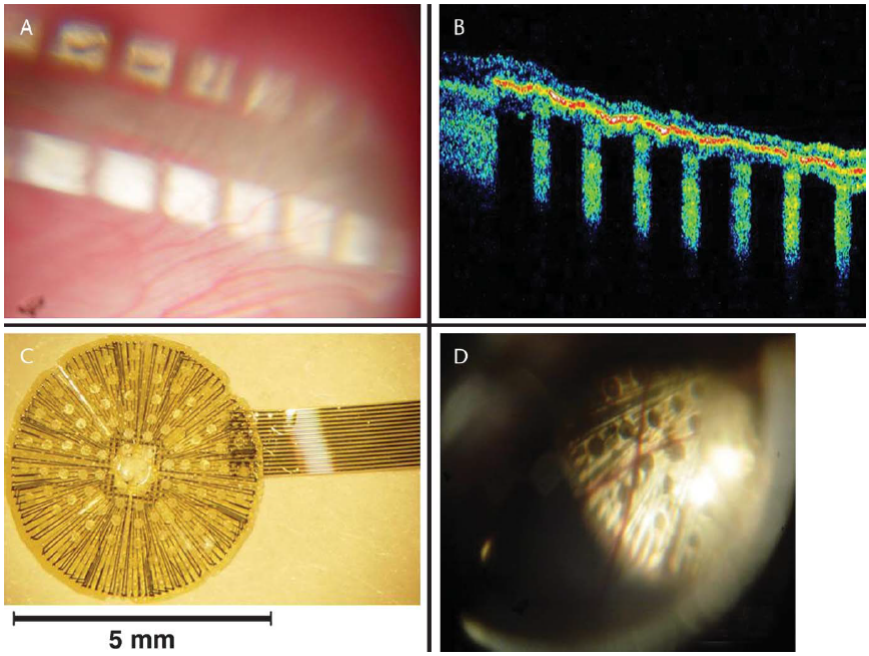

Figure 8: Images of 2 different types of electrode arrays, manufactured by the Boston Retinal Implant Project. A. Fundus photograph of an electrode array 3 months after implantation in a rabbit retina. B. Optical coherence tomography of the same electrode array seen as a highly reflective (falsely colored) red line under the retina. The electrode array is tightly apposed to the retina over the length of the array. C. Ten-micrometer microfabricated polyimide array with 100 electrodes. D. Fundus photograph of the same array 3 months after implantation in a pig retina. This is the widest electrode array ever implanted into the subretinal space of an animal [17].

Schanze et al. developed a microsystem-based epiretinal implant fabricated on a flexible polyimide substrate with integrated platinum electrodes [18]. The device uses a wireless communication between a camera and the stimulator, which is encapsulated in a parylene/silicone seal. The power supply comes from an implanted four silicon-based PIN photodiodes connected in series on the polyimide substrate, providing the voltage needed for the stimulation. The design of the implant consists of two units, both implanted: one, named IOL (intraocular lens part), is the unit responsible of the image acquisition and processing and it is implanted replacing the lens, while the other is the epiretinal stimulator. The layout of the stimulator has a substrate consisting in a ring-like structure with footprints for the four photodiodes to be embedded into an artificial intraocular lens. Then, conductive leads from the substrate communicate with the stimulator, which is made of two electrodes fabricated with micromachining techniques. The implant was tested both in vitro and in vivo on cats, stimulating with 100 and 200 µs impulses at different light intensity and distances between LED and eye, recording the evoked neuronal responses.

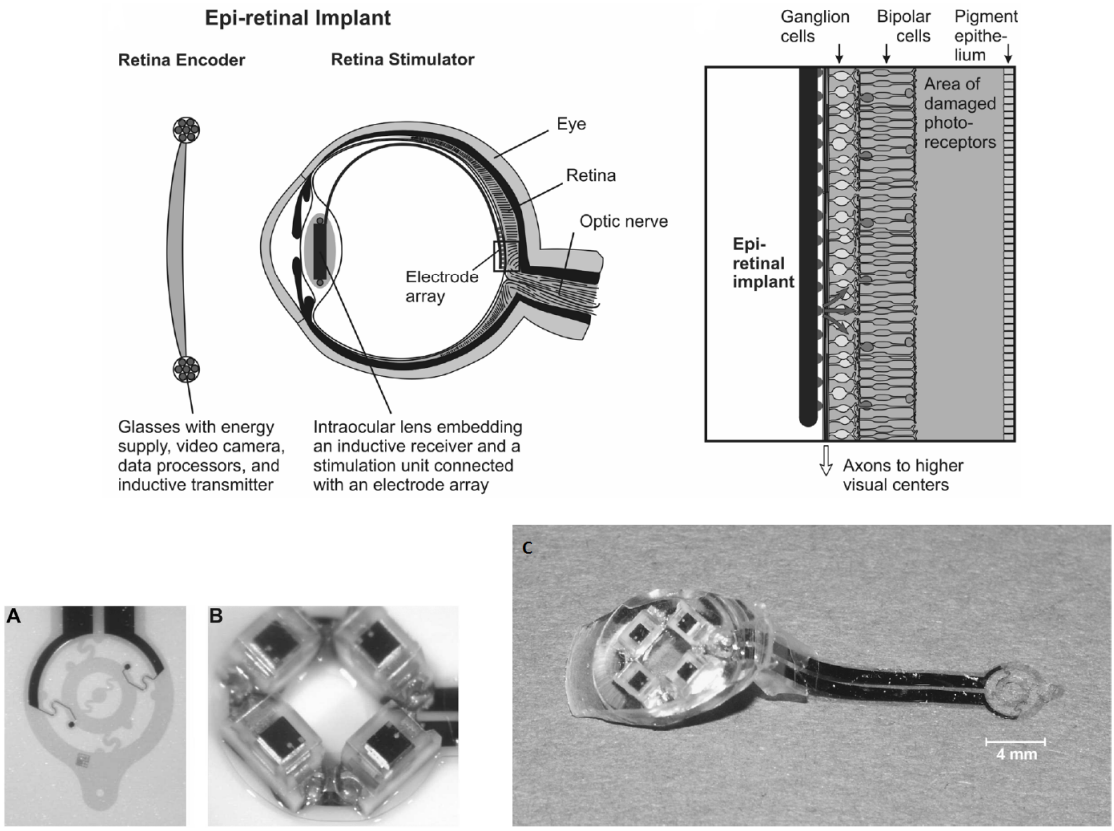

Figure 9: Epiretinal implant from Schanze et al. [18]. Electrode on polyimide substrate (A). Parylene coated IOL part (photodiodes) of the stimulator (B). Silicone encapsulated epiretinal stimulator (C).

Wong et al. presented a suprachoroidal implant consisting of 14 planar platinum electrodes embedded within a silicone rubber carrier [19]. The animal model chosen for the implant was the cat, and the validation was realized recording electrically evoked potentials (EEPs) on the primary cortex with a 32-channel surface electrode. They demonstrated that, for the suprachoroidal approach, the thresholds are higher then the previous one due to the charge being spread throughout the choroid and the retinal pigment epithelium (high impedance structures). The coverage of the stimulation sites is substantially larger than the one in epiretinal implants, and it comes without apparent consequences in choroidal blood flow.

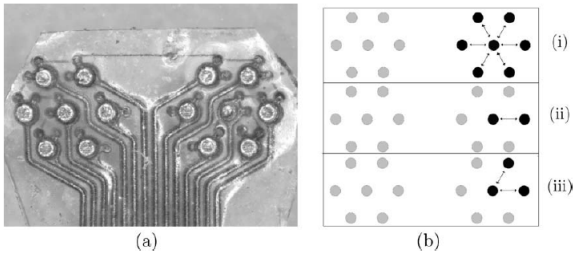

Figure 10: (a) The 14-channel platinum stimulating electrode array tip. Electrodes are grouped into two hexagons with the circular contacts with a diameter of 230 lm. (b) The electrode can be used to stimulate in three different electrode configurations, (top) six-return electrodes, (middle) a single-return electrode, and (bottom) two-return electrode stimulation. These configurations can be moved so that any electrode can act as the stimulating or return electrode [19].

Zhou et al. developed another suprachoroidal implant composed by an internal unit for retinal stimulation and an external one for the control of the stimulation and the battery charging [20]. The two units are linked

by two RF coils like in the previous analysis we made. The controlled parameters of the stimulation are amplitude, duration and rate, and the modulation technique is the PWM as explained in 1.3.1 with the only difference in duty cycle values for the codification of binary values (0=25% and 1=75%, with 50% duty cycle meaning the end of frame bit). The power recovery of the implanted unit is realized through a rectification and a low pass operation. A p-MOS switch separates the stimulation phase from the battery charging phase. The device is protected by a hermetic housing in a metal package consisting of a biocompatible titanium shell, platinum feedthroughs and a ceramic plate. The feedthroughs connects the electrode array and receiver coil to the retinal stimulator. The stimulator itself is a polyimide-based seven channel one with gold electrodes, and the chosen animal model is the rabbit. The validation was realized with a cortical registration of EEPs and VECPs (Visually Evoked Cortical Potentials), whose shapes and latencies are comparable to the other results in literature. Also the long term follow up (16 months) of the implant was measured with OCT and fundus oculi photography. It was demonstrated that the implant did not cause chorioretinal inflammation or structural deformity.

Zrenner et al. designed a subretinal implant containing an array of 1500 active microphotodiodes which acquires external images, and 16 implanted stimulating electrodes [21]. Their approach is the only one in literature where the photodiode-amplifier-electrode set is contained within a single pixel such that each electrode provides an electrical stimulus to the remaining neurons nearby, hence reflecting the visual signal that would normally reach an healthy retina. The validation was made on two male patients and one female with hereditary retinal degeneration, using four psychophysical tests concerning light detection, basic temporal resolution, object localization and movement detection. If passed successfully, the validation continues with tests for recognition of stripe patterns, localization and recognition of common objectives, and after these follows more complex tasks to fulfill. Tests were performed in “power ON” and “power OFF” conditions in order to define a baseline response. Zrenner’s work also briefly discussed the problem of image fading, cellular interface, and the role of learning and cognition in the perception process.

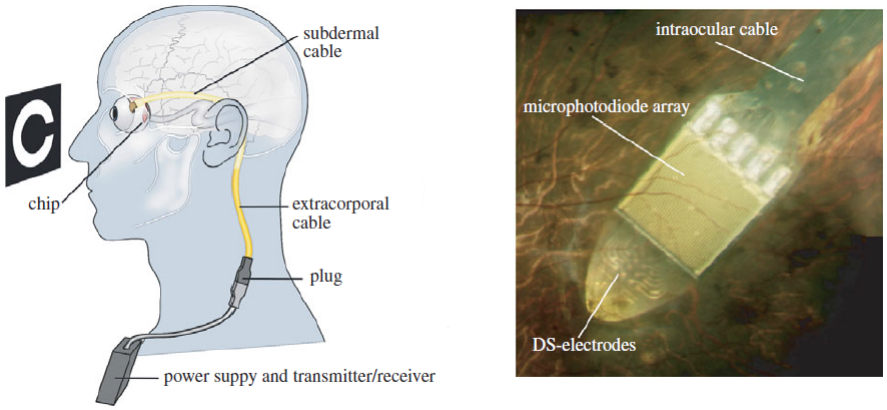

Figure 11: Zrennel et al. subretinal implant [21].

1.3.3 Organic Approach and Demonstration of Feasibility

The inorganic artificial retina has several limitations which hinder its applications and its spreading in the clinical practice. Silicon-based electronics and the implementation of an implanted microcontroller generate heat release to tissue, hence leading to cellular degradation and necrosis. The solid, non-flexible nature of inorganic electronics implies a heavily invasive surgical procedure for the implantation, and a non-ideal coupling between tissue and device. Also, the non-ionic nature of the signals produced by the device represents a forced communication tool which can generate cellular fatigue and necrosis, other than being less efficient than the ionic signals commonly used by biological entities. The organic approach to the design of an artificial retina overcomes these limitations but pays the price in terms of quantum efficiency of the photodetector. A demonstration of feasibility of the organic approach can be found in Ghezzi et al. [23]. In this work, the authors realized a bioorganic interface between an organic semiconductor and a network of cultured primary neurons. The organic semiconductor acts like a photodetector and transforms incident light into an electrical charge, like the CCD camera does in the inorganic artificial retina. The organic polymer was a blend of regio-regular poly(3-hexylthiophene-2,5-diyl) with phenyl-C61-butyric-acid-methyl ester (rr-P3HT:PCBM), spin coated onto a glass substrate pre-coated with indium-tin oxide (ITO) and covered with poly-L-lysine (PLL) to improve adherence. The neuronal culture consisted in primary rat embryonic hippocampal neurons, grown on top of the PLL layer. In order to maintain the cell survivability, the device was immersed in a culture medium (acqueous solution of NaCl) after thermal treatment and sterilization. The hybrid solid-liquid photodetector uses ITO as anode and the sodium chloride solution as cathode. In order to demonstrate that the polymeric layer does not affect cellular survivabiliy, the primary neurons were grown both on PLL treated ITO-P3HT/PCBM and on control glass substrates covered by ITO and PLL only, and a statistical analysis of cell mortality was performed :

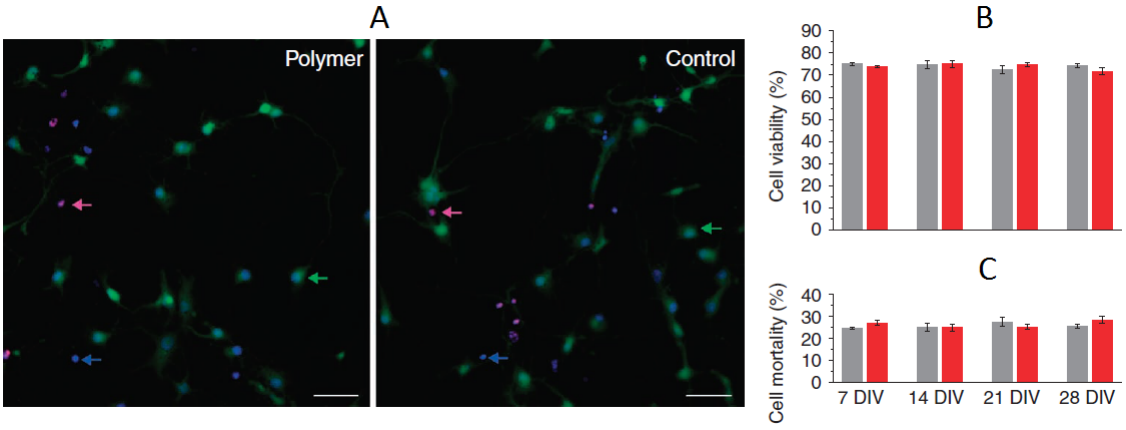

Figure 12: (A) Propidium iodine/fluorescein diacetate staining assay carried out at 21 DIV. Green, blue and violet arrows indicate viable cells, apoptotic cells and necrotic/apoptotic cells, respectively. Scale bars, 25 μm. (B) Statistical analysis of cell viability on control (grey) or polymer-coated (red) substrates (P = 0.558, one-way ANO VA, n = 6) at four time points: 7 DIV, 14 DIV, 21 DIV and 28 DIV. (C) Statistical analysis of cell mortality (P = 0.445, one-way ANOVA, n = 6) at the same time points of panel. Ghezzi et al. [23].

The functionality of the device was tested through the patch clamp technique and the use of Multiple Electrode Arrays (MEA), since a photogenerated ionic current is able to depolarize the cells and to induce an action potential. The resting membrane potential, and frequency and amplitude of spontaneous excitatory postsynaptic currents were measured for both cultures and it showed similar results. Also, polymer coated and non-coated MEAs did not show differences in spontaneous firing rate as shown in figure 13:

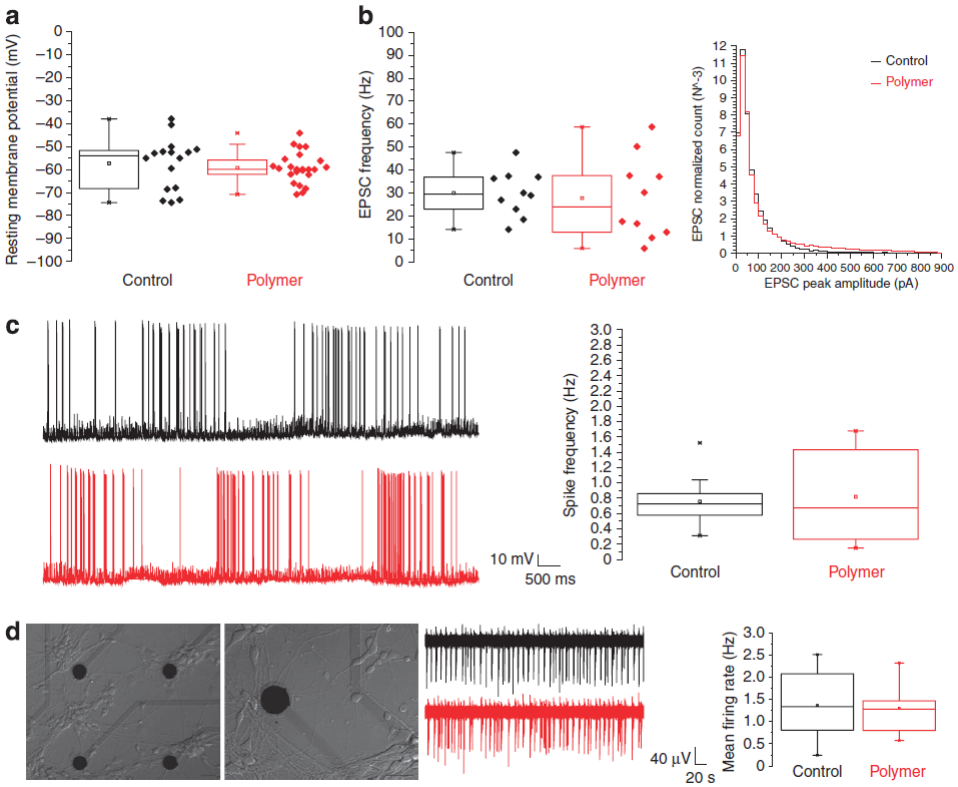

Figure 13: Spontaneous electrical activity of primary hippocampal neurons cultured onto bioorganic active interfaces. (a) The resting membrane potential of neurons cultured on either poly-L-lysine (PLL)-treated ITO/rr-P3HT:PCBM devices (red, n = 24) or control glass substrates covered only with ITO and PLL (black, n = 16) was measured (t-test, P = 0.506). (b) Analysis of the frequency (left; t-test, P = 0.736, n = 10) and amplitude distribution (right; n = 6, bins 20 pA) of spontaneous excitatory postsynaptic currents (EPSCs). (c) Example of whole-cell recordings from neurons cultured on either polymer (red) or control (black) substrates. The analysis of neuronal firing rates in ITO/rr-P3HT:PCBM devices (red, n = 10) and control substrates (black, n = 10) did not show any significant difference (left, t-test, P = 0.780). (d) Network mean firing rates (MFRs) computed with multielectrode array devices. Sample traces show a representative example of extracellular spikes recorded in the presence (red) or absence (black) of polymer deposition. Statistical analysis (t-test, P = 0.843, n = 9) did not show any difference between the two conditions. Scale bars, 30 µm. Box plot limits represent the 25th and 75th percentile and whiskers represent the outliers (coefficient 1.5) of the distribution. The mean (square), maximum and minimum values of the distribution are also shown. [23].

These data shows that the organic materials of the photodetector are higly biocompatible and that they maintain the healthy physiological behavior of the neuron culture. As far as the spatial selectivity is concerned, it was studied applying a 3x3 stimulation grid to the neuronal layer and it was measured the electrical response to an optic input signal. The results demonstrate a deterministic correspondence between the photostimulation site in the polymeric layer and the underlying cell body, being the action potentials evoked only within a cell-body diameter (in all directions) from the optical stimulus:

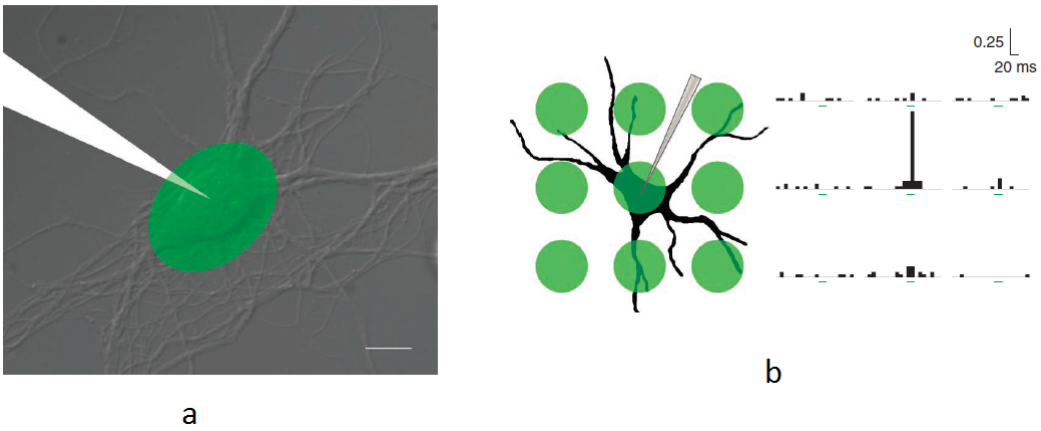

Figure 14: Optical stimulation of neurons cultured onto an ITO/rr-P3HT:PCBM device. (a) Schematic representation of the optical stimulation paradigm including the localization of the stimulus in a region surrounding the patched neuron (scale bar, 10 μm). (b) Spatial properties of the photostimulating interface. A grid of nine spots (diameter 20 μm, spacing 30 μm) was overlaid to a patched neuron and spikes were counted. PSTHs, arranged in a similar grid, represent the spike counts normalized for the total number of sweeps in all recorded neurons (n = 10, bins 10 ms). Each histogram represents the count of the spikes recorded at the soma by the corresponding stimulation spot. [23].

The physiological integrity of the culture was assessed through pH monitoring, ensuring that the photostimulation does not generate short-term degradation effects.

The concept of an organic artificial retina is based on these preliminary observations, that is good biocompatibility and ionic nature of signals. Moreover, the liquid nature of the organic polymers which constitute the photodetector allows their deposition on top of a flexible substrate, with the advantage of a smoother surgical procedure and an high adaptability of the device to the fundus oculi. Finally, the concept of trichromatic color vision can be theoretically achieved with a chemical tuning (doping) of the active layers, even if this topic is a very complex one and still subject of studies. The potentialities of the organic approach to sight restoration are enormous but still very young and with a lot of room for improvement. The aim of this thesis work is to fabricate and characterize an organic artificial retina based on bombyx mori silk fibroin as substrate, organic active layer responsible for the phototransduction and a physiological cathode, the vitreous humor. In order to realize that, we are going to understand the basic principles of Organic Bioelectronics and the difference between organic photodetectors and inorganic ones, studying and justifying every choice of passive and active materials, and finally characterizing the structural, chemical, optical, electrical and mechanical properties of the device.

Bibliography

[1] R. Kandel, H. Schwartz, M.Jessel. "Principles of neural science" 4/e. Mc Graw-Hill, 2000.μ

[2] Guyton & Hall. "Textbook of Medical Physiology", eleventh edition. Elsevier Saunders.

[3] J.M McNeil, "Americans with disabilities: 1991-92,". U.S. Census Bureau,1991.

[4] E.L. Berson, B.Rosner, M.A.Sandberg, K.C. Hayes, B.W. Nicholson, C. Weigel-DiFranco, and W. Willettw, "A randomized trial of vitamin A and vitamin E supplementation for retinitis pigmentosa," Arch.Ophthalmol., vol 111, pp. 761-772, 1993.

[5] E.D.Cohen, "Prosthetic interfaces with the visual system: biological issues", J.Neural Eng.4 (2007) R14-R31.

[6] Wang D Y, Chan W M, Tam P O, Baum L, Lam D, Chong K K, Fan B J and Pang C P, "Gene mutations in retinitis pigmentosa and their clinical implications", Clin.Chim.Acta (2005).

[7] Tassiker G E. 1956, US Patent 2760 483.

[8] G.S.Brindley, W.S.Lewin, "The sensations produced by electrical stimulation of the visual cortex", J.Physiol.196, pp.479-493 (1968).

[9] J.D.Weiland, M.S.Humayun, "A Biomimetic Retinal Stimulating Array", IEEE Engineering in Medicine and Biology Magazine, September/October 2005.

[10] X. Beebe and T.L. Rose, "Charge injection limits of activated iridium oxide electrodes with 0.2 ms pulses in bicarbonate buffered saline," IEEE Trans. Biomed. Eng., vol. 35, no. 6, pp. 494–495, June 1988.

[11] A.J.Bard, L.R.Faulkner. "Electrochemical Methods. Fundamentals and Applications". John Wiley & Sons, Inc., 2001.

[12] Liu W, McGucken E, Clements M, DeMarco C, Vichienchom K, Hughes C. "Multiple unit artificial retina chipset system to benefit the visually impaired".Theodorescu N.,ed. Raton B, FL:CRC, ch.2; 2000.

[13] J.M.Seo, S.J.Kim, H.Chung, E.T.Kim, H.G.Yu, Y.S.Yu. "Biocompatibility of polyimide microelectrode array for retinal stimulation". Material Science&Engineering, C 24 (2004) 185-189, Elsevier.

[14] K.Koo, H.Chung, Y.Yu, J.Seo, J.Park, J.Lim, S.Paik, S.Park, H.M.Choi, M-J.Jeong, G.S.Kim, D.D.Cho. "Fabrication of pyramid shaped three-dimensional 8x8 electrodes for artificial retina". Sensors and Actuators A 130-131 (2006) 609-615, Elsevier.

[15] E.T.Kim, J.Seo, S.J.Woo, J.A.Zhou, H.Chung, S.J.Kim. "Fabrication of Pillar Shaped Electrode Arrays for Artificial Retinal Implants". Sensors (2008), 8, 5845-5856; DOI: 10.3390/s8095845.

[16] T.Stieglitz, M.Schuettler, K.P.Koch. "Implantable Biomedical Microsystems for Neural Prostheses". IEEE Engineering in Medicine and Biology Magazine 0739-5175/05, September/October (2005).

[17] Joseph F.Rizzo III. "Update on Retinal Prosthetic Research: The Boston Retinal Implant Project". J.Neuro-Ophthalmol. 2011; 31: 160-168.

[18] T.Shanze, L.Hesse, C.Lau, N.Greve, W.Habener, S.Kammer, T.Doerge, A.Rentzos, T.Stieglitz. " An Optically Powered Single-Channel Stimulation Implant as Test System for Chronic Biocompatibility and Biostability of Miniaturized Retinal Vision Prostheses". IEEE Transactions on Biomedical Engineering, vol.54, no.6, june 2007.

[19] Y.T.Wong, S.C.Chen, J.M.Seo, J.W.Morley, N.H. Lovell, G.J.Suaning. "Focal activation of the feline retina via a suprachoroidal electrode array". Vision Research 49 (2009), 825-833, Elsevier.

[20] J.A.Zhou, S.J. Woo, S.I.Park, E.T.Kim, J.M.Seo, H.Chung, S.J.Kim. "A Suprachoroidal Electrical Retinal Stimulator Design for Long-Term Animal Experiments and In Vivo Assessment of Its Feasibility and Biocompatibility in Rabbits". Journal of Biomedicine and Biotechnology, Volume 2008, Article ID 547428, Hindawi Publishing Corporation.

[21] E.Zrenner, K.U. Bartz-Schmidt, H.Benav, D.Besh, A. Bruckmann, V.Gabel, F. Gekeler, U.Greppmaier, A.Harscher, S.Kibbel, J.Koch, A.Kusnyerik, T. Peters, K. Stingl, H.Sachs, A.Stett, P.Szurman, B.Wilhelm, R.Wilke. "Subretinal electronic chips allow blind patients to read letters and combine them to words". The Royal Society, doi: 10.1098/rspb.2010.1747, 2010, FirstCite e-publishing.

[22] C.Rao, X.Yuan, S.Zhang, Q.Wang, Y.Huang. "Epiretinal prosthesis for outer retinal degenerative diseases".

[23] Ghezzi, D. et al. "A hybrid bioorganic interface for neuronal photoactivation". Nat. Commun. 2:166 doi: 10.1038/ncomms1164 (2011).

Chapter 2

The Physics of Organic Polymers

2.1 Organic Bioelectronics

Organic Bioelectronics is a new and interdisciplinary field of science which integrates Electronic and Biology in order to study, understand and design electronic devices based on carbon and semiconducting materials (organic crystals, conjugated polymers, small molecules, etc..). The carbon-based nature of these devices is well suited for the interaction with biological elements like cells, proteins, micro-organisms, oligonucleotides, therefore opening new possibilities for the design of biocompatible implants and prosthesis, biosensors, drug delivery devices, neural interfaces. Organic bioelectronics also finds implementations in the field of energy, with devices like OLED (Organic Light Emitting Diodes), OTFT (Organic Thin Film Transistors), organic photoelectrochemical cells, organic photovoltaic cells, organic photodetectors and so on. The advantages of organic devices lie in the flexibility of their substrates, biocompatibility, cheapness of the fabrication, low production of heat, good interactions with photons thanks to the easy tuning of their optoelectronic properties, and good interactions with electrolytes due to the ionic nature of their electrical signals. The working principles behind the organic artificial retina are strongly connected to the charge generation process for organic semiconductors, and in particular for conjugated polymers because of their photovoltaic features. In order to understand the behavior of these materials, it is necessary to review concepts like molecular orbitals, hybridization, and energy levels. In 2.1.2 the main features of conjugated polymers are discussed, while in 2.1.3 the definition of exciton and its basics properties are introduced. Finally, the two main theory behind the charge generation process in organic materials are briefly discussed.

2.1.1 Molecular Orbitals and Hybridization

In the periodic table of elements the Carbon element has atomic number 6 and belongs to the period 2, group 14. Its electron configuration is $1s^2 2s^2 2p^2$, meaning that it has two electrons in its internal shell and four in its external shell. Carbon is a non metallic element with medium electronegativity and it tends to share electrons rather than catching or giving away. The 2s and 2p orbitals can interact between them creating from two to four covalent bonds, sp, sp2 or sp3. This interaction between atomic orbitals and their energy levels is called hybridization:

- sp3 hybridization: linear superposition of 2s, $2p_x$, $2p_y$and $2p_z$orbitals. The process creates tetrahedral structures like methane (CH_4);

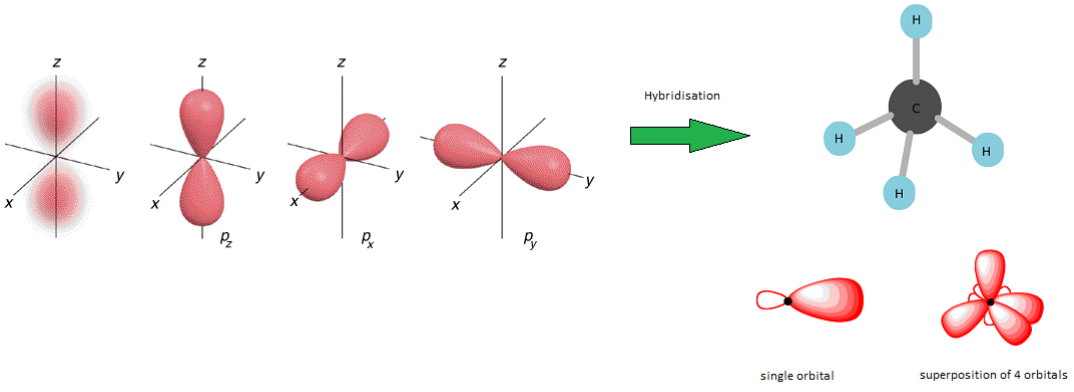

Figure 15: Methane and sp3 hybridization

- sp2 hybridization: linear superposition of 2s, $2p_x$, $2p_y$ orbitals. The process creates planar structures like ethylene (C_2H_4);

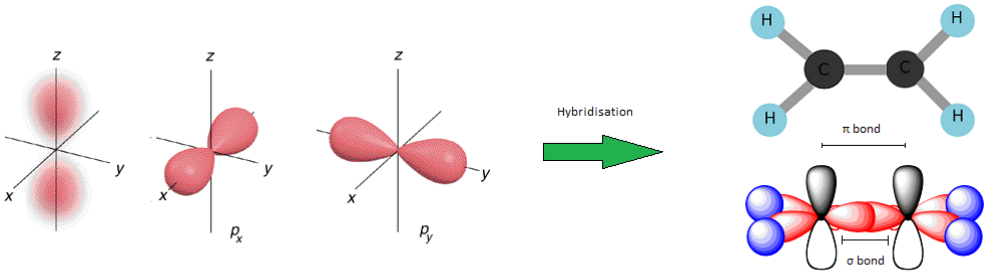

Figure 16: Ethylene and sp2 hybridization

- sp hybridization: linear superposition of 2s and $2p_x$orbitals. The process creates linear structures like acetylene (C_2H_2);

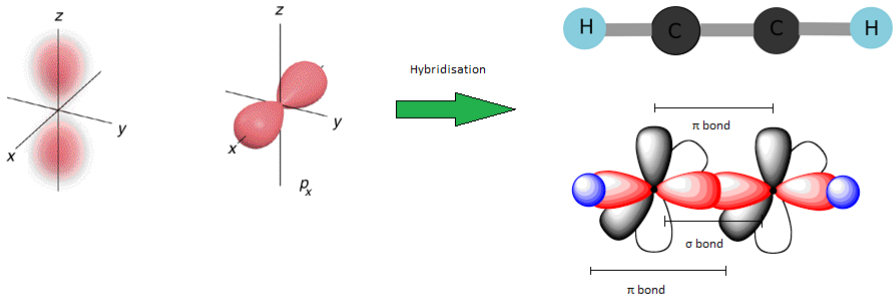

Figure 17: Acetylene and sp hybridization

A molecular orbital is defined as the region inside a molecule in which there is a high probability to find an electron occupying the orbital. Molecular orbitals can be achieved as solutions of the Schrödinger equation, a partial differential equations which fully describes the quantum state of a physical system. The linear superposition of orbitals (or LCAO, Linear Combination of Atomic Obritals) is a necessary approximation, since for complex molecules there are no exact solutions to the Schrödinger equation. The direct consequence of this approximation is the hybridization itself. In sp3 hybridization the energy of the hybridized orbital is between the energy of the 2s orbital and the 2p one (slightly more towards the sp orbital). The four electrons in $CH_4$are equally distributed in the four sp3 hybridized orbitals because they have the same energy. The tetrahedral geometry derives from the repulsion of the electrons in every hybridized orbital, therefore the configuration with the minimun potential energy is the one in which every orbital has an orientation of 109,5° with respect to the others. The sp2 hybridization is the more interesting one for conjugated systems. In this configuration, the $2p_z$orbital is left unchanged and it is perpendicular to the plane generated by the other three orbitals, hence creating strong σ bonds in planar structures and weak π bonds out of plane. Also in this configuration the energy of a sp2 hybridized orbital is between the energy of the 2s orbital and the 2p one, and the geometry is planar trigonal due to the electron repulsion. The orientation between orbitals is equal to 120°. The remaining $2p_z$ orbital does not partecipate in the hybridization and its minimum potential energy can be achieved only by the positioning along the plane orthogonal to the one identified by the sp2 hybridized orbital. The same considerations can be made for the sp hybridized orbital and its linear geometry. In this configuration there are two π bonds, each one located in an orthogonal direction with respect to the linear structure of the sp hybridized orbital, and one σ bond along the two carbon atoms.

An organic molecule can be univocally described by its molecular orbital diagram, which shows the energy levels of a molecule compared to the constituent atomic orbitals. These diagrams are focused on the wave-

nature of electrons and the energy levels are determined by the sum of waves (electrons) that can be in phase or out of phase. The simplest case is the H_2 molecule. When the two H are summed in phase a bonding orbital is created, while when they are summed out of phase an antibonding orbital is created. Antibonding orbitals have higher energy than bonding orbitals, therefore they are not stable configurations. in nature.

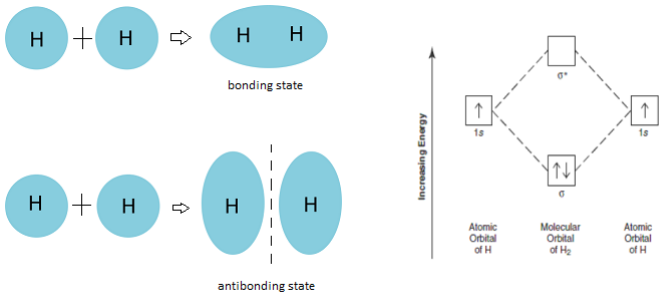

Figure 18: Bonding and antibonding orbitals for the H_2 molecule

When the atoms have enough electrons to occupy p orbitals and they have π overlapping, the situation changes as follows:

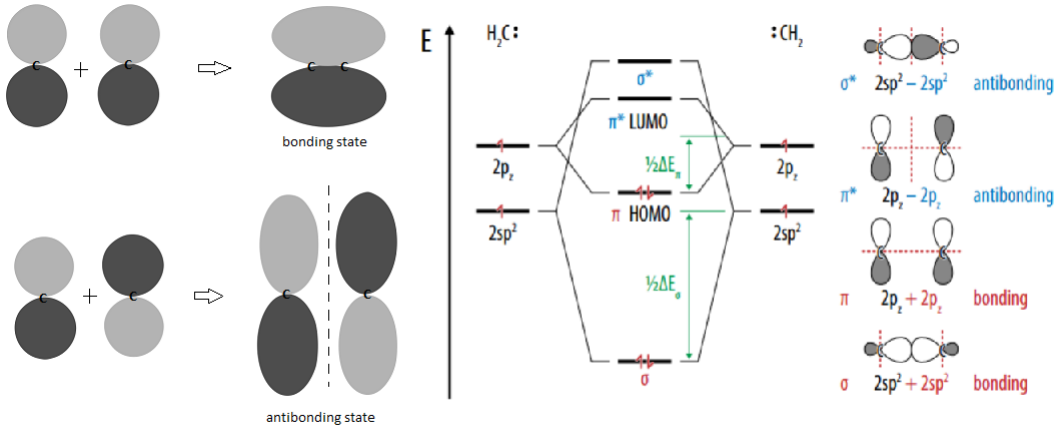

Figure 19: Bonding and antibonding orbitals for π bonds

In this configuration it exists a bonding and antibonding condition for both σ bonds and π bonds, and the generation of four energy levels. σ bonds have lower energies than π bonds because the proximity of s orbitals creates strong interactions and stability. We can define a classification of organic semiconductors based on the energy levels and their gaps, in a similar way as the valence band and conduction band for inorganic semiconductors. For this purpose we define:

- HOMO: Highest Occupied Molecular Orbital;
- LUMO: Lowest Unoccupied Molecular Orbital;

HOMO can be roughly considered as the valence band for organic semiconductor, and the same is for LUMO and the conduction band. However the similarities between the two frameworks is only formal, and not practical, since organic semiconductors present several differences with inorganic one and it is not accurate to talk about energy bands for them. This concept will be discussed in a different section. At the moment we are interested in materials whose energy gap between HOMO and LUMO is compatible with a semiconducting behavior. The energy gap in particular has to be low enough to allow the transition of a electron-hole couple from HOMO to LUMO after an optical excitation. Conjugated polymers have all these features and they are well-suited for the design of a biocompatible device which interacts with photons.

2.1.2 Conjugated Polymers

Conjugated polymers are a special kind of polymers which alternate single and double bonds in their backbone chain. The conjugation consists of the overlapping of all the $p_z$orbitals (and $p_y$orbitals for the sp hybridization), and of the generation of a monodimensional delocalized electrons cloud (bidimensional for sp hybridization). The simplest organic molecule is ethylene. If we replicate n times the ethylene molecule we obtain polyacetylene, which is the simplest conjugated polymer. In this structure there is a π simmetry, hence every carbon atom has sp2 hybridization and the electronic density is localized on the plan created by the hybridized orbitals. For the p orbitals, instead, the strength of the bond is not enough to confine the electrons, therefore we can talk of charge delocalization along the entire polymeric chain. The electrons are free to move in this preferential direction, and if an electrical potential is applied, it can generate ionic currents in the material. Hence, delocalization implies an easy conduction along the molecular plane and it establishes the bases for plastic electronics. For n carbon atoms inside a chain, the energy levels get splitted into n levels and the distance between levels decreases proportionally with the increase of n. Also, the energy gap between HOMO and LUMO decreases with the increase of n. For n tending to infinity, the energy levels are continuous (energy bands), the energy gap is zero and the material behaves like a metal. However, in a real organic material there is always a minimum gap of 1,5 eV between HOMO and LUMO, because the alternating single and double bonds in the conjugated polymer show different bond length and energy. This difference is known as *Peierls distortion,* and it doubles the period of repetition of every CH=CH structure with respect to the equispaced chain.

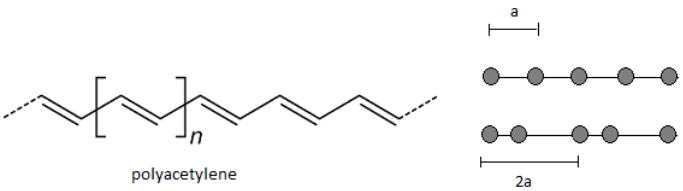

Figure 20: Polyacetylene and Peierls dirtortion

Conjugated polymers are liquid at ambient temperature.Various examples of conjugated systems besides linear single and double bonds alternation are benzene and aromatic compounds, polycyclic benzenoid hydrocarbons, cyclic polyenes, heterocycles, dendrimers, 5-membered heterocycles etcetera. The spatial distribution of their molecules has an amorphous component, in which weak Van Der Waals interactions happen, and a crystalline component in which there are a strong superposition of p_z orbitals and a good electronic conductance. The balance between amorphous and crystalline components does not only influence the conductance but also the mechanical properties of the polymer, since amorphous components are more flexible than crystalline ones. A good conjugated polymer designed for biocompatible application should have enough crystalline chains to guarantee a good conduction along the molecular plane, but also a percentage of amorphous structures in order to achieve flexibility and adaptability to the various possible implant sites. For artificial retina applications in particular, the device must be flexible enough to allow the least possible invasivity during the implantation process, and to adapt his shape to the fundus oculi. The tuning between these two conditions can be set through a thermal treatment called *annealing*, which will be discussed in chapter 3. It is also possible to tune the optoelectronic properties of conjugated polymers through doping and chemical treatments, in order to modify for example the solubility or the conductivity of the chains, the flexibility, the absorption spectra etcetera.

2.1.3 Excitons and Charge Generation

In the physics of semiconducting polymers there are two different theories that try to explain the charge generation process and the excited states. One of them is the band theory already used for inorganic semiconductor, since for increasing delocalization lengths the energy gap between HOMO and LUMO tends to zero. As a matter of fact, several experimental evidences showed that the theory used for large organic molecules is well suited for the description of conjugated polymers. The band theory assumes that if a photon with energy at least equal to the energy gap strikes the material, a delocalized electron-hole pair is created with low binding energy. The problem of this theory is that a real polymeric chain cannot be approximated to an infinite succession of repeating units, and the band-like framework collapses since there is not a real continuum for energies.

The model also does not accurately describe the interaction between photogenerated electron-hole pairs. The molecular approach seems more adequate for the description of the system. This model considers an organic polymer as an array of conjugated chains described by their molecular properties. The primary photoexcitation in conducting polymers is the *singlet neutral exciton states* [1], that is an excited molecular state consisting in a bound electrone-hole pair localized on a single molecule. The exciton is electrically neutral and therefore is not subjected to drift phenomena but only to its mechanical diffusion for both interchain and intrachain environments. The charge photogeneration for an organic system has to overcome two different energy gap, the electronic one and the optical one. The optical gap is the energy amount needed to generate a bound electrone-hole pair, while the electronic gap is the amount of energy needed to separate the bound electrone-hole pair against its Coulombian attraction. For inorganic systems, the electronic gap is in the order of few kT, and at ambient temperature the thermal energy of electrons and holes is sufficient to separate the bound pair. In organic materials this energy is higher and the reason for that is the different dielectric constant. If we analyze the Coulomb law and its dependence on the dielectric constant, and if we consider that the dielectric constant of silicon (which we assume to be representative of a generic inorganic material) is about ten times higher than the carbon one, we conclude that the increased Coulombian attraction for organic materials is the reason why the bound electrone-hole pair needs additional energy for its dissociation. Excitons can be classified into Frenkel, Wannier-Mott and Charge transfer excitons:

- Frenkel exciton: it is the typical exciton for materials with a small dielectric constant (organic materials, as we discussed before). It has a strong Coulombian interaction between electron and hole, the binding energy can range within the 0,1-1 eV gap. The exciton is strongly localized inside the single molecule;
- Wannier-Mott exciton: it is the typical exciton for materials with a high dielectric constant (inorganic materials and some liquid). The Coulombian interaction between electron and hole is reduced by the screening from the electric field, and the exciton is delocalized. The binding energy is about 0,01 eV;
- Charge Transfer exciton: it is the typical exciton for molecular crystals or polymers made up of ordered crystals and very few amorphous components. It is an intermediate case between Frenkel and Wannier-Mott exciton because it is composed by an electron and a hole located in another adjacent chain. This distance between the bound pair is responsible for a low binding energy, about to 10-100 meV;

Figure 21: Different types of excitons

In conjugated polymers we mostly deal with Frenkel excitons and we have to overcome both the optical and the electronic gap. The separation of the bound electrone-hole pair creates a *polaron* pair, that is a quasiparticle composed by an electron/hole and its interaction with the surrounding environment. This separation can be achieved with the application of an electric field, internal to the material. Several complex mechanism happen in this process, including the creation of a metastable state between the Coulombian bonding and the generation of the polaron pair, called *charge-transfer* state. In this state the distance between electron and hole is higher than in the bound state but there is still a significant Coulombian attraction between them. If this metastable state decades to the bound condition we talk about *geminate recombination*. If the pair manages to separate instead, the two polarons start to drift towards their minimum potential energy condition (anode and cathode generally), and the charge transfer may happen for both intrachain and interchain paths. For a complete and exhaustive understanding of charge generation processes the interested reader can consult the bibliography of the end chapter.

2.2 Organic Photodetectors

The understanding of concepts like molecular orbitals, conjugation, and charge generation in organic polymers is the basis of the design process of an organic photodetector. The main feature of such a device is the conversion of photon into electrical charge. The purpose of the conversion may have roots in the photovoltaic field, that is the generation of electrical energy from solar radiation, or it may be focused on the acquisition of an absorption spectrum in order to analyze the physical/optical/chemical properties of a material. Also, the goal may be a combination of the two mentioned categories, that is the acquisition of an optical signal and the extrapolation of energy from the same signal. The artificial retina application falls on the latter category, since the design of the device allows the acquisition of the visual signals generated from the outside environment, and the extraction of energy from the same signal can be used to feed the processing itself. In the organic artificial retina the energy extraction is not needed because the device is fed by the light signal itself and there is no artificial processing. In this section the main features of an organic photodetectors are discussed. The configuration that leads to the highest quantum efficiency possible, that is the stack of P3HT-PCBM bulk heterojunction and PEDOT-PSS is analyzed in 2.2.2 and 2.2.3. Finally, the detailed architecture of the artificial retina device is presented, which is the main topic of this thesis.

2.2.1 The Transduction Process

The transduction of a photon into electrical charge is a process that can be rigorously described by analyzing four different phases:

- photon absorption: the absorption of electromagnetic radiation can be studied by the Beer-Lambert law, which states that there is a logaritmic dependence between transmissivity of light through a material, its absorbance and the distance of traveling. If I is the intensity of the radiation coming out of the sample, I_0 is the intensity of the radiation entering the material, T is the transmissivity, A is the absorbance, x is the distance and μ is the coefficient of linear attenuation, we have the following relationships:

$$I = I_0 e^{-\mu x}$$

$$T = {}^{I}/_{I_0} = e^{-\mu x}$$

$$A = -log_{10} T$$

Figure 22: Beer-Lambert law

  μ depends on the material composition and its density. We can introduce a coefficient of mass absorption normalizing with respect to the density, and this new physical quantity depends on three absorption mechanism: the photoelectric absorption, the scattering (elastic and inelastic), and the production of electron-hole pairs. The photon absorption can generate an exciton if the energy of the photon is at least equal to the optical gap;

- exciton diffusion: the diffusion process is described by the two Fick's law, the first one relates the flux of diffusion to the concentration, and the second one predicts how the diffusion can induce changes in the concentration. If J is the flux, D is the diffusion coefficient, x is the distance, φ is the concentration in mol/m^3, and t is the time, the relationships are the following:

$$J = -D\frac{\delta\varphi}{\delta x}$$

$$\frac{\delta\varphi}{\delta t} = D\frac{\delta^2\varphi}{\delta^2 x}$$

Figure 23: Fick's laws

- exciton separation: we mentioned that the separation of the bound electrone-hole pair, that is the overcoming of the electronic gap, can be achieved with the application of an electrical field. In organic photodetectors this electrical field can be generated at the interface of a *donor/acceptor* system. A donor is defined as a chemical entity which donates electrons to another one, while an acceptor is defined as a chemical entity which accepts electrons transferred from another one. When an organic photodetector is designed, the energy levels of the donor/acceptor system must be accurately selected in order to guarantee the creation of an eletrical field at the interface. This electrical field is the direct consequence of the two layered materials reaching thermal equilibrium. Also the geometry of the system plays an important role. The first solution to this problem was the stacking of the two photoactive layers, one on top of the other, and the deposition of a cathode and an anode to the extremities of the device. This structure takes the name of *heterojunction*, and the most efficient choice of the materials led to the layering of P3HT (Poly-3-hexylthiophene), one of the most efficient electron donor, with PCBM (Phenyl-C61-butyric acid methyl ester), a fullerene derivative of the C_{60} bulkyball and one of the most efficient electron acceptor:

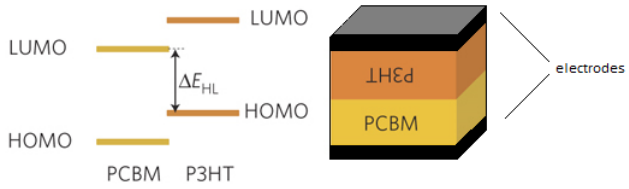

Figure 24: A primitive example of organic photodetector

The problem of this structure was not the choice of the materials, to this day still the best donor/acceptor interface for exciton separation, but its geometry. The diffusion length of the exciton, between 5-10 nm for organic materials, entails a stringent design parameter since the exciton must be separated (hence it must find a donor/acceptor interface) between 5-10 nm from its generation site. A layering thickness of P3HT/PCBM higher than 5-10 nm is useless for the charge generation and it lowers the quantum efficiency of the device, but a layering thickness similar to the excitonic diffusion length generates a device with a very low conductivity. Also the process of the photons absorption is not compatible with the thicknesses we are talking about. Hence for thick devices it is penalized the charge generation, and for thin ones the charge transfer and the absorption. The solution to this dilemma is a *bulk heterojunction*, that is a nanoscale blend of donor and acceptor materials. The blend creates a sea of P3HT in which the PCBM is distributed with many domains, and this architecture generates several donor/acceptor interfaces. The quantum efficiency is strongly increased because it is very likely that an exciton meets an interface, and therefore the energy needed for its separation, whithin the 5-10 nm of its diffusion. A bulk heterojunction can be simply obtained blending the two donor/acceptor materials, liquid at ambient temperature, and letting the mixed solution at rest in order to assemble the interpenetrating network of structures. The detailed process to create a bulk heterojuction is described in chapter 3. In some case it can be added a third component to the heterojunction, precisely a second p-type donor polymer, in order to introduce an alteration of the absorption spectrum. In this work we will not consider this possibility because the behavior of such a device is far more complex than the one for a standard bulk heterojunction, and because the price to pay for the fine tuning of the absorption spectrum is a decreased quantum efficiency.

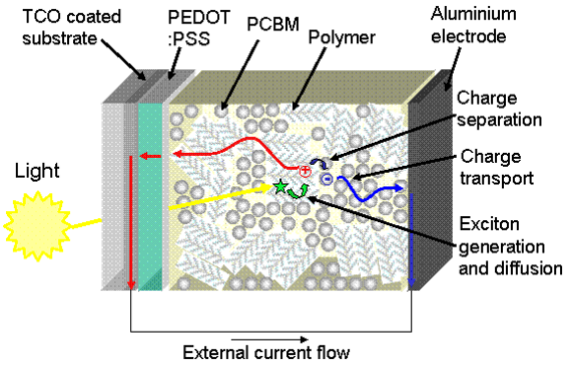

Figure 25: Example of a bulk heterojunction based organic photodetector

- charge collection: the two polarons generated with the mechanism we already discussed must be collected in order to avoid recombination processes. The best way to do it is to apply an external electrical field which can induce the polarons drifting. Usually for organic photodetector a good choice for the anode is the ITO (Indium Tin Oxide), and the cathode is an aluminum electrode. An increase in quantum efficiency can be achieved with the introduction of other two layers in the stack, usually PEDOT:PSS coupled with ITO and LiF coupled with the aluminum electrode. Those two transitioning layers promote the charge transfer of the polarons towards the electrode, and lower the work function of the latter. Another important factor in charge collection efficiency is the mobility of the charge carriers, that can be improved with functional substitution in the polymeric chain, with the tuning of its molecular weight and with doping.

Finally we discuss the concept of quantum efficiency in photodetectors. The quantum efficiency is defined as the ratio between the charge amount generated by a photodetector and the number of photons in input. It is usually calculated as a percentage, being an adimensional quantity, for example a QE=100% means that the photodetector generates an electrical charge for every single incident photon. The concept of quantum efficiency is further splitted into other two definitions:

- EQE (External Quantum Efficiency) = ratio between incident photons and number of charges collected from the photodetector. If I is the current generated from the photodetector, e is the elementary charge, P is the incident luminous power, h is the Planck constant and ν is the frequency of the optical radiation, we have:

$$EQE = \frac{I/e}{P/h\nu}$$

- IQE (Internal Quantum Efficiency) = ratio between incident photons which are actually absorbed by the photodetector and the number of charges collected. If R is the reflectivity of the photodetector we have:

$$IQE = \frac{EQE}{(1-R)}$$

The difference between EQE and IQE lies in the transmission and reflection properties of the photodetector, since a perfect optical coupling between the incident photon and the absorbing material would give matching EQE and IQE. The EQE can be directly measured from the device, while the IQE must be estimate knowing its transmission and reflection spectra. The IQE provides information on the efficiency of the donor/acceptor interface (dissociation efficiency), the recombination processes, and the efficiency of the charge collection, while the EQE takes into account also the efficiency of light absorption. A detailed description of the quantum efficiency in photodetector can be found in several reviews that cover the topic and in the end chapter bibliography.

2.2.2 P3HT/PCBM Bulk Heterojunction

Polythiophenes are polimerized thiophenes linked through their 2,5 position. Thiophenes are sulfur heterocyclic compounds with formula C_4H_4S, colorless liquids at room temperature. The thiophene molecule is flat and presents the typical charge delocalization of conjugated polymers, but it has poor solubility and processing properties. Furthermore, polythiophenes are made of amorphous films with low structural order, short π-conjugation lenght and poor carrier mobility [2]. In order to overcome these limits it is possible to create polymers derived from polythiophenes with alkyl-substitution in 3 and 3,4 positions. One of the most interesting Polythiophene is P3HT, Poly-3-hexylthiophene. It has an excelent solubility in organic solvents like chlorobenzene and it is well suited for the deposition in thin films. A good conductive polythiophene must have crystalline microstructures which allow the overlapping of intermolecolar orbital, and this happens in regioregular head-to-tail Poly-3-hexylthiophene. In this polymer the thienylene structures are planar and this greatly increases the alignment of p orbitals and therefore the π-conjugation. As a direct result, the carrier mobility increases from about $10^{-3}cm^2/Vs$ (of the regiorandom polythiophene) to about 0,1 cm^2/Vs.

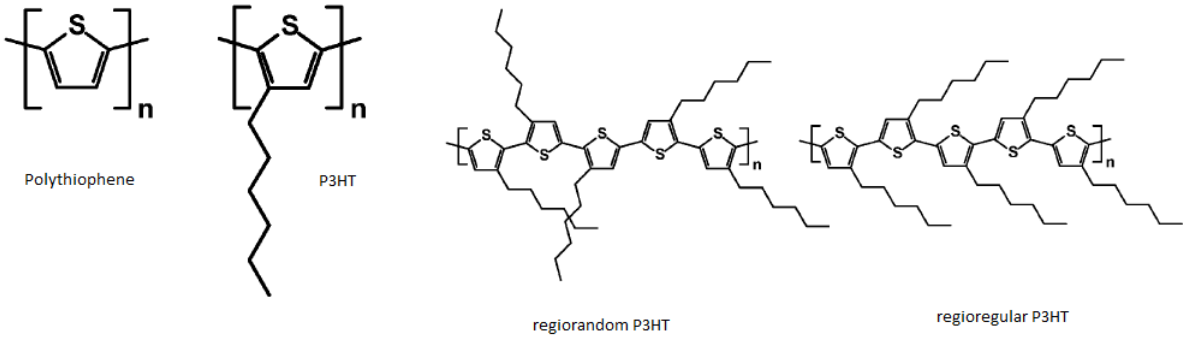

Figure 26: Polythiophene and Poly-3-hexylthiophene

Carrier mobility is also influenced by the molecular weight of the polymer, the degree of regioregularity and the speed of deposition. The downside of this structure is that the increased π-conjugation makes the material very susceptible to photoinduced oxidation, hence the device encapsulation is a common solution for organic photodetectors based on regioregular P3HT.
PCBM (Phenyl-C61-butyric acid methyl ester) is a fullerene derivative that is considered to be the best electron acceptor to be coupled with P3HT. Like P3HT it is soluble in chlorobenzene and this feature makes it an optimal choice for the polymer/fullerene blending, in order to create a bulk heterojunction.

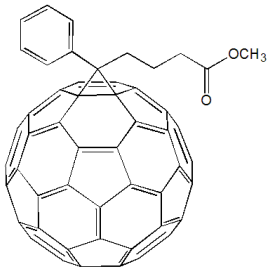

Figure 27: PCBM (Phenyl-C61-butyric acid methyl ester)

We want to discuss now the feature of the P3HT/PCBM bulk heterojunction in relation with the quantum efficiency. The first aspect of a good quantum efficiency is the photon absorption process, since, if a remarkable part of incident photons is not absorbed, the charge amount generation is hindered. The general UV-Vis spectrum for P3HT/PCBM shows a typical Gaussian shape with a peak between 450nm and 600 nm, but the shape of the spectrum is heavily influenced by several parameters, like the P3HT/PCBM ratio, the thermal annealing duration, the thickness of the device and others. As far as the optimal ratio of polymer/fullerene

is concerned, there are studies and reports which states that the best combination is a 1:1 ratio [11][12]. An increasing concentration of PCBM in the blend generates a blue shift of the absorption peak in the spectrum:

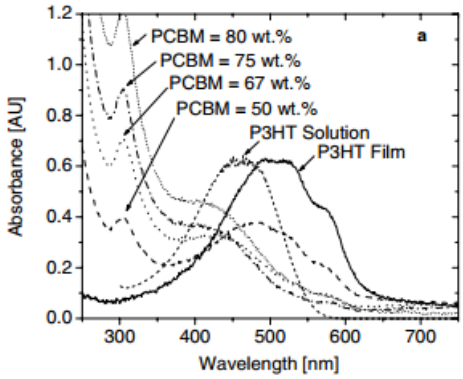

Figure 28: P3HT/PCBM absorption spectrum for different blend ratio [10]

Also the absorption of the P3HT solution shows a blue shift with respect to the P3HT film. Both shifts may be caused by an increased delocalization of π conjugated electrons, in one case because of the liquid state in itself, and in the other one because of the PCBM lowering the interaction among P3HT chains in the other. Another reason for the thin film is the charge transfer between P3HT and PCBM, since P3HT is a good electron donor and tends to be oxidized while PCBM is a good electron acceptor and tends to be reduced. A proof for this theory can be supplied through the substitution of PCBM with the C_{60} bulkyball. The alkyl side chain in PCBM helps the fullerene with its solubility problems, and if the blue shift is only caused by the low interaction between P3HT chains generated by PCBM obstruction, then the blue shift should be greater for PCBM rather than for C_{60}. Experimental evidences show that the opposite situation is true, hence proving the presence of an irreversible charge transfer.
The blue shift caused by the blend of polymer/fullerene may be compensated with a process named *thermal annealing*. Thermal annealing is a heat treatment which modifies the mechanical, chemical and physical properties of a material. In particular the temperature of the material must exceed its glass transition temperature, keeping it steady for a while, and then cooling it down to the room temperature. This process increases the degree of order of the polymeric chains and therefore its crystallinity, its stiffness and electrical conductance. Thermal annealing for P3HT/PCBM is usually executed around 120°C for 30 min. The increased regularity of the annealed film causes a red shift that it is still not enough to fully compensate the blue shift induced by the blending, because of the irreversible charge transfer process we discussed before. Figure 29 depicts the blend absorption spectrum at different annealing temperatures, showing that the induced red shift generates the broadening of the spectrum itself:

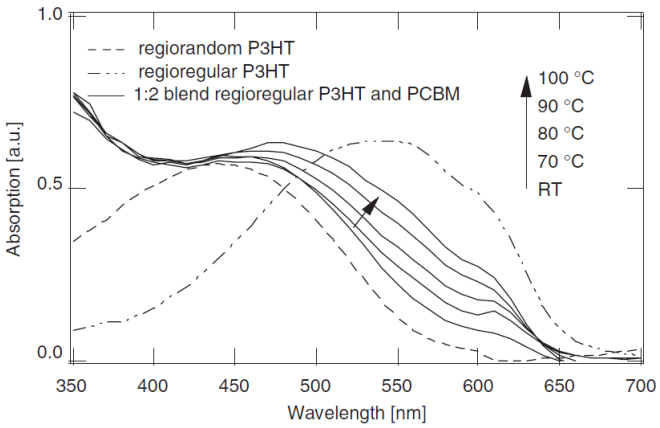

Figure 29: P3HT/PCBM absorption spectrum for different annealing temperatures [7]

After the thermal annealing process, the absorption peak shifts to about 530 nm. The peak around the green component of the spectrum along with the broadening it experiences after thermal annealing, makes the material well suited for its application as photoactive layer in an organic artificial retina. Furthermore, the matching of the absorption spectrum with the spectrum of the incident light is very important for high quantum efficiencies, hence the broadening of the photoactive spectrum is a well accepted consequence also for this perspective. The thickness of the photoactive layer is another parameter of efficiency, since according to Beer-Lambert law a thin device may not be able to catch photons. This law also takes into account the effect that multiple internal reflections, diffraction phenomena and photoelectric absorption have on the absorption process.
Geminate recombination is a big limiting factor for high quantum efficiencies. In order to avoid that phenomenon, there must be a high probability that the exciton finds a polymer/fullerene interface within its diffusion range. That probability is very high when the two interpenetreting nanostructures of the blend are mixed in a 1:1 ratio. If the domain sizes are too large, the exciton may degenerate before meeting an interface. If the two phases are too thin then there is a high interfacial area and geminate recombination is promoted because the Coulomb capture radius is higher than the domain size [2].
The last contribution to quantum efficiency is the charge collection efficiency, and as we mentioned before it has been proven that the carriers mobility strongly depends on regularity and crystalline order of the nanostructures. Thermal annealing treatments greatly improve the regularity of domains, the charge transport and reduce the geminate recombination, while they induces a lower efficiency of exciton quenching. It is possible to tune these two effect until an optimum is reached, that is a condition in which the decrease in exciton dissociation matches the improvement of the charge-tranfer state separation.
We can introduce an additional definition for EQE which summarizes all the topics we discussed. This definition takes into account the single efficiencies of the internal processes responsible for the total quantum efficiency. If A is the absorption efficiency of the photoactive material, Q is the charge collection efficiency for the electrodes and $\eta_d$is exciton dissociation efficiency, we have the following relation:

$$EQE = A * \eta_d * Q$$

2.2.3 PEDOT:PSS

PEDOT:PSS or poly(3,4-ethylenedioxythiophene) polystyrene sulfonate is a material composed of the conjugated polymer poly(3,4-ethylenedioxythiophene) and sodium polystyrene sulfonate.

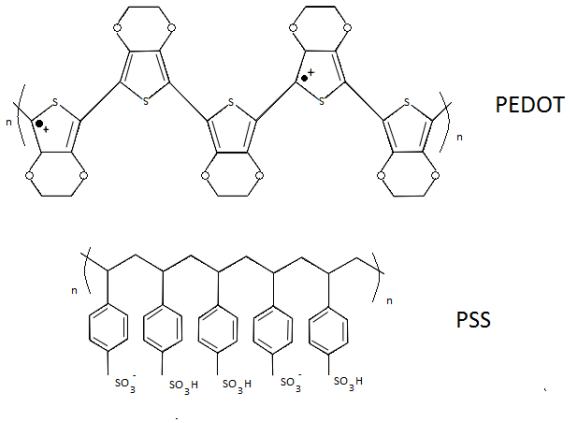

Figure 30: PEDOT:PSS

PEDOT has several features which make it a widespread choice in plastic electronic and bioengineering applications. It is conductive, being a conjugated polymer. It is fairly transparent in the visible spectrum, stabile and biocompatible, and it has a low redox potential. The mixture with PSS helps its solubility problems allowing it to be dispersed in water, simultaneously enhancing its conductivity and also being a template for polymerization [16]. PEDOT and PSS form a macromolecular salt, since the first has positive charges in his aromatic ring, and the second has negative charges through part of its sulfonyl groups. The implementation of PEDOT:PSS in the photovoltaic field is also justified by its high work function and its tendency to act as a hole injection layer. This feature allows to use PEDOT:PSS as an electrode in organic solar cells, replacing ITO or other metallic thin films on condition that other additives are used in order to further increase its conductivity. A common additive is DMSO or DiMethyl SulfOxide, which greatly increases PEDOT:PSS conductivity with respect to the pristine polymer one (below 10 S cm^{-1}). This increase in conductivity can reach the 1000 S/cm value. Other additives for PEDOT:PSS can be used in order to enhance its wettability, since its acqueous nature is not optimal to the coupling with hydrophobic organic surfaces like P3HT. Such additives should reduce the surface tension, therefore surfactants like Zonyl or organofunctional silanes like (3-Glycidyloxypropyl)trimethoxysilane (GOPS) are widely used in this regard. The concentration of additives must not affect the absorption spectrum of PEDOT:PSS (its transparency). It has been proven that a DMSO concentration up to 10% does not significantly change the total transmittance in the visible range [20].

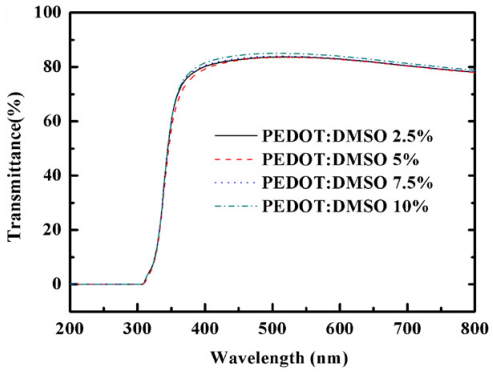

Figure 31: PEDOT:PSS transmittance with increasing DMSO concentrations

The deposition of PEDOT:PSS can be realized through spin coating, spray coating or printing techniques. A thermal annealing treatment can significantly affect the performance, in particular it has been studied that

the work function of PEDOT:PSS monotonically decreases with the annealing temperature without changing the ohmic nature of the contact [21]. The conductivity increases in a thermal range between 100°C and 200°C and decreases for values outside this range. Temperatures over 200°C generate over-oxidation and degradation of the polymer, while temperatures between 100°C and 200°C induce a benefic increase in oxidation state. Thermal annealing also affects the thickness of the PEDOT:PSS layer and the smoothness of its surface, being this latter fluctuating for annealing temperatures around 140°C and smoother above 200°C.

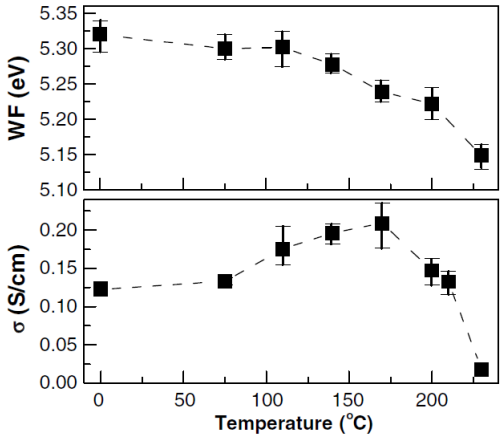

Figure 32: Work Function (WF) and conductivity (σ) of PEDOT:PSS with respect to annealing temperature [21]

2.2.4 The Organic Artificial Retina

The main topic of this thesis is the fabrication and the characterization of a silk-based organic artificial retina. The working principle of the device is based on the physics of organic polymers we reviewed in this chapter, with particular emphasis on the behavior of organic photodetectors. The device is composed of the following layers:

- Substrate: the purpose of this layer is to supply the mechanical structure of the device, since the photoactive polymers are liquid at room temperature and they must be deposited on a solid structure. The substrate determines the total flexibility and almost the total thickness of the device. It has to be a transparent material with a high degree of flexibility, biocompatibility and stability in ionic ambients. For this application, it was chosen a bombyx mori silk fibroin film whose characterization is discussed in Chapter 4 of this thesis;
- Photoactive layer: it is the layer in which photons are absorbed and the generated excitons are splitted into charged polarons. The material used for this purpose is a P3HT:PCBM bulk heterojunction;
- Electrodes: they are responsible for the charge collection from splitted excitons. The anode is a high-conductivity PEDOT:PSS mixture which in this application replaces the ITO, commonly used in most of organic photovoltaic devices. The cathode is a liquid electrolyte, more specifically the vitreous humor inside the eye;

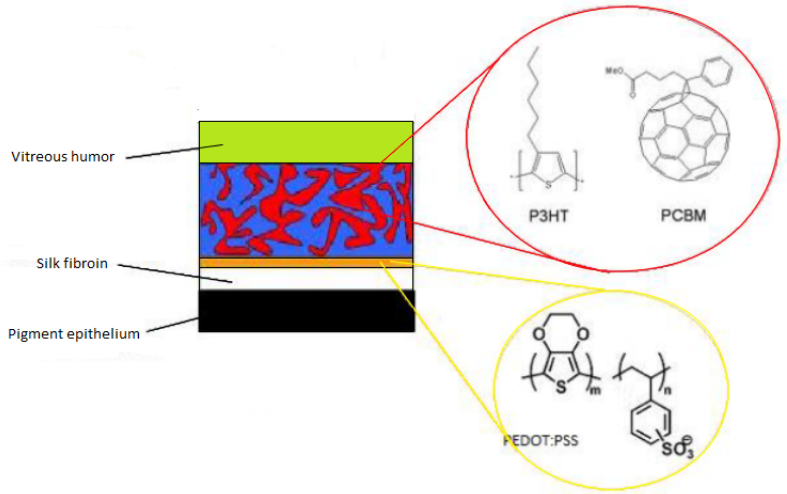

Figure 33: Overview of the device. The thicknesses are not scaled for the sake of readability

PEDOT:PSS can be deposited on silk through spin coating or spray coating (see Chapter 3) and it acts like a hole conductor. P3HT:PCBM is deposited on PEDOT:PSS through spin coating and works as an electron conductor. The energy diagram for the physical system is the following:

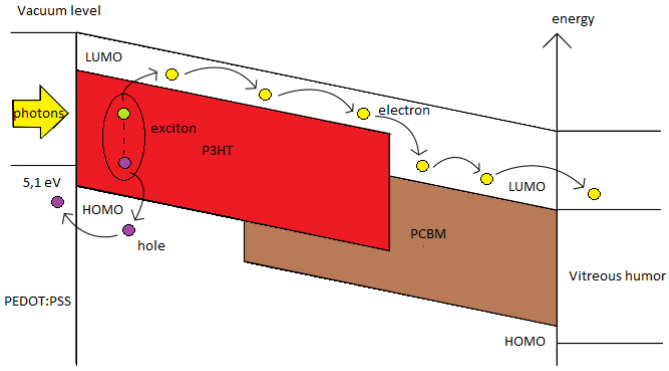

Figure 34: Energy diagram for the organic artificial retina

This device has a lot of advantages with respect to an inorganic artificial retina. First of all, it is a flexible device since its substrate, silk fibroin, is processed in order to be sufficiently malleable and well suited to work in aqueous environments. The flexibility is a great value in the process of the in-vivo implantation, and in its ability to adapt to the fundus oculi curvature. Secondly, the device is carbon-based and biocompatible in every layer. Moreover, the device has a virtually infinite resolution since both the absorption surface and the stimulating surface are continuous domains. However, in a practical analysis the resolution is limited by the resolution (density) of the bipolar cells which collect the transduced signal. Another great advantage lies in the absence of a power supply for the device. The energy needed for the functioning is simply the one carried by the incident photons, and this strongly limits overheating problems and heat-related necrosis to tissues. Finally, the output signal of the device has a ionic nature, hence a typical shape for the communication in biological systems. The disadvantages of this approach are the low quantum efficiency of organic devices, the absorption spectrum not entirely matched with the trichromatic nature of human vision, and a certain lack of information about the long-time stability of the implant in aggressive environments like physiological mediums. In chapter 3 it will be provided a detailed description of the fabrication process, while in chapter 4 it will be discussed the complete characterization of the device.

Bibliography

[1] Marcus, R.; "Electron Transfer Reactions in Chemistry: Theory and Experiment". Nobel Lecture, December 8, 1992.

[2] Klauk, H.; "Conducting Polymers for Carbon Electronics Themed Issue". Chem. Soc. Rev. 10.1039/b909902f.

[3] Perzon, E.; Wang, X.; Zhang, F.; Mammo, W.; Delgado, J.L.; Cruz, P.; Inganäs, O.; Langa, F.; Andersson, M.R. "Design, Synthesis and Properties of Low Band Gap Polyfluorenes for Photovoltaic Devices". Synthetic Metals 154 (2005) pp.53-56;

[4] Al-lbrahim, M.; Ambacher, O. "Effects of solvent and annealing on the improved performance of solar cells based on poly(3-hexylthiophene): Fullerene". Appl.Phys.Lett. 86 201120 (2005);

[5] Hoppe, H.; Sariciftci, N.S. "Organic solar cells: An overview". J.Mater.Res., Vol.19, No.7, Jul (2004);

[6] Mayer, A.C.; Scully, S.R.; Hardin, B.E.; Rowell, M.W.; McGehee, M.D. "Polymer-based solar cells". Materials today, Vol.10, No.11, Nov. (2007) pp.28-33;

[7] Vanlaeke, P.; Swinnen, A.; Haeldermans, I.; Vanhoyland, G.; Aernouts, T.; Cheyns, D.; Deibel, C.; D'Haen, J.; Heremans, P.; Poortmans, J.; Manca, J.V. "P3HT/PCBM bulk heterojunction solar cells: Relation between morphology and electro-optical characteristics". Solar Energy Materials & Solar Cells, 90 (2006), pp.2150-2158;

[8] Reyes-Reyes, M.; Kim, K; Carroll, D.L. "High-efficiency photovoltaic devices based on annealed poly(3-hexylthiophene) and 1-(3-methoxycarbonyl)-propyl-1-phenl-(6,6)C61 blends". Appl. Phys. Lett., 87 (2005) 083506;

[9] Poelking, C.; Daoulas, K.; Troisi, A.; Andrienko, D.; "Morphology and Charge Transport in P3HT: A Theorist's Perspective". Adv.Polym.Sci. DOI: 10.1007/12_2014_277. Springer-Verlag Berlin Heidelberg 2014;

[10] Shrotriya, V.; Ouyang, J.; Tseng, R.J.; Li, G.; Yang, Y., "Absorption spectra modification in poly(3-hexylthiophene) : methanofullerene blend thin films". Chemical Physics Letters 411 (2005) 138-143, Elsevier;

[11] Y. Kim, S.A. Choulis, J. Nelson, D.D.C. Bradley; " Device annealing effect in organic solar cells with blends of regioregular poly(3-hexylthiophene) and soluble fullerene" Appl. Phys. Lett. 86 (2005) 063502;

[12] D. Chirvase, J. Parisi, J.C. Hummelen, V. Dyakonov; "Influence of nanomorphology on the photovoltaic action of polymer–fullerene composites". Nanotechnology 15 (2004) 1317;

[13] Abe, T.; Ichikawa, M.; Hikage, T.; Kakuta, S.; Nagai, K.; "Relationship between the morphology of poly(3-hexylthiophene)/methanofullerene composite and its photoelectrode characteristics in the water phase". Chemical Physics Letters 549 (2012) 77-81, Elsevier.

[14] Clarke, T., M.; Durrant, J., R.; "Charge Photogeneration in Organic Solar Cells". Chem. Rev. 2010, 110, 6736-6767.

[15] Shukla, M.; Brahme, N.; Kher, R., S.; Khokhar, M., S., K.; "Elementary approach to calculate quantum efficiency of polymer light emitting diodes". Indian Journal of Pure & Applied Physics, Vol. 49, February 2011, pp.142-145.

[16] Kim, Y., H.; Sachse, C.; Machala, M., L.; May, C.; Müller-Meskamp, L.; Leo, K.; "Highly Conductive PEDOT:PSS Electrode with Optimized Solvent and Thermal Post-Treatment for ITO-Free Organic Solar Cells". Advanced Functional Materials, 2011, 21, 1076-1081.

[17] Peh, R., J.; Lu, Y.; Zhao, F.; Lee, C., K.; Kwan, W., L.; "Vacuum-freeprocessed transparent inverted organic solar cells with spray-coated PEDOT:PSS anode". Solar Energy Materials & Solar Cells, 95 (2011) 3579-3584.

[18] Xia, Y.; Ouyang, J.; "Significant Different Conductivities of the Two Grades of Poly(3,4- ethylenedioxythiophene):Poly(styrenesulfonate), Clevios P and Clevios PH1000, Arising from Different Molecular Weights". Applied Materials & Interfaces, 2012, 4, 4131-4140.

[19] Isaksson, J.; Kjäll, P.; Nilsson, D.; Robinson, N., D.; Berggren, M.; Richter-Dalfors, A.; "Electronic control of Ca2+ signalling in neuronal cells using an organic electronic ion pump". Nature Materials, 22 July 2007; doi:10.1038/nmat1963.

[20] Park, J.; Lee, A.; Yim, Y.; Han, E.; "Electrical and thermal properties of PEDOT:PSS films doped with carbon nanotubes". Synthetic Metals 161 (2011) 523–527.

[21] Kim, Y.; Ballantyne, A., M.; Nelson, J.; Bradley., D., C.; "Effects of thickness and thermal annealing of the PEDOT:PSS layer on the performance of polymer solar cells". Organic Electronics 10 (2009), 205-209, Elsevier.

[22] Lanzarini, E.; "Fotodiodi organici a catodo liquido". 2009.

[23] Bellani, S.; "Caratterizzazione chimico-fisica dell'interfase tra polimeri semiconduttori ed elettroliti salini per applicazioni energetiche e in campo biologico". 2011.

[24] Antognazza, M., R.; "Processi fondamentali della fotofisica dei semiconduttori organici: lo stato di tripletto". 2003.

[25] Grancini, G.; "Ultrafast Dynamics at Organic Interfaces for Photovoltaics". 2011.

[26] So, F.; "Organic Electronics: Materials, Processing, Devices and Applications". CRC Press, 2010.

[27] Lanzani, G.; "The Photophysics behind Photovoltaics and Photonics". Wiley-VCH, 2012.

Chapter 3

Methods and Materials

3.1 Silk Fibroin

As we discussed in the final part of chapter 2, the passive layer of the organic artificial retina is composed of silk, in particular a Bombyx Mori silk fibroin type. Silk is well known in literature for its biocompatibility thanks to its non-immunogenic response with respect to in-vivo implantations, its good mechanical properties, a good resistance to degradation, and the good tunability of its chemical/physical properties through chemical engineering and surface functionalization. The main applications for silk fibroin in material science field are the fabrication of hydrogels, suture materials, tubes, sponges, composites, fibers, microspheres and thin films [1].
A silk fiber is a polyamino acid-based fibrous protein composed by a crystalline part and minority amorphous structures. The morphology of silk has been studied using techniques as SEM, TEM and AFM, demonstrating that its nanostructures are arranged in oriented fibrils. These fibroin fibrils are surrounded by a sericin matrix which occupies 25-30% of the whole fiber [2]:

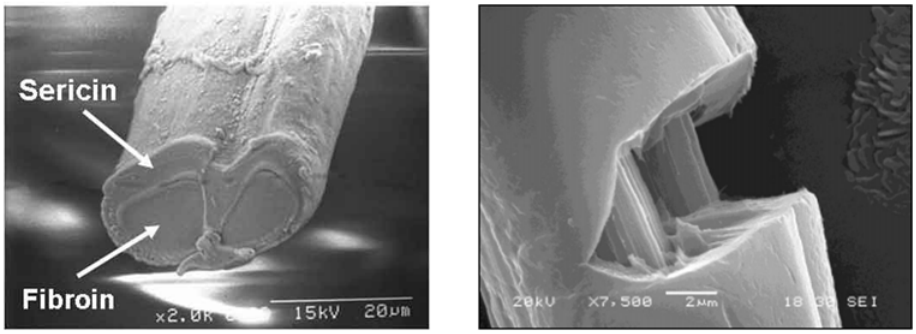

Figure 35: Silk fibroin structure

As depicted in figure 35, Bombyx Mori fibroin has heavy protein chains (molecular weight of 350 kDa) alternated with light chains (about to 26 kDa), linked by a covalent disulfide bond [2]. The crystalline component of the heavy chains consists of the repetitive hexameric units $(Gly\text{-}Ala)_n$ while the light chains consists of non-repeating amino acid units like tyrosine and valine, but its exact structure is not yet fully understood:

GAGAGSGAGAGSGAGAGSGAGAGSGAGAGSGAGAGYGAGVGVGYGAGYGAGAG
AGYGAGAGSGAASGAGAGSGAGAGSGAGAGSGAGAGSGAGAGSGAGAGSGAGA
GSGAGAGSGAGAGSGAGAGSGAGVGSGAGAGSGAGAGVGYGAGAGVGYGAGAG
SGAASGAGAGSGAGAGSGAGAGSGAGAGSGAGAGSGAGAGSGAGAGSGAGAGSG

Figure 36: Bombyx Mori silk fibroin acid sequence. The heavy chain is shown in red, while the light one is shown in black [2].

Natural unprocessed silk fiber are called “Silk I”, while heavy chains with conformation of an antiparallel β-sheet are commonly referred as “silk II” . This silk II conformation is considered to be the main factor responsible for the remarkable mechanical properties of fibroin. In fact, it is believed that the toughness of a silk fiber is superior to the Kevlar one [4]. “Silk III” is instead referred to the silk in proximity to the air water and/or organic-water interface, and it differs from the other silks because of the chemical reaction happening at the interface.
The processing of silk fibroin is a fascinating topic and, nowadays, the precise mechanism with whom Bombyx Mori or spiders are capable of producing it is not completely understood. In particular, there are several issues about the secretion, stabilization of large modular gene structures, and the determination of metabolic demands during production [4]. The synthetic processing of silk is bio-inspired, and its complete characterization for

the organic artificial retina application can be found in chapter 4 of this thesis. An important feature is that the sericin component of silk is not biocompatible with in-vivo environments, hence it must be removed and separated from fibroin (process called “degumming”). Sericin swells and dissolves in alkaline hot water, but water molecules produces a plasticizing effect also on fibroin as well, changing its mechanical properties [6]. Fibroin is mostly composed of hydrophobic chains but there is also an hydrophilic component located at the end chain terminus (and also in other random positions). That component is the one interacting with water. These interactions cause the increase of plastic deformation for the silk, and an increase in Young’s modulus. The macroscopic effect for prolonged exposition to water is an heavy pleating and the damaging of silk structures. The challenge in the silk processing is the developement of a silk film that has a good interaction with aqueous environments, and thanks to a fine tuning of the silk processing this can be achieved. In chapter 4 it will be discussed how using a Teflon petri for the solvent casting of a silk solution may increase the hydrobobicity of one film layer, and how the application of photoactive organic polymers on top of that layer increases the stability of the device in water. These polymeric layers act as a mechanical support for the whole structure and their natural hydrophobicity (expecially for P3HT/PCBM) limits water-induced damages to the silk substrate.

3.2 Setup for Polymer Preparation and Deposition

In this section, the full setup used for the preparation and deposition of PEDOT:PSS and P3HT/PCBM will be described. The preparation is realized by the use of pristine polymers, dopants and laboratory tools. The deposition is made using spin coating and a spray coating techniques. Finally, the samples undergo a thermal treatment inside a glove box.

3.2.1 Laboratory Tools

The main tools used for the preparation of samples are the following ones:

- Spatula: used for the polymer dosage;
- Tweezers: for the handling and repositioning of various materials;
- Precision balance: OHAUS (model dv215cd), with a resolution of 0,01 mg and standard deviation of 0,2 mg;
- Single-channel pipette: used for the dosage and withdrawal of liquid substances;
- Petri dishes: normal glass petri for general tasks, Teflon petri for the silk solvent casting;
- Nitrogen gun: for cleaning substrates and other laboratory tools. Also used to dry wet objects;
- Sonicator: Branson (model 2510). It consists in a chamber in which water is oscillating under a forcing sinusoidal mechanical wave. The ultrasounds generate a cavitation phenomenon, useful for cleaning substrates (included silk films) and for stirring polymeric solutions. The ultrasonic bath has a tunable temperature which depends on the application (usually between 20°C and 60°C);
- Nitrogen glove box: sealed chamber with controlled atmosphere. Used for the thermal annealing of P3HT/PCBM in low oxygen conditions;
- Thermal plate: used for the thermal annealing of polymers. Thermal annealing for P3HT/PCBM is carried out inside of glove box, while the one for PEDOT:PSS is outside it;
- Fume hood: a station under which managing all chemicals. It has a glass window in order to avoid eye contact with substances and an extractor fan which constantly draws chemical vapors;

3.2.2 Polymeric Materials

The two polymeric material used for the fabrication of the artificial retina are PEDOT:PSS and P3HT/PCBM:

- **PEDOT:PSS**: Clevios™ PH-1000 from Heraeus [8]. The Clevios™logo comprehends a family of polymers whose basic chemistry of the polimerization process is the following one:

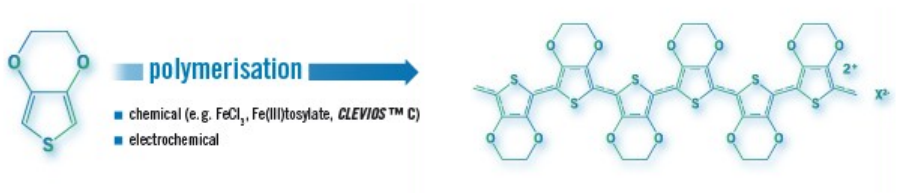

Figure 37: Clevios™ PEDOT:PSS

The technical specifications are shown in the datasheet:

	min.	max.	Unit
Physical Characteristics[1]			
Solid content	1.0	1.3	%
Specific conductivity*	850		S/cm
Viscosity	15	50	mPas
Technical Data (guide values, not a specification)			
Form		liquid	
Odour		odourless	
Colour		dark blue	
PEDOT:PSS ratio		1:2.5 (by weight)	
pH (at 20°C)		1.5 – 2.5	
Density (at 20°C)		1 g/cm^3	
Boiling Point		approx 100°C	

*After the addition of 5% Dimethyl sulfoxide. Measured on the dried coating.

Figure 38: PH 1000 datasheet

The initial choice was a IJ-1005 from Orgacon which had a very good conductivity but a bad viscosity and it was performing poorly during spray coating sessions. The choice of PH-1000 instead is justified by its good conductivity and its relatively low viscosity. The conductivity was measured for different kind of PEDOT:PSS with the Van Der Pauw method and the results were between 250-300 S/cm for PH 1000:

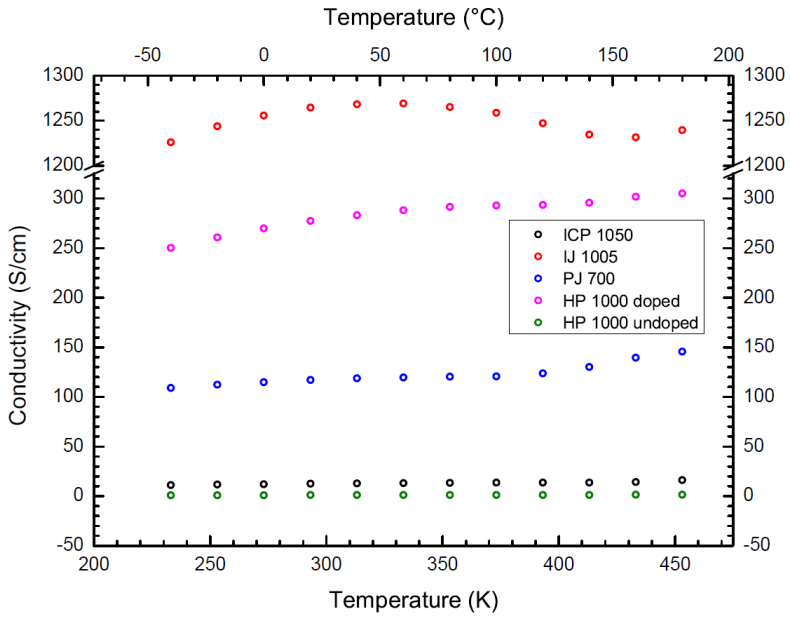

Figure 39: Conductivity of various PEDOT:PSS

PEDOT was doped with the addition of GOPS, DMSO and Zonyl (see chapter 4 for the exact ratio). DMSO is used in order to enhance the conductivity [9], GOPS decreases the PEDOT:PSS film solubility and Zonyl is a surfactant which decreases the polymer viscosity. The dopants were produced from Sigma-Aldrich.

- **P3HT**: regioregular Poly(3-hexylthiophene-2,5-diyl) from Sigma-Aldrich

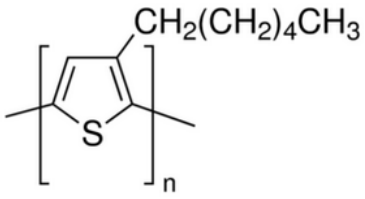

conductivity	~10^3 S/cm (when doped with iodine)
mp	238 °C
	238 °C
fluorescence	λ_{ex} 443 nm; λ_{em} 568 nm in chloroform
Orbital energy	HOMO 5 eV
	LUMO 3 eV
OPV Device Performance	ITO/NiO/P3HT/PC61BM/LiF/Al[2] • Short-circuit current density (J_{sc}): 11.3 mA/cm^2 • Open-circuit voltage (V_{oc}): 0.64 V • Fill Factor (FF): 0.69 • Power Conversion Efficiency (PCE): 5.16 %
	ITO/PEDOT:PSS/P3HT:PC61BM (1:08)/Al[3] • Short-circuit current density (J_{sc}): 9.5 mA/cm^2 • Open-circuit voltage (V_{oc}): 0.63 V • Fill Factor (FF): 0.68 • Power Conversion Efficiency (PCE): 5 %
semiconductor properties	P-type (mobility=1E-4-1E-1 cm^2/V·s)

Figure 40: P3HT datasheet

- **PCBM**: [6,6]-Phenyl C_{61} butyric acid methyl ester from Sigma-Aldrich

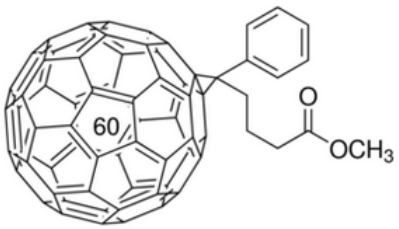

description	functionalized fullerene
assay	>99%
solubility	chlorobenzene: soluble
	organic solvents: soluble
	toluene: soluble
Orbital energy	HOMO 6.1 eV
	LUMO 3.7 eV
semiconductor properties	N-type (mobility=0.21 cm^2/V·s)

Figure 41: PCBM datasheet

3.2.3 Polymer Deposition

The methods chosen for polymer deposition are spin coating and spray coating:

- **Spin coating**: it is a deposition technique capable of deposing a thin film on top of a solid flat substrate. The thickness of the thin films ranges between few nanometers and tens of microns. The substrate dimension must be in the order of magnitude of $cm^2$and the thin film must be deposited from few µl of a highly volatile solution. A spin coater consists in a flat surface, the chuck, which rotates with known speed and acceleration. That rotating motion spreads the solution thanks to the centripetal acceleration. The rotation is also responsible for the solvent evaporation other than the spreading. The substrate is kept coupled with the chuck through the application of vacuum from a vacuum pump, and the suction force lasts for the whole deposition process. An example of a spin coater setup is depicted in the following figure:

Figure 42: Spin coater

The spin coating procedure can be described in four steps:

1. Deposition: firstly the solution is heated on a thermal plate at 50 °C. The substrate is then kept on top of the chuck by the vacuum pump. A certain volume of solution is poured on top of the substrate using a single-channel pipette. If the solution is deposed before the chuck starts rotating we talk about *static deposition*, otherwise it is a *dynamic deposition*. A static deposition is preferable for low viscosity solutions, and all the polymers used for the artificial retina fabrication are deposed under static conditions.

2. Spin up: in this step the chuck starts rotating at a desired speed and acceleration. The solvent immediately starts to evaporate but its distribution is not yet homogeneous because of its inertia. Once a good portion of solvent is evaporated, the solvent spreading wins the inertia and it starts following the substrate rotation. This step is the main one which determines the final thickness for the thin film. Of course the final thickness is also influenced by the initial volume of polymer, but for sufficiently long spinning time this contribute becomes negligible.

3. Spin off: this phase consists of the substrate acceleration in order to evaporate the remaining solution. The acceleration generates viscous forces responsible for the film thinning. Edge effects, that is the stockpile of material to the extremity of the substrate, can be minimized increasing the acceleration. Anyway, the central portion of substrate is the one with the most homogeneous polymer distribution and the minimum edge effect.

4. Evaporation: in this step the angular velocity is constant and the viscous forces overcome the centrifugal force. The final thickness of the device is set at the end of this phase. A final evaporation step can be performed on a thermal plate, often in conjunction with the thermal annealing process.

The deposition of P3HT/PCBM and of one layer of PEDOT:PSS are realized through spin coating. The spin coater used for the fabrication of the artificial retina is a model from Laurell Technologies.

- Spray coating: it is a deposition technique which deposes a thin film through the nebulization process of the solvent. It is optimal for the first PEDOT:PSS deposition on top of a silk substrate, because of the bad interaction between silk and water (PEDOT being water-based). The process does not require any kind of surface treatment apart from the normal substrate cleaning. For spray coating the wettability of the solution is essential to obtain high surface coverage and smooth film formation [10]. This can be achieved by the addition of a surfactant, Zonyl in the case of PEDOT:PSS deposition. When a solution is spray-coated on top of a substrate, the solvent nebulizes. Hence, it divides itself into many little droplets which reach the substrate and generate a thin film stockpiling on it. The spray coater realizes a nebulization by flowing an air stream at high speed into the solution, and letting it pass through a little opening. From a thermodynamic point of view, this is an adiabatic transformation. The droplets generated from nebulization have a certain diameter which is inversely proportional to the evaporation speed. This diameter directly influences the quality of the deposition and the film thickness. The substrate coverage, in fact, generates some gaps in the thin film due to the stochastic nature of the nebulization-generated filling. Droplet diameter, gap-free substrate coverage and solution wettability are intimately connected. An homogeneous coverage can be achieved using low surface tension liquids, high erogation pressures (being it inversely proportional to the droplet diameter) and an optimal erogation time. With good wetting conditions the droplet dries almost immediately after reaching the substrate, and the droplet stockpiling generates a “coffee stains” patterning:

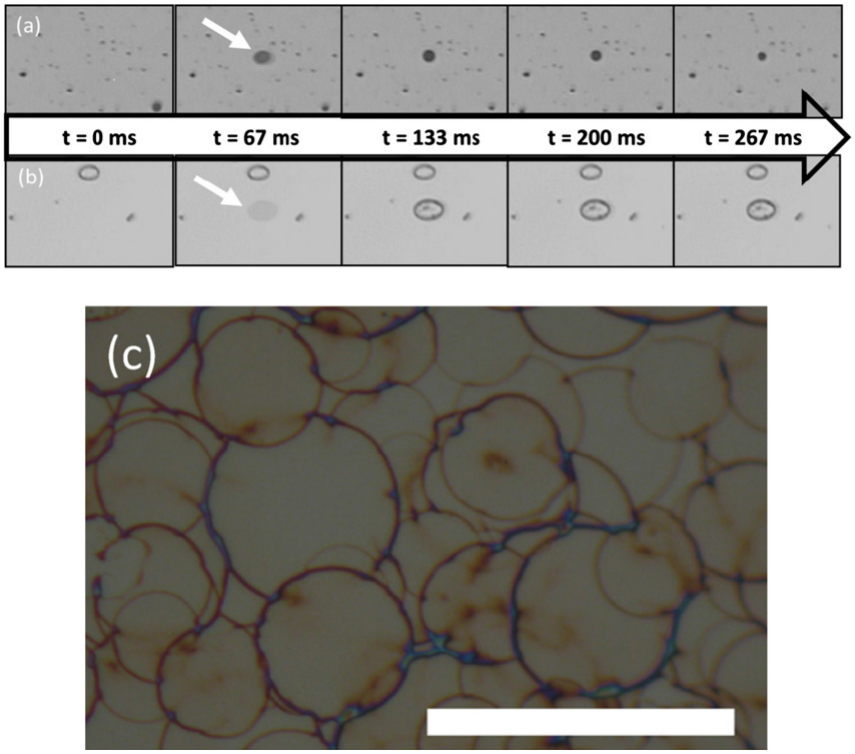

Figure 43: Optical microscope images of PEDOT:PSS spray-coated droplets. (a) PEDOT:PSS droplet did not wet the surface. The droplet shrunk as it was drying. (b) Favorable wetting of PEDOT:PSS , the droplet spread and almost dried immediately on impact. (c) Coffee stains patterning. The scale-bar represents 50 μm. [10].

Profilometry analyses show that the substrate coverage is not flat as the one achieved by a spin coating. Also, a gap-free homogeneous deposition usually implies high thicknesses, because the stochastic filling of the substrate can be optimized only by high deposition time. For these reasons, an optimal PEDOT:PSS deposition

can be achieved by a first spray coating step in which homogeneity is not important, and the purpose is to "prepare" the silk substrate to a second step of spin-coated PEDOT:PSS. This final step allows to control the thicknesses in a better way, and to achieve a good homogeneity without submitting the silk substrate to a direct contact with water.

The spray coater adopted for the first PEDOT:PSS deposition layer was an aerograph, connected to a gas compressor through a pipe. The systems works in a feedforward way, hence the erogated pressure is not finely tuned through any kind of feedback mechanism. Any turbulence generated by the intrinsic erogation process, or by any viscosity inhomogeneities, requires a manual correction of the erogation pressure. A rigorous study of spray coating optimization is described in chapter 4 of this thesis, as well as the characterization of a spray-coated PEDOT:PSS layer on top of a silk substrate.

3.3 Photocurrent Setup

The photocurrent setup described in this section was used in order to realize the electrical characterization of the artificial retina. The photocurrent measurement is based on a hybrid system in which the anode is the PEDOT:PSS film and the cathode is a saline solution. Samples are placed inside a cuvette in a vertical orientation, and the cuvette is filled with the solution letting dry only the upper part of the device. The saline solution has a concentration that can be quantified by its molarity, hence the number moles of solute per litre of solution. In order to achieve a desired molarity, a certain mass of salt must be weighted according to the following relationships, where m is the mass, MM is the molecular mass, n is the number of moles, V is the solvent volume and M is the molarity:

$$n = \frac{m}{MM}$$

$$M = \frac{n}{V}$$

The salts used for the artificial retina hybrid cathode are purchased from Sigma-Aldrich and they are pure at 99,5%. The weighted salt is put into a volume V of ultrapure water and the solution is left into a sonicator for a period of time between 30-60 min. After this ultrasonic bath the salt is completely dissolved into ultrapure water.
In order to measure a photocurrent, the hybrid system must have two electric contacts which enable an operational amplifier to close the circuit. One of the two contacts is a platinum wire immersed into the saline solution, with the only precaution of keeping it always separated from the artificial retina. Even the smallest contact, in fact, creates a short circuit and the amplifier cannot measure any photocurrent. Then, the upper portion of the platinum wire is clamped by a crocodile clip. The second contact must be created on the artificial retina. Since the contact has to reach the PEDOT:PSS anode, the upper portion of the device was treated with chlorobenzene (selectively removing the P3HT/PCBM blend). The contact is realized with a silver paste connection, which must not be in direct contact with the saline solution in order to avoid short circuits. An example of device/cuvette system is depicted in the following figure:

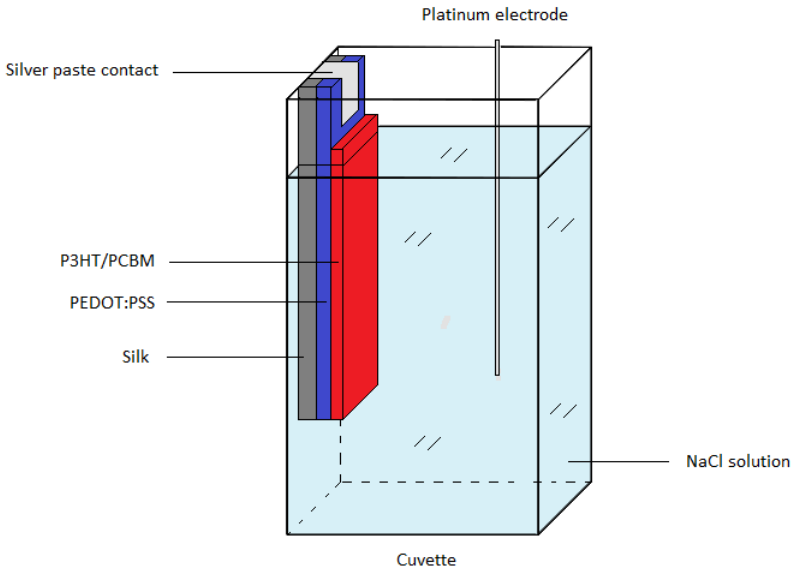

Figure 44: Device/cuvette system

The photocurrent setup consists of a device/cuvette system, a LED lamp, a lens system, a monochromator, a mechanial chopper and a lock-in amplifier. A schematic picture of the setup is shown below:

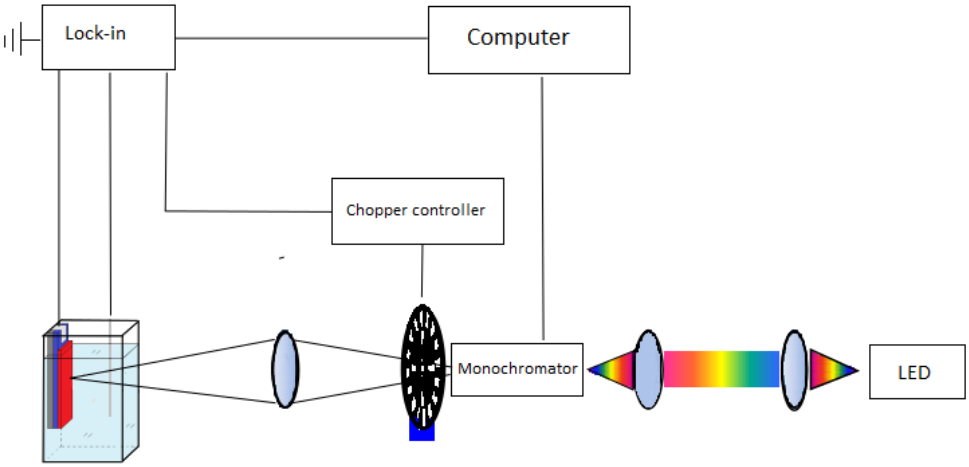

Figure 45: Photocurrent setup

The photocurrent measurement starts with the projection of photons from a LED device. Photons always strike the device from the solution side rather than the silk side (in order to avoid absorption phenomena). In order to reconstruct a photocurrent spectrum, the LED starts projecting from the infrared wavelength, continuously advancing towards the ultraviolet, and the photocurrent is measured step by step. The LED is excited with an electrical tension, whose amplitude and waveform determines the stimulation type. The model used is an ASB-W-030 from Spectral Products, a Tungsten alogen lamp emitting a divergent beam. The beam is firstly collimated and then focused towards the monochromator fissure using two lenses, both with focal length of 12,5 cm. The LED emission spectrum ranges from 300 to 2600 nm, and it can be measured by a calibration photodetector (a FDS100-CAL model from Thorlabs in this case). The photodetector responsivity has the following shape:

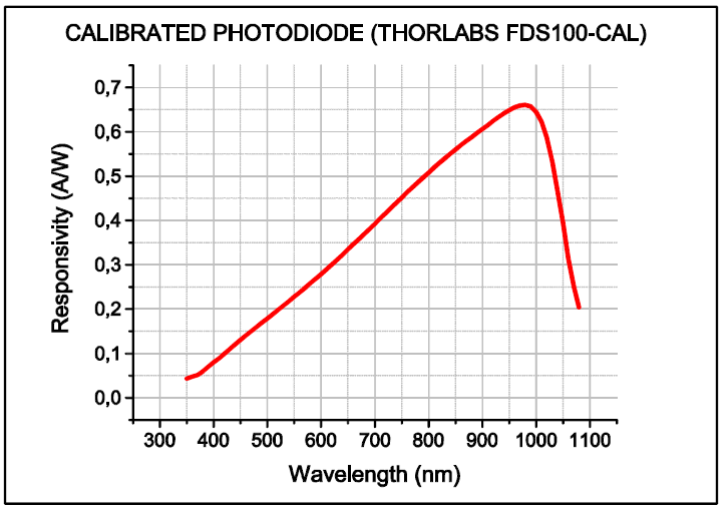

Figure 46: Photodetector responsivity

The optical power, instead, can be measured with an Optometer. An optometer is a device in which a photodetector is positioned inside an integrating sphere, that is an empty sphere with an internal surface which allows a total reflection of photons. The LED beam enters the sphere through a fissure, and the photons are trapped inside the sphere where the optical power can be measured. The sensitivity of this system is in the order of magnitude of μW. The knowledge of the LED optical power is important in order to calculate the quantum efficiency of the device.

A typical optical stimulation consists of a step signal (light off-on condition) or a square wave (ligth on-off-on-off-...- condition), and the choice depends on the desired frequency content with whom we want to excite the device. The LED radiation is filtered by a monochromator and then focused on the device using a plano-convex lens. The monochromator is a CM110-L model from Spectral Products, and its operating range is within 350-800 nm. Its working principle consists of the filtering of an input signal through a diffraction grating system. This system has fixed input/output fissures, selected at 0,6 mm, while the diffraction grating rotates with an angle proportional to the desired wavelength. Since the photocurrent acquisition is carried out by a lock-in amplifier, the input signal must undergo a frequency modulation from a mechanical chopper. A chopper is a rotating wheel with opened windows, positioned before or after the monochromator,which artificially induces a light-dark condition and, therefore, a modulation. At this point, the lock-in amplifier is fed by the photocurrent from the artificial retina. The lock-in amplifier is a correlation filter capable of extracting a signal modulated by a non-modulated noise and background [11]. It is commonly used in order to measure the amplitude of slowly varying signals. Its block diagram is depicted in the following figure:

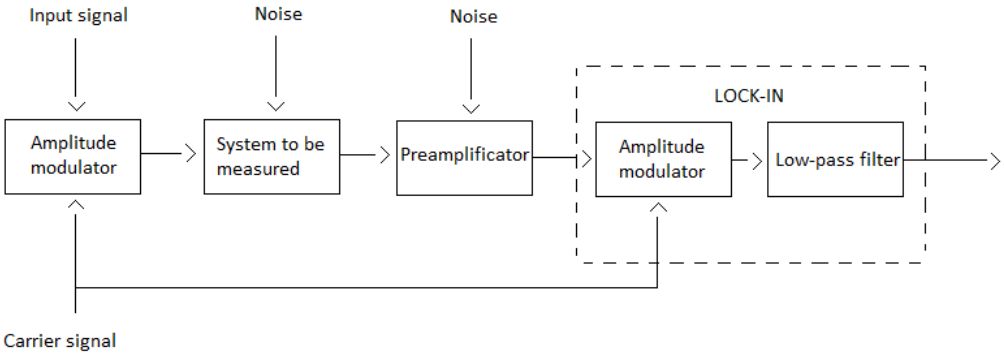

Figure 47: Lock-in amplifier block diagram [11]

Firstly, the input signal is used to modulate the amplitude of a carrier signal, and this is the reason why it has to have a low frequency content. The carrier is usually a periodic signal with a frequency much higher than the input signal one. Thanks to this modulation, the low frequency content of the input signal can be translated into the frequency range of the carrier signal. In our case, the modulation is made from the mechanical chopper which can rotate at a very high frequency, much higher than the LED signal one. If the modulation is carried out in an early stage of the acquisition system, possibly near the signal source, the probability to modulate also the noise component lowers. The preamplificator, then, amplifies the signal in order to prepare it for the lock-in filtering. The amplitude modulation comes really handy at this stage, because the preamplificator often introduces a 1/f noise component that is particularly high in the frequency range of the input signal. Once the signal is acquired from the lock-in, it is demodulated back in its original frequency content. The demodulation is performed by the same carrier applied to the input signal. However, the carrier undergoes now a different path and because of that its phase displacement must be measured and compensated. This operation can be performed by a phase controller (not depicted in the block diagram), before the demodulation process. Finally, a low-pass filter selects the bandwidth of interest, filtering the noise component at high frequencies. Details about the working principle of a lock-in amplifier can be found in [11].

3.4 Setup for Structural and Chemical Characterization

The structural and chemical characterization consists of profilometry measurements, optical imaging, SEM imaging, and contact angle analysis. The characterization is discussed in chapter 4, while the working principle of all the involved tools and devices will be described in this section.

3.4.1 Profilometry

Profilometry is a measuring technique aimed at quantifying the roughness and the waviness of a surface. The device used for this work is an Alpha-Step IQ model from KLA-Tencor. It is a contact profilometer in which a conical diamond stylus is moved both vertically and horizontally on top of a surface. These movements are capable of measuring small surface variation with a vertical sensitivity under 1 nm and a maximum excursion of 1mm, while the horizontal resolution is controlled by the scan speed and data sampling rate. Also, the force of the stylus can be selected and it ranges between 1 and 50 mg. As far as the physical quantities are concerned, a profilometer mainly measures the following quantities:

- Roughness: quantified by the deviations in the direction of the normal vector of a real surface from its ideal form. The concept of roughness is often used in mechanical engineering in order to study and control the friction between surfaces. In our case, however, it will be used in a static way quantifying the quality of interfaces between different layers of the artificial retina. The profilometer calculates the roughness as follows:

$$R_q = \sqrt{\frac{1}{n}\sum_{i=1}^{n} y_i^2}$$

where n is the total number of data points, y is the vertical position measure from the average surface height (which is assumed to be positive along the upward direction) and R is the roughness. Before using this formula, the raw data have to be low-pass filtered from the very high frequencies, being them related to vibrations or debris on the surface. Then, the signal is deprived of its baseline or "form", forcing it to oscillate around a constant mean line. This operation corresponds to a high-pass filtering with cutoff frequency equal to the baseline oscillation. The overall filtering process, therefore, consists of a band-pass filtering with cutoff frequencies established by the previous considerations. An example of roughness calculation is shown below:

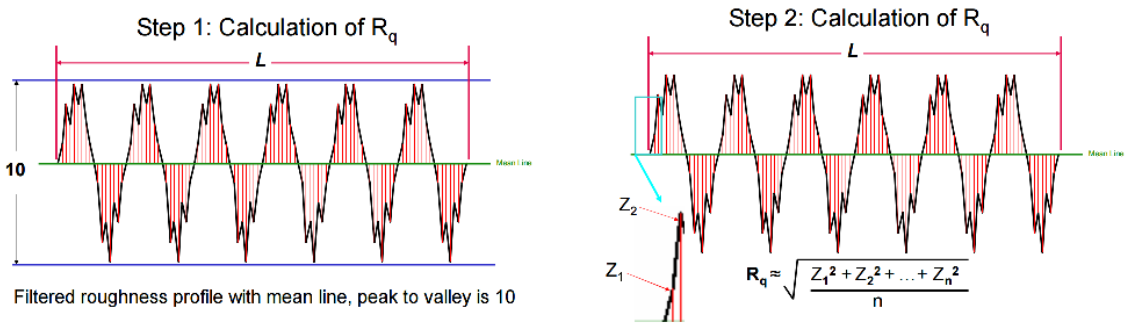

Figure 48: Example of roughness calculation (signal is aready filtered and deprived of its form) [12]

- Waviness: quantified as the more widely spaced component of a surface texture. The waviness calculation has not a default expression given in current ISO standards. It is derived from profilometer data with an operation of band-pass filtering, with the difference of the band being higher than the one for roughness measurement. This filtering is aimed at removing the surface oscillation, keeping only the slow baseline oscillation. A comparison between the band-pass bandwidth for roughness and waviness is depicted in the following chart:

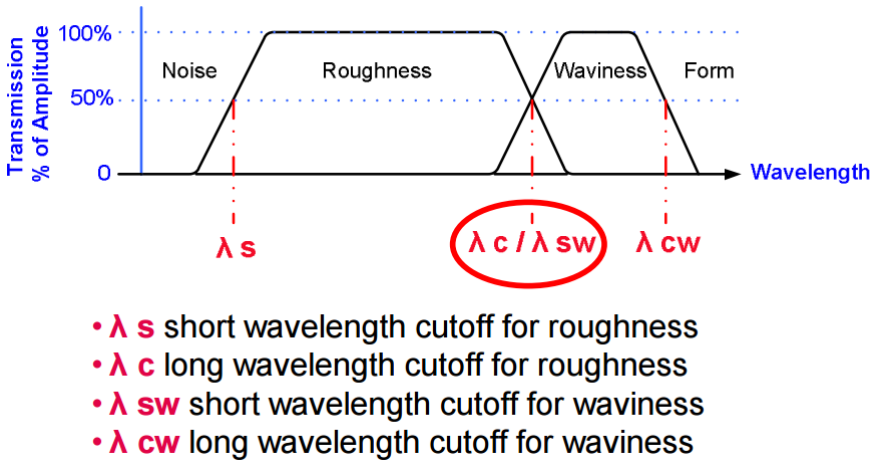

Figure 49: Different bandwidth for roughness and waviness measurement [12]

After the filtering process, the waviness is empirically determined as the maximum peak-to-valley distance in the signal:

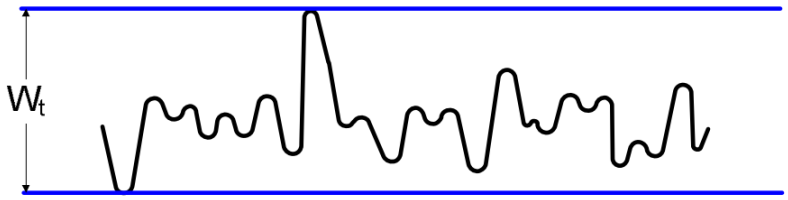

Figure 50: Waviness height [12]

A final example of roughness and waviness extraction from raw data is the following one:

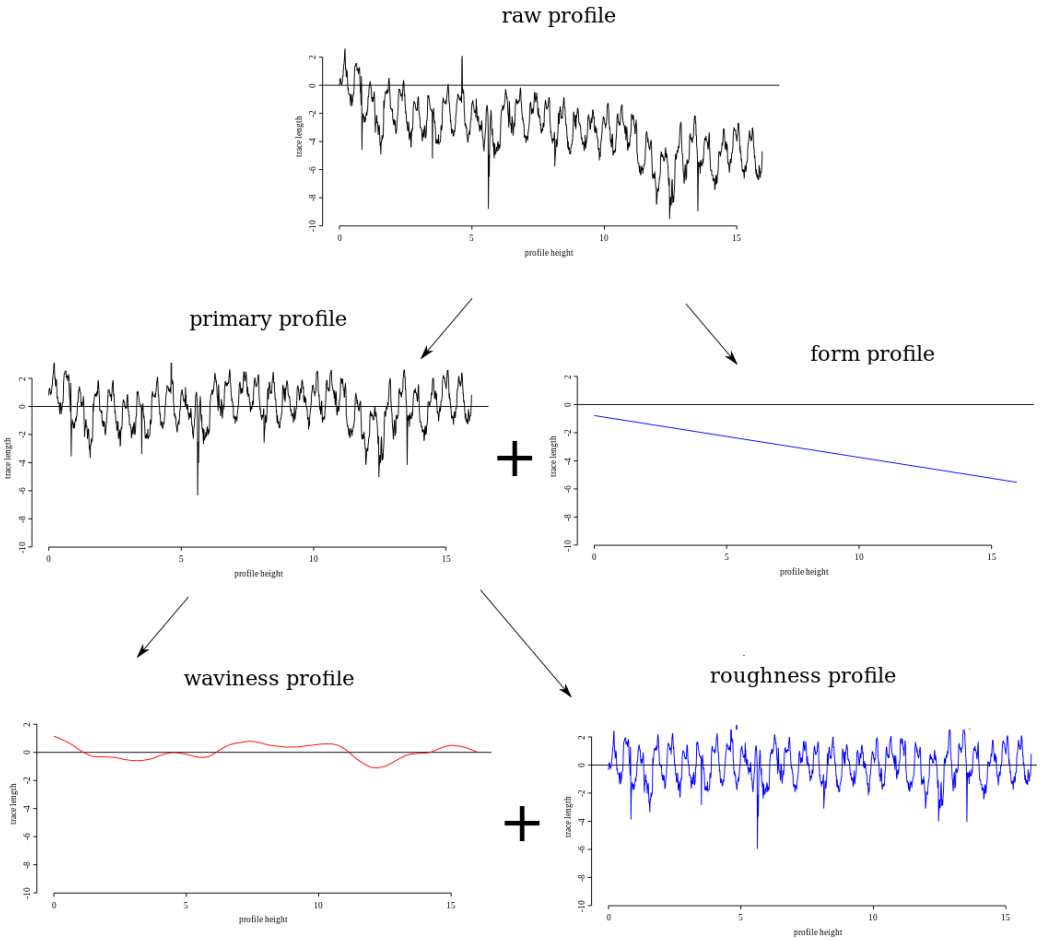

Figure 51: Roughness and waviness extraction from raw data

3.4.2 Contact Angle

Contact angle measurements are realized in order to characterize the hydrophobicity of a solid surface. The measurement technique consists of a water drop deposition, whose volume establishes the sensitivity of the process, on top of a solid surface to be characterized. An optical microscope, then, acquires the drop image from a perspective that is perpendicular to the normal vector of the surface. The image acquisition is supported by the application of a back light, which allows to create a strong contrast between the drop and the background. A processing software takes a snapshot of the image and the contact angle calculation is based on this static acquisition, because the water drop changes its shape and its physical properties through time. The image processing software determines the drop baseline, approximating it to a straight line, and the tangent line to the drop hemisphere. For materials with a high hydrophobicity coefficient the drop shape is more similar to an ellipse than a hemisphere, and the software is able to identify this difference and to adapt it to the elliptical geometry. In any case, the angle identified by the baseline and the tangent line is defined as the contact angle. The quality of measurement depends on the surface regularity (roughness and waviness), the water drop volume, and on the quality of the image processing. An example of a contact angle measurement setup is shown below:

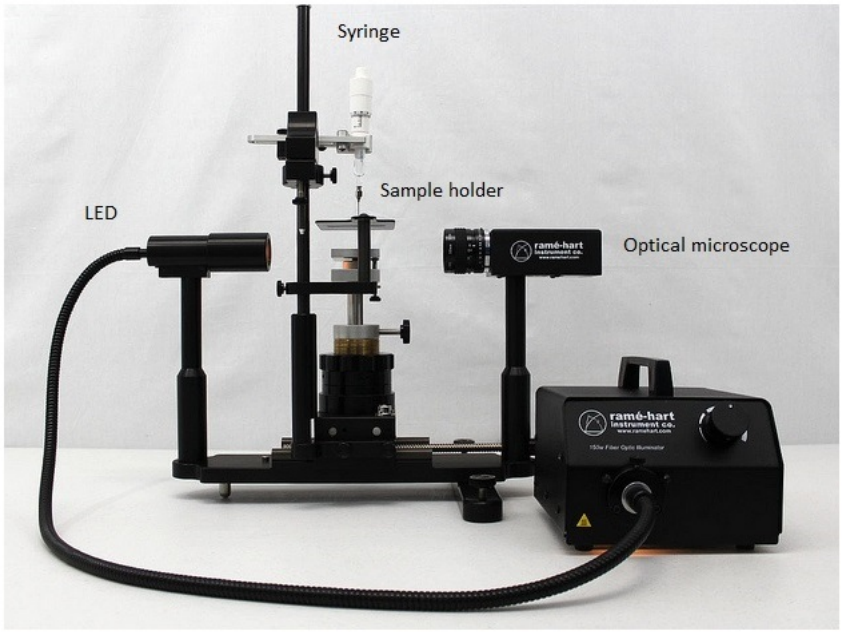

Figure 52: Example of contact angle measurement setup (from Ramè-hart instrument)

The water erogation from the syringe is activated by a robotic system which allows the deposition of drops in the microliter order of magnitude. A typical acquisition from a contact angle setup is depicted in the following figure:

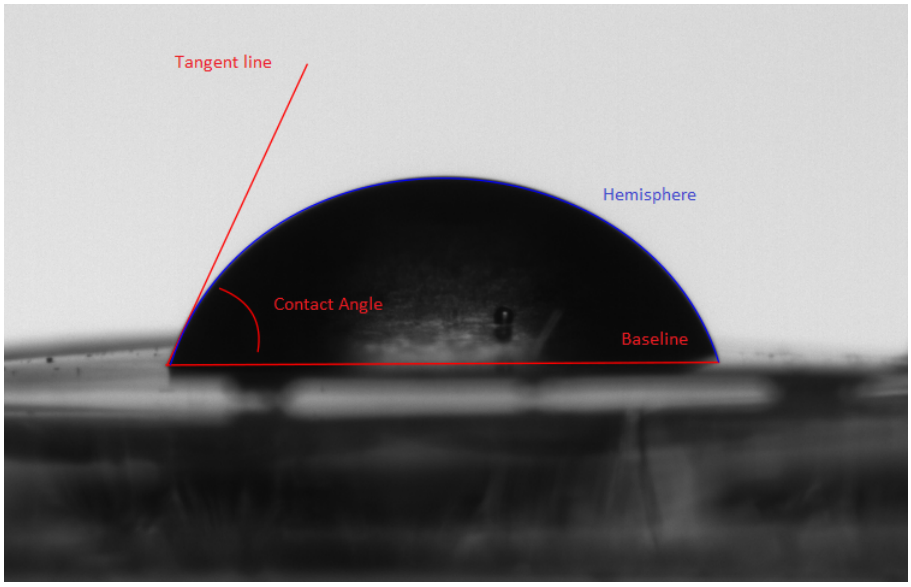

Figure 53: Contact angle acquisition

The shape of the water drop, and therefore its contact angle, give information about the surface hydrophobicity. If the surface has a high hydrophilicity coefficient, the water drop tends to flatten itself generating low contac angles. If the surface has a high hydrophobicity coefficient, instead, the drop assumes an elliptical profile because the repulsion from the surface tends to push away water molecules. This behaviour generates high contact angles that can also be higher than 90° (critical point in which an hemispheric profile becomes elliptical), like it happens for P3HT/PCBM surfaces. Details about the physics of liquid/vapor interfaces, contact angles calculation and hysteresis can be found in [13]. A deep analysis of contact angles for every surface of the artificial retina, instead, is carried out in chapter 4.

3.4.3 SEM Imaging

SEM (Scanning Electron Microscope) imaging is a microscopy technique aimed at scanning the structure of a material using a focused beam of electrons. When an electron beam strikes a material, the following physical phenomena happen:

- Transmission: the electron does not interact with the target material and it keeps its starting trajectory and energy;
- Fluorescence: the energy of the accelerated electron produces the emission of an electron belonging to an internal shell. An electron of a next shell takes the place of the ejected electron. The process produces a X photon of definite energy equal to the difference between the two energy levels:

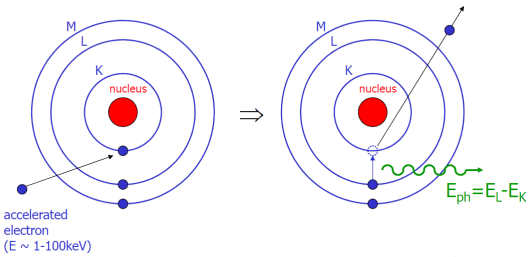

Figure 54: Fluorescence [14]

- Bremsstrahlung: produced when an electron changes its tangential velocity following the Coulombian interaction with the atomic nucleus. Larger the emission, more energetic the electron is. Also, the atomic number Z of the absorbing material proportionally increases. The energy emitted as X rays has a continuous spectrum from 0 to E_{max}(the kinetic energy of the incoming electron, in the case it is fully absorbed in the interaction):

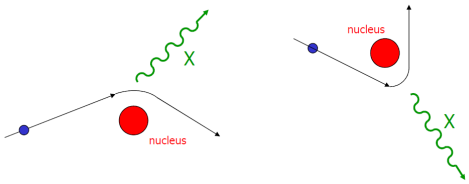

Figure 55: Bremsstrahlung [14]

- Elastic scattering (or Rutherford scattering): the incoming electron changes its trajectory without losing significant portion of its kinetic energy. Larger atoms (high atomic number Z) have a high probability of producing elastic collisions because of their greater cross-sectional area;

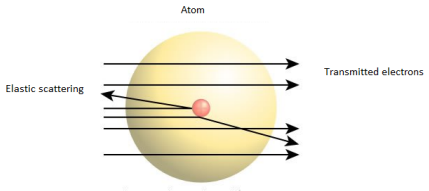

Figure 56: Elastic scattering

- Backscatter diffraction: accelerated electrons can be diffracted by atomic layers in crystalline materials. The detection of these electrons gives information about the crystalline structure and the crystallographic orientation of the target material. Diffraction happens because of the electron wave-particle duality;

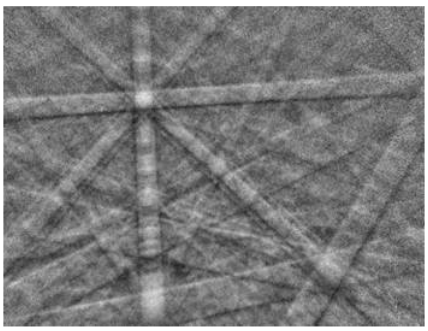

Figure 57: Example of diffraction grating

- Chatodoluminescence: physical phenomenon that happens when a high energy electron strikes a semiconductor. The energy of the incoming photon promotes electron from their valence band to the conduction band, leaving behind a hole. When electron and hole recombine there is a finite probability for a photon to be emitted. The energy of the emitted photon depends on the material, its purity, and its defect state;
- Heat release: the incoming electron loses its energy due to one of the aforementioned phenomena (elastic interactions excluded), and this energy is transformed into heat;

All these physical phenomena can be exploited in a SEM in order to achieve a microscopic image of the target material, and they are summarized below:

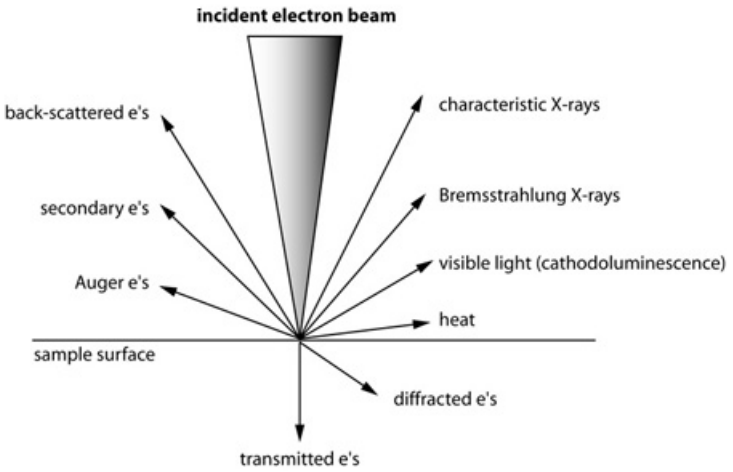

Figure 58: Summary of phisical phenomena happening in a SEM

A SEM machine is generally composed of an electron source, a sample hoder, detectors (X-ray detectors and secondary electron detectors), electron lenses and a display. Then, a series of other infrastructures and machines are necessary for its functioning, like a power supply, a vacuum system, a cooling system. a vibration-free floor and a shielded room. An example of an internal block scheme for a SEM machine is depicted below:

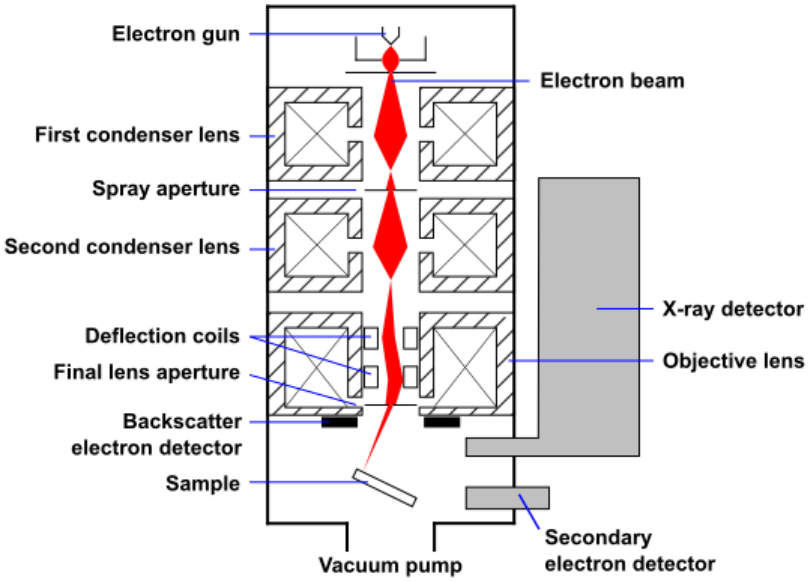

Figure 59: Internal block scheme of a SEM machine

The electron gun is capable of emitting electron beams generated by a thermoionic effect (with a Tungsten filament cathode). The energy of the beam usually ranges between 0,2 and 40 keV. After its generation, the electron beam is accelerated by the condenser lenses, while the deflection coils focus it towards the scanning point. When the beam strikes the sample, the aforementioned phenomena happen. The emission of secondary electrons is detected by a scintillator-photomultiplier system, while backscattered electrons are detected by dedicated scintillators. X-rays are usually detected by Gas detectors, but it is also possible to measure them with scintillators or direct semiconductor detectors (or a combination of these two). Every collected analogic signal is converted into digital, processed by an imaging software, and the image is then displayed and stored in a digital format.
In this work, SEM imaging is applied in order to characterize the quality of surfaces and interlayers of the materials which compose the artificial retina. The model used is a GeminiSEM from Zeiss:

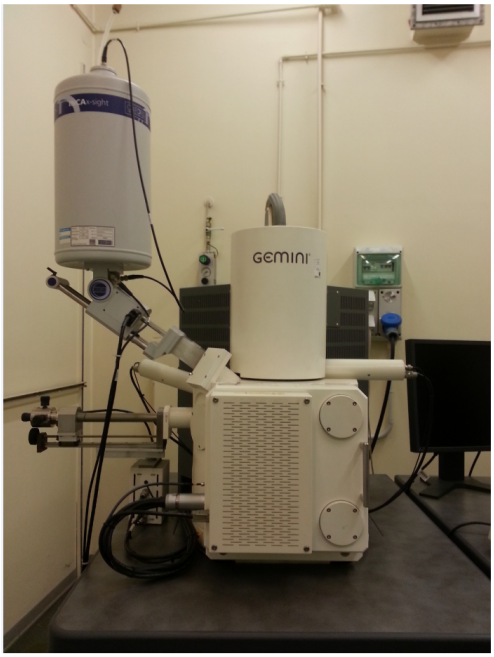

Figure 60: SEM model GeminiSEM from Zeiss, used for the artificial retina characterization

One of the biggest problem with SEM imaging of polymeric materials is their attitude to accumulate negative charges and consequently rejecting incident electrons for successive scans. Usually metals and some kind of semiconductor materials are capable of dispersing this charge, but this is not the case for polymers. In order to enhance the conductivity of the artificial retina before a SEM imaging process the devices were coated with silver paste. This guarantees an escape path for the electrons accumulated in the sample. Also, another defence mechanism against sample charging is to tilt them at a high angle relatively to the beam. This provides a more favourable geometry for the escape of secondary electrons (internally generated during the scanning) from the sample surface [15]. In order to acquire a section image of the artificial retina, which shows the thicknesses and the quality of every layer, the last requirement to fulfill is to perform a neat cut of the device. A neat cut is fundamental for the safeguard of every layer and interface, and it is the only technique that allows to see an uncorrupted image of the thicknesses. For this application it was chosen a liquid nitrogen-based neat cut. Details of the sample fabrication, preparation and measuring are explained in chapter 4. For a more detailed description of SEM imaging in general, instead, the interested reader can consult the chapter 3 bibiliography.

3.5 Laser Cut

Before their implantation into RCS rats, the artificial retina need to be cut and shaped into a particular geometry. The mechanical cut generates devices with sharp edges, which are not compatible with the implantation into test animals. In fact, sharp edges cause continuous micro-injury, bleeding, and the recurring renewal of fibrosis mechanisms. The laser cut, instead, produces smooth edges due to the vaporization effect and it leaves a high quality surface finish. The ablation processes can be distinguished in photolytic and pyrolytic. In photolytic processes, the most interesting ones for our application, the photon energy is directly applied to overcome the chemical bonding energy of macromolecules. In the case of polymers they are broken into smaller often gaseous monomer [18]. In particular, the UV photons are absorbed within a layer of about 0,2 μm and they cause the break of long chain molecules, which are then removed from the material in the form of vapor or small particles. A schematic of a laser beam cutting system is depicted below:

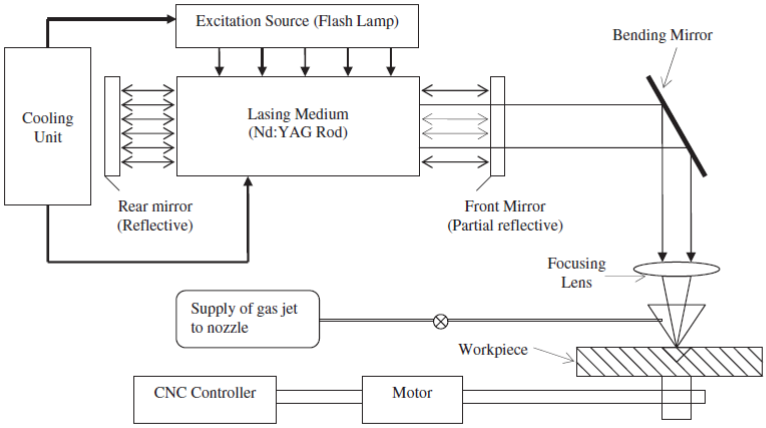

Figure 61: Schematic of a laser beam cutting system [19]

In a setup like that, the lasing material is stimulated by a flash lamp while a couple of mirrors (rear and front in the picture) reflect the light beams, until they become sufficiently energetic to leave the material in the form of coherent monochromatic light. Bending mirror and focusing lens direct the monochromatic beam towards the target sample. The supply gas unit is used in order to remove the leftover small particles or melted debris. Finally, a robotic holder moves the target sample according to a precise trajectory, which is responsible for the creation of a desired geometry in the cut.
The model of the laser cutting machine used in this work is a PHAROS laser from Light Conversion. It is a femtosecond laser system whose output parameters can be tuned by the software SCA (System Control Application).

Bibliography

[1] Rockwood, D., N.; Preda, R., C.; Yücel, T.; Wang, X.; Lovett, M., L.; Kaplan, D., L.; "Materials fabrication from Bombyx mori silk fibroin". Nature Protocols, Vol. 6 No. 10, 2011.

[2] Liu, X.; Zhang, K.; "Silk Fiber: Molecular Formation Mechanism, Structure-Property relationship and Advanced Applications". DOI: 10.5772/57611.

[3] Li, X.; Wu, L.; Huang, M.; Shao, H.; Hu, X.; "Conformational Transition and Liquid Crystalline State of Regenerated Silk Fibroin in Water". Biopolymers Volume 89, Number 6 (2007), DOI 10.1002/bip.20905.

[4] Omenetto, F., G.; Kaplan, D., L.; "New Opportunities for an Ancient Material". Science 329, 528 (2010), DOI: 10.1126/science.1188936.

[5] Lawrence, B., D.; Marchant, J., K.; Pindrus, M., A.; Omenetto, F., G.; a,c, Kaplan, D., L.; Silk film biomaterials for cornea tissue engineering". Biomaterials 30 (2009) 1299–1308.

[6] Lawrence, B., Wharram, S.; Kluge, J., A.; Leisk, G., G.; Omenetto, F., G.; Rosenblatt, M., I.; Kaplan, D., L.; "Effect of Hydration on Silk Film Material Properties". Macromol Biosci. 2010 Apr 8; 10(4): 393–403. DOI: 10.1002/mabi.200900294.

[7] Benfenati, V.; Stahl, K.; Gomis-Perez, C.; Toffanin, S.; Sagnella, A.; Torp, R.; Kaplan, D.; Ruani, G.; Omenetto, F., G.; Zamboni, R.; Muccini, M.; "Biofunctional Silk/Neuron Interfaces". Advanced Functional Materials (2012). DOI: 10.1002/adfm.201102310.

[8] Xia, Y.; Ouyang, J.; "Significant Different Conductivities of the Two Grades of Poly(3,4- ethylenedioxythiophene):Poly(styrenesulfonate), Clevios P and Clevios PH1000, Arising from Different Molecular Weights". dx.doi.org/10.1021/am300881m | ACS Appl. Mater. Interfaces 2012, 4, 4131−4140.

[9] Park, J.; Lee, A.; Yim, Y.; Han, E.; "Electrical and thermal properties of PEDOT:PSS films doped with carbon nanotubes". Synthetic Metals 161 (2011) 523–527.

[10] Peh, R., J.; Lu, Y.; Zhao, F.; Ken Lee, C.; Kwan, W., L.; "Vacuum-free processed transparent inverted organic solar cells with spray-coated PEDOT:PSS anode".

[11] Cova, S. "Appunti e Bibliografia per il corso di Sensori, Segnali e Rumore". Libreria Clup.

[12] MacKenzie, D.; "Surface Texture Measurement Fundamentals". Technical Seminar Metrology Center Open House, April 9-10, 2008.

[13] Kwok, D., Y.; Neumann, A., W.; "Contact Angle Measurement and Contact Angle Interpretation". Advances in Colloid and Interface Science, 81 (1999) 167-249, Elsevier.

[14] Fiorini, C.; "Electronic Design for Biomedical Instrumentation". Lez 14.

[15] Butler, J., H.; Joy, D., C.; Bradley, G., F.; Krause, S., J.; "Low-voltage scanning electron microscopy of polymers". Polymer vol. 36 No. 9, pp. 1781-1790, 1995. Elsevier Science Ltd.

[16] Joy, D., C.; "Scanning electron microscopy for materials characterization". Current Opinion in Solid State & Materials Science 1997, 2:465-458.

[17] Bogner, A.; Jouneau, P.-H.; Thollet, G.; Basset, D.; Gauthier, C.; "A history of scanning electron microscopy developments: Towards "wet-STEM" imaging". Science Direct, Micron 38 (2007), 390-401. Elsevier.

[18] Meijer, J.; "Laser Beam Machining (LBM), State of the Art and New Opportunities". Journal of Materials Processing Technology 149 (2004), 2-17. Elsevier.

[19] Dubey, A., K.; Yadava, V.; "Laser beam machining - A review". International Journal of Machine Tools & Manufacture 48 (2008) 609–628. Elsevier.

Chapter 4

Device Characterization

4.1 Silk Characterization

The organic artificial retina realized in this work is composed of several layers, each one responsible for different features of the device. In this section the silk fibroin layer will be analyzed, which is a passive layer defining the mechanical properties of the entire device. An important requirement of the passive layer is its optical transparency in the visible spectrum, since the incident photons must reach the active layer without being subjected to spectral distortion. The flexibility of the silk fibroin layer plays an important role during the surgical procedure of the implantation and for the device adaptability to the eye curvature. The complete characterization of the silk layer consists of the fabrication process description, the optical microscopy, the Scanning Electron Microscopy (SEM), and the contact angle analysis.

4.1.1 Fabrication Procedure of Silk Fibroin Films

- The starting point of the procedure is the cut of the Bombyx Mori cocooons and the disposal of the worm :

Figure 62: Bombyx Mori cocoons

- Degumming: the procedure of sericin removal from fibroin. The cocoons are placed in a becher with 40 ml of water per silk gram, and their immersion in water is kept with the application of some kind of weight. The becher is put into an autoclave, which has its serpentine completely covered with distilled water. The work cycle in the autoclave is 120°C for 30 min. After 30 min the autoclave proceeds to cool the cell down, and after it reaches 80°C the samples can be extracted. The remaining sericin is removed with the application of 5-6 washing cycles with water at 50-60 °C, until the water becomes transparent. The remaining fibroin is left to dry at ambient temperature, then the degummed cocoons are placed in a conditioned chamber (T = 20 ± 2 °C, U.R = 65 ± 2 %).

- Solubilization: silk fibroin is solubilized in a saturated solution of LiBr. Cocoons and LiBr are placed in a flask , with a weight/volume ratio of 1:10 g/ml. The flask, hermetically closed, is put into a thermostated bath at 60 ± 2 °C for 3 hours (with occasional shaking and venting). After 3 hours the solution of silk fibroin and LiBr is diluted with distilled water (inside the 60 °C bath) in a 1:50 g/ml ratio.

- Silk fibroin film preparation: once an homogeneous blend is obtained, the solution is filtered with a unit porosity filter and a water pump. Then, the solution undergoes a dialysis process in order to remove the salt, using preconditioned cellulose tubes (cut-off 12400 kDa). The tubes are immersed in bechers filled with distilled water under mechanical agitation, the water being renewed 10 times (roughly 3

times per day). The resulting dialyzed solution is composed by fibroin diluted in distilled water, with a concentration of 2% weight/volume, and it is filtered for a last time in order to remove possible solid traces from the unit porosity filtering. Finally the thin film is obtained from the deposition of 15 ml of the solution per Petri dish (diameter = 5,5 mm without plasma treatment in order to achieve a better interaction with cells), after two days of solvent casting.

- NB: the preconditioning of cellulose tubes is realized with their immersion in cold distilled water and their following heating up to 65-70 °C (not over 80°C). The operation is repeated twice, the last time with ultrapure water, and the tubes are left in ultrapure water until their use. The LiBr solution is prepared by solving 500 g of LiBr in 300 ml of distilled water, with gradual steps due to its exothermic nature. Once completely dissolved, the solution is placed into a dark glass bottle which is kept under cold water and shaked until the first crystals are formed. The bottle is then kept in a conditioned chamber (T = 20 ± 2 °C, U.R. = 65 ± 2 %). The regeneration of LiBr is achieved placing the LiBr bottle (with crystals) inside a thermostated bath at 60°C. Then, 5-10 ml of distilled water are added and once the crystals are dissolved, the bottle is held under cold water and shaked until the first crystals are formed. The bottle is kept in a conditioned chamber (T = 20 ± 2 °C, U.R. = 65 ± 2 %).

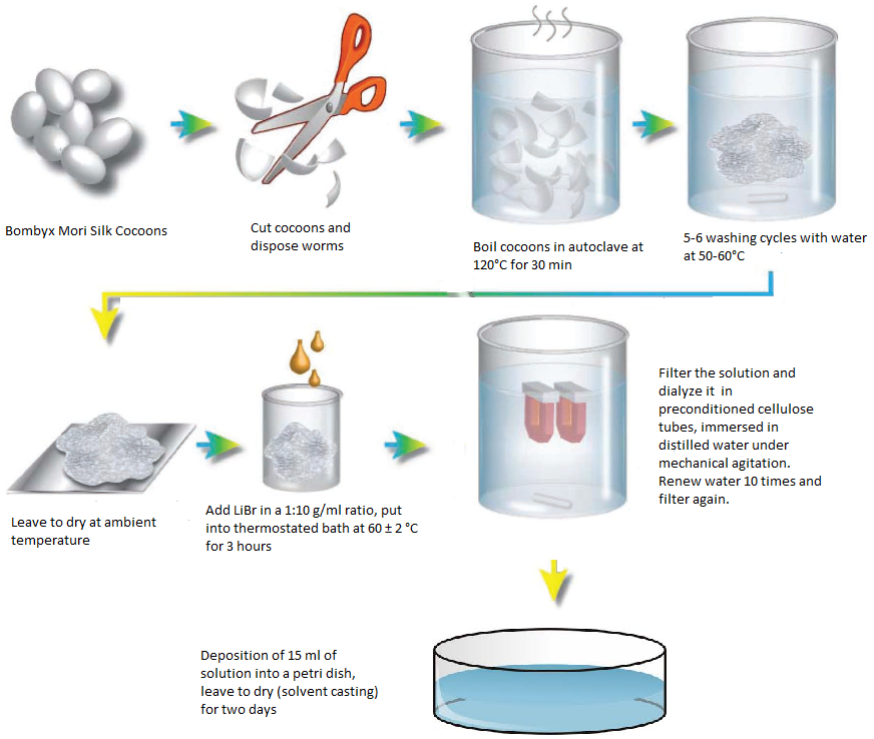

Figure 63: Summary of the silk films fabrication

At the end of the whole fabrication process, a silk fibroin film looks like this:

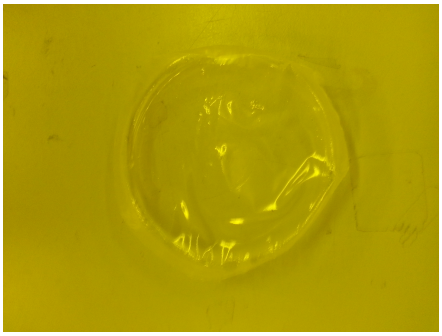

Figure 64: Final result of the silk fibroin film fabrication process

The main procedure for the fabrication of silk fibroin films can be slightly modified in order to tune different properties of the material, mainly its stiffness and its transparency. The choice of the optimal material led to three alternatives:

- Silk 1: Fibroin film obtained from water solution, treated for 20 hours at 105°C, with solvent casting on aluminum foil substrate. Very transparent, high flexibility but the immersion in aqueous environment makes the film too soft and malleable;
- Silk 2: Fibroin film obtained from water solution, treated for 20 hours at 105 °C, with solvent casting on Teflon film; Slightly opaque, it has medium flexibility outside aqueous environment but good flexibility inside;
- Silk 3: Fibroin film obtained from formic acid solution on Teflon film. Highly opaque, it shows a yellowish color because of the formic acid solution, and it is very stiff and fragile;

The comparison between the three film types shows that the silk 1 is significantly more hydrophilic than silk 2 and silk 3. The solvent casting on Teflon film generates a layer of the solution in contact with the Teflon and a layer in contact with the air. The Teflon side is basically inert, while the air side undergoes an oxidation process which increases the hydrophilicity of the layer. This difference in contact angles between the two different sides of the same film will be analyzed in the next paragraph. For now it is important to notice that silk 3 shows bad flexibility, it often cracks during its handling and it isn't totally transparent in the visible range. Silk 1 and 2 appear to be better materials for the substrate of an organic artificial retina, since they show a good mechanical behavior and adaptability in liquid environment (like could be the vitreous humor) and are almost completely transparent. The final choice for the substrate can be made performing a contact angle analysis, a rigorous study of the hydrophilicity of the film that is carried out in the next paragraph.

4.1.2 Contact Angle Analysis

The idea of a contact angle analysis was born from the observation of a high unrepeatability in mechanical properties of the organic artificial retinas. The fabrication process for the entire artificial retina, described in section 4.2, includes the deposition of organic polymers on top of the silk passive layer, hence the interaction of the silk film with liquid substances. The deposition of aqueous polymers like PEDOT:PSS on top of silk fibroin films showed very different behaviours, sometimes the film was very flat and regular and other times it was pleated and irregular. These observations suggested a difference in hydrophilicity between the two sides of a silk fibroin film, rather than a difference in hydrophilicity between different types of silks (mainly silk 1 and silk 2, the most suited for the application). As mentioned before, this difference is provoked by the solvent casting procedure, which intrinsecally has the two layers of the solution in contact with different mediums (substrate and air). The substrate can be more or less inert, Teflon being more inert than aluminum foil, while the air promotes oxidations and an increase in hydrophilicity. All these features are demonstrated by a rigorous study of contact angles for the silk fibroin film. The following measurement protocol was chosen in order to select the best silk type:

- measurements were performed on six samples, three silk 1 (from water solution on aluminum substrate) and three silk 2 (from water solution on Teflon substrate);
- the contact angle is measured three times for every sample in order to collect a statistic;

- the silk layer that was in contact with air during the solvent casting procedure will be called Top layer, while the silk layer in contact with the substrate will be called Bottom layer:

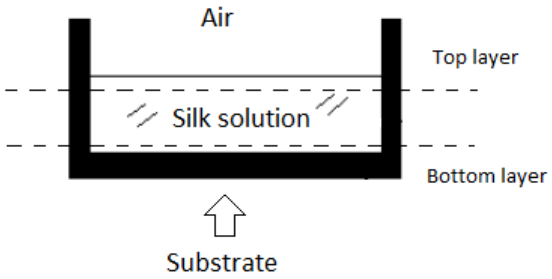

Figure 65: Definition of Top layer and Bottom layer

- measurements for Top layer and Bottom layer are realized from different pieces of the same sample, because of the degeneration effect that the water drop applies on silk;
- the resolution of the measurement is equal to the volume of the water drop, 4 μl in this experiment;
- silk samples are secured to the holder and they cannot move during the experiment;
- the contact angle is computed by an image processing software which works on a snapshot acquired immediately after the application of the water drop;

Measurements and snapshots are shown in Figure 66:

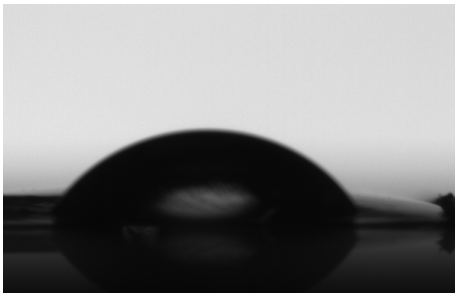

(a) Silk1 Top1: CA = 55,4 / 50,9 / 49,7

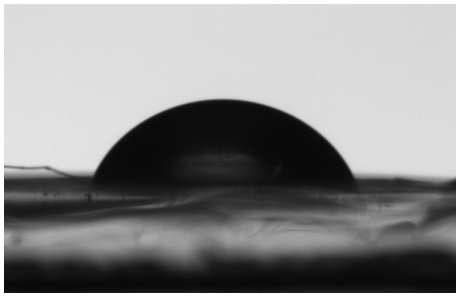

(b) Silk1 Bottom1: CA = 65,8 / 62,5 / 64,9

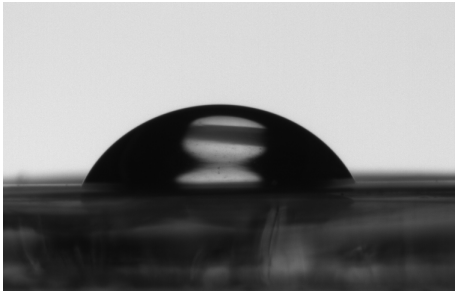

(c) Silk1 Top2: CA = 61,9 / 60 / 57,7

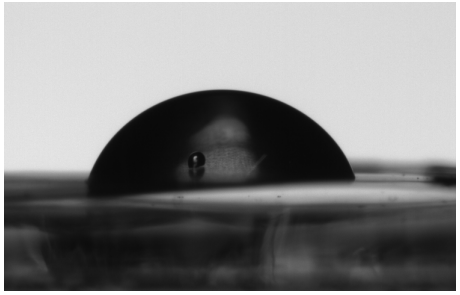

(d) Silk1 Bottom2: CA = 67,1 / 68,4 / 69,4

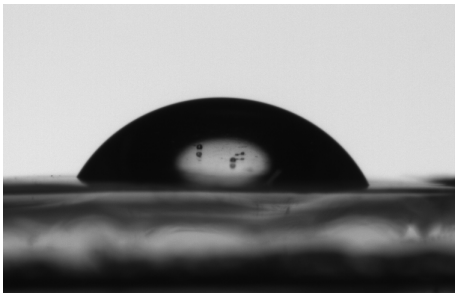

(e) Silk1 Top3: CA = 58,9 / 54,1 / 58,3

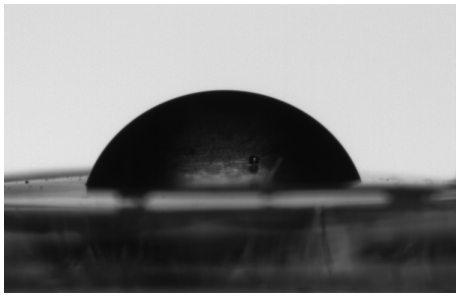

(f) Silk1 Bottom3: CA = 67,7 / 69,5 / 65,2

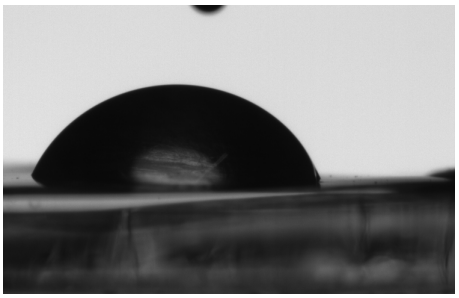

(g) Silk2 Top1: CA = 65,4 / 64,5 / 61,9

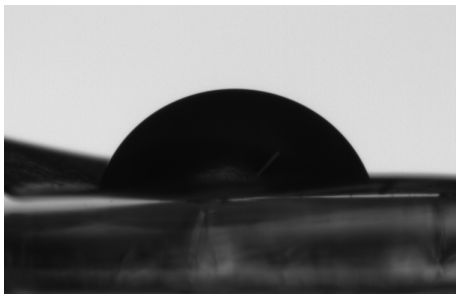

(h) Silk2 Bottom1: CA = 76,0 / 73,8 / 73,5

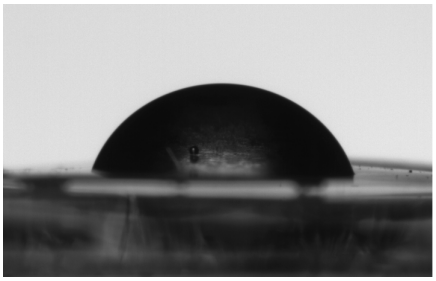

(i) Silk2 Top2: CA = 70,6 / 65,6 / 65,5

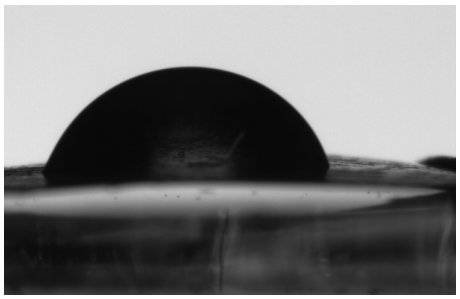

(j) Silk2 Bottom2: CA = 74,3 / 73,1 / 76,8

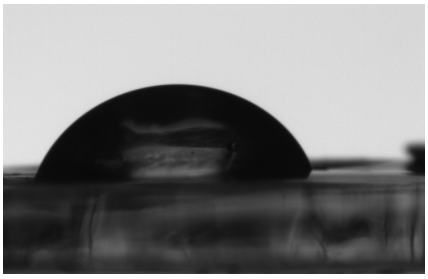

(k) Silk2 Top3: CA = 64,4 / 64,3 / 70,1

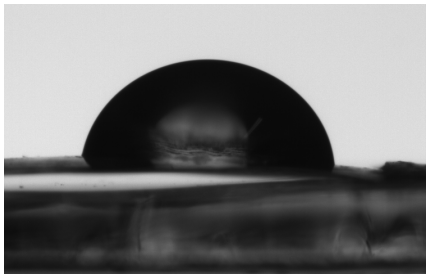

(l) Silk2 Bottom3: CA = 75,6 / 73,2 / 73,4

Figure 66: Contact Angle measurements

The results of the contact angle analysis show that the silk bottom layer is generally more hydrophobic than the top layer, because of the oxygen reaction we mentioned before. That difference in hydrophilicity is less pronounced for silk 2, being the Teflon substrate more inert than the aluminum foil one. Furthermore silk 2 is generally more hydrophobic than silk 1 for both top layer and bottom layer, once again because of the Teflon inertia. These features are summarized in the following graph, in which the mean contact angle (ϑ) is plotted with respect to the different silk types and layers (whiskers represent the standard deviation of the contact angle):

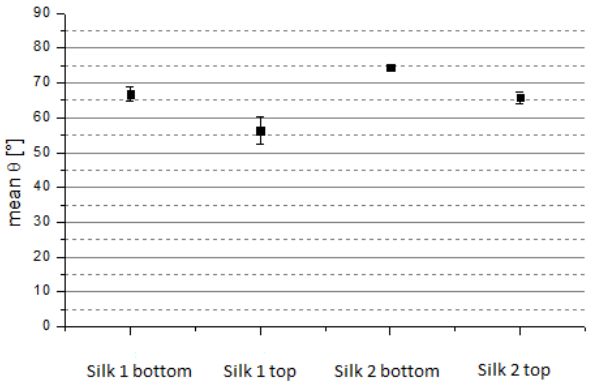

Figure 67: Statistical analysis of contact angles

At this point we have all the elements for the choice of the optimal silk. Considering that the silk layer must be in direct contact with the PEDOT:PSS layer, an aqueous organic polymer, and that the interaction between silk and water is rather destructive for the silk integrity and flatness, an hydrophobic material is more suitable. An hydrophobic material endures the spin coating of an aqueous polymer more than an hydrophilic one because, during the limited time in which the water touches the substrate before evaporating, the contact is less sticking. Last but not least, the hydrophobic silk shows better mechanical properties (mainly flexibility and manageability) when immersed in a liquid. Therefore, silk 2 is the elective material for this application, but that is not the only important result of the contact angle analysis. The other valuable information is that there is a preferential silk side on top of which the spin coating of PEDOT:PSS is optimal, that is the one we defined bottom layer (the hydrophobic one).

4.1.3 Structural and Chemical Characterization

A preliminary structural characterization for the silk fibroin can be realized through SEM imaging. This technique can show the quality of the fabrication process and can quantify the thickness of the film. A review of the working principle behind SEM imaging can be found in chapter 3 of this thesis. As far as the measurement protocol is concerned, every test sample must be electrically conductive and this can be achieved by covering the silk film with silver paste. Then, in order to acquire a good image of the film section, the silk film must be cut in a neat way. A liquid nitrogen cut was chosen for this application. In particular, the sample was immersed in liquid nitrogen for less than a minute and then the cut was realized using two metallic forceps. SEM images show thicknesses around 40 μm for silk films fabricated with the aforementioned protocol :

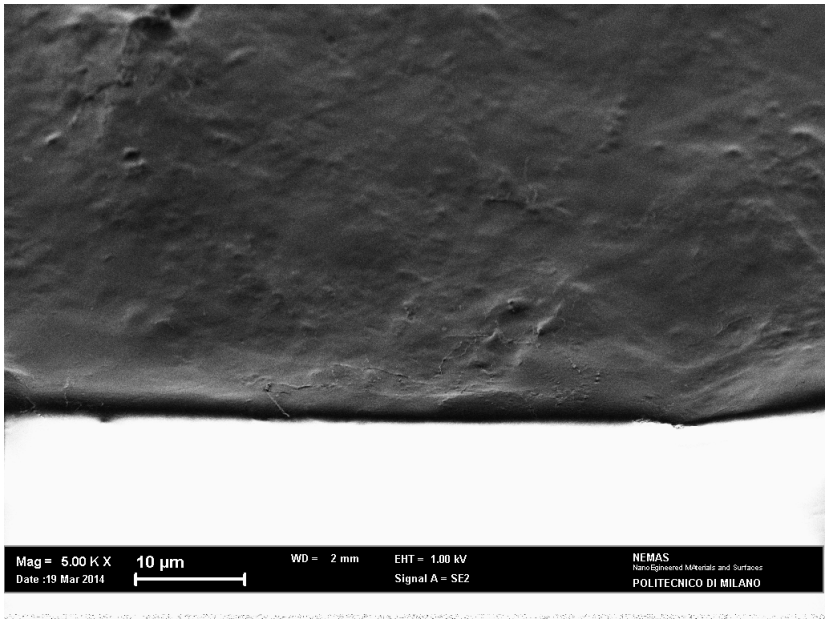

(a) Zoomed section

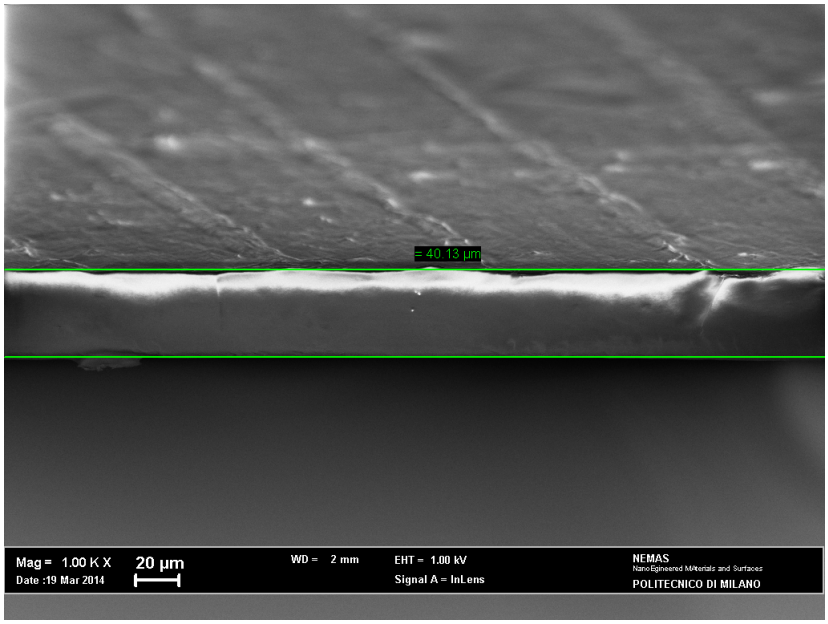

(b) Thickness of the silk film

Figure 68: SEM images of a silk film section

A SEM image of the silk surface shows a periodic circular patterning with a repetition period approximately

equal to 80 μm. This is probably caused by the solvent casting process:

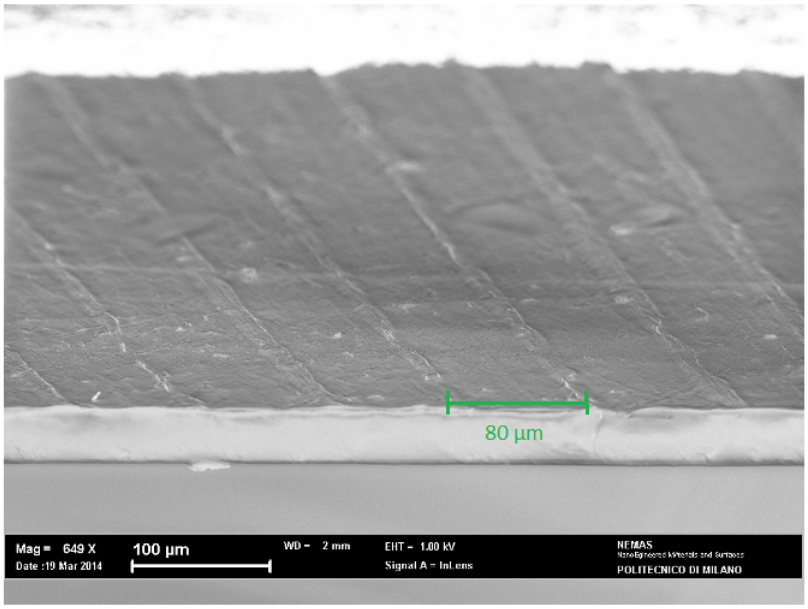

Figure 69: Silk surface patterning

An interesting structural and mechanical characterization could be realized by stress-strain tests. This kind of characterization can be useful in order to analyze the Young's modulus, the elastic limit, the breaking point and their variations with temperature. It could also be possible to study how the addition of PEDOT:PSS and P3HT/PCBM to the silk substrate modifies the aforementioned quantities. A stress-strain test, however, is really difficult to realize for our device. The material testing machine required samples with 7 cm x 1 cm dimensions, and a spin coating procedure on such a substrate generates highly variable results. Firstly, the device starts to bend itself under its own weight, and when the polymer is poured it is distributed in an anisotropic way. Furthermore, after the spin coating, the spinned material is layered with a space-variant thickness due to different evaporation gradients along it. As analyzed in chapter 3, during a spin coating process there are two forces in action, the centrifugal force and the viscous force. Long substrates have long radius and therefore small centrifugal forces located at the sample extremes, and this implies different evaporation mechanics during the spin coating. A device entirely realized through spray coating could satisfy the requirements for a stress-strain test, but the results would not be related to the artificial retina fabricated under our usual protocol. Despite these limitations, a stress-strain test still remains an important characterization tool that could be someway designed for future developments.

4.2 Polymeric Layer Characterization

In this section the deposition of the organic layers will be discussed, specifically for PEDOT:PSS (the anode of the organic photodetector) and for the P3HT:PCBM blend (the photoactive layer). The main deposition technique, spin coating and spray coating, are applied in order to stack the polymeric material on top of the silk substrate. The interfaces between each layer are analyzed through SEM images, and then the surfaces are characterized through optical microscopy, profilometry and SEM.

4.2.1 PEDOT:PSS Deposition

The first step of the polymer deposition is the silk substrate cleaning. This is carried out with an ultrasonic bath firstly into acetone and then into isopropanol. Poly(3,4-ethylenedioxythiophene) and sodium polystyrene sulfonate, or PEDOT:PSS, is the first polymeric layer that is deposed on top of the silk layer. Before its deposition the polymer is doped with the addition of DMSO, Zonyl and GOPS (details about PEDOT:PSS and its additives can be found in section 2.2.3 of this thesis or in the relative bibliography). Studies of the literature and analysis of the optimal conductivity for the polymer led to the following doping ratio: 10% DMSO, 1% GOPS, 0,2% zonyl (percentages of the total volume). For example, 10 ml of PEDOT:PSS are doped with 1ml of DMSO, 100 μl of GOPS and 20 μl of zonyl. The deposition of the polymer can be made with several techniques but in this work we will analyze only the spray coating and the spin coating ones, those being the most suitable for the application:

- **Spray coating**: this is the elective technique in order to deposit PEDOT:PSS on top of a silk film. As analyzed in chapter 3, the nebulization phenomenon allows the deposition of PEDOT:PSS droplets minimizing the amount of solvent deposition (water), on condition that the spray coating session is carried out at a certain distance between spray gun and target. Nebulization is a key factor because of the bad interaction between water and silk. The limits of this technique are the long duration of the spray deposition, incompatible with a mass production of device without having an appropriate facility, and the low conductivity of the pedot layer so obtained. In order to achieve stability and repeatability in the device fabrication, a deposition protocol must be established. For a spray coating session there are three main control parameters responsible for the final output of the deposition, that are the distance between spray gun and target, the time duration of spray coating and the pressure at which the spray is dispensed. We know from literature that there is an optimal spray distance, under which the nebulization process does not come into play (or comes in a minor extent) and above which both polymer conductivity and time length of the spray session are unacceptable. For the deposition of PEDOT:PSS on top of a silk film that distance is about 10 cm, because shorter distances caused a remarkable degradation of the silk substrate and higher ones produced low conductivity devices with huge deposition timings. The time length of the spray coating is chosen around 10 minutes, because shorter sessions lead to low conductivity depositions and longer sessions can produce thick films and an increase in resistivity. Moreover, long spray sessions are not suitable for a mass production of devices, and the mass production (around 100 samples) is fundamental for the implantation in test animals. Some numbers relating to this process are the following: for 30 seconds of spray coating it is achieved a pedot film with a thickness between 100 and 200 nm, while for 15 minutes the thickness can increase up to 1 μm. As far as the erogation pressure is concerned, the spray gun (an aerograph) introduces a limitation to the 1-2 bar range. Under 1 bar the pedot distribution is simply too feeble and over 2 bar turbulence phenomena are very frequent, and they heavily disrupt stability and repeatability of the process. In order to choose an optimal pressure, a profilometry study of the deposited PEDOT:PSS surface was carried out. Mean thickness and roughness were measured for two silk films, one coated with a pressure of 1,5 bar and the other with a pressure of 2 bar. The two samples were kept steady and stable between two laboratory slides during the whole coating process. Finally, the coating was applied to the silk bottom layer, being it the most hydrophobic side of the silk film (as discussed before). After the spray coating, a thermal annealing for 5 minutes at 120 °C under normal air atmospheric conditions was performed. The profilometry analysis was realized on the laboratory slides rather than on the silk coated samples, because they were subject to the same PEDOT:PSS flux but the glass flatness does not corrupt the measures like a highly irregular silk surface would. The difference of regularity between a glass covered surface and a silk covered surface can be enlightened with optical microscopy images:

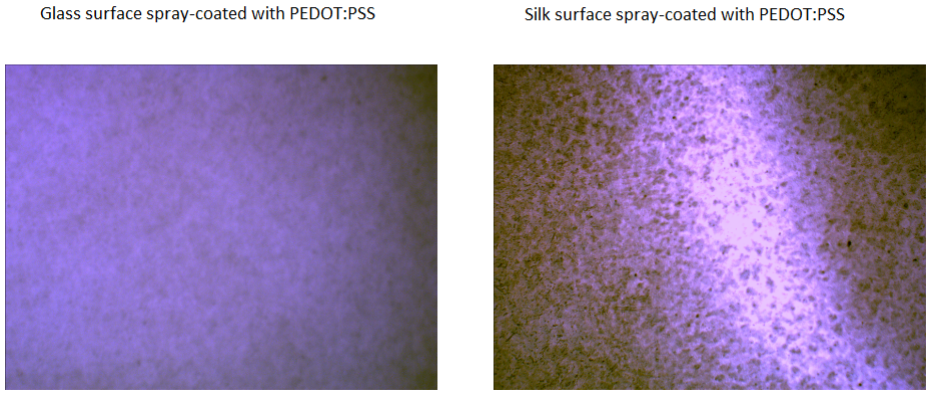

Figure 70: Difference between a glass covered surface and a silk covered surface, shown with optical microscopy

Measurements of roughness were performed three times in different sites, for both samples, in order to collect some statistics. The results of the profilometer analysis are shown in figure 71:

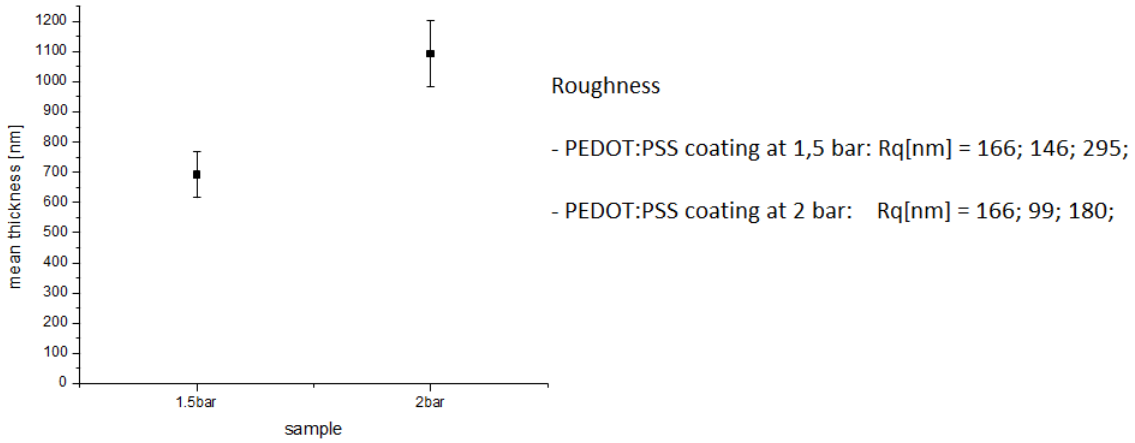

Figure 71: Profilometry of spray-coated PEDOT:PSS on a silk film, performed at 1,5 bar and 2 bar

Higher spray coating pressures generate higher thicknesses than low pressures, but also more variance and therefore less homogeneity. The roughness instead shows better flatness for high pressures, because of an increased efficiency in filling the gaps. The optimal pressure seems to be 1,5 bar because of the reduced variance and of the lower thickness, which imply a lower resistivity. The definitive spray coating protocol is therefore a deposition session performed at 10 cm of distance, for 15 minutes at 1,5 bar, on top of the silk bottom layer, followed by a thermal annealing for 5 minutes at 120 °C in air. Under these conditions we can apply the spray coating procedure to every silk type we analyzed before (silk 1, silk 2 and silk 3), and measure the mean thickness in order to further examine the effect of PEDOT:PSS on the substrates. Being profilometry measurements very variable, because of the low repeatability of a spray coating session and of the intrinsic silk irregularity, the analysis was performed on top of two sample batches fabricated in two different sessions. The following chart shows the mean thicknesses of PEDOT:PSS spray coated on top of the three different silk types:

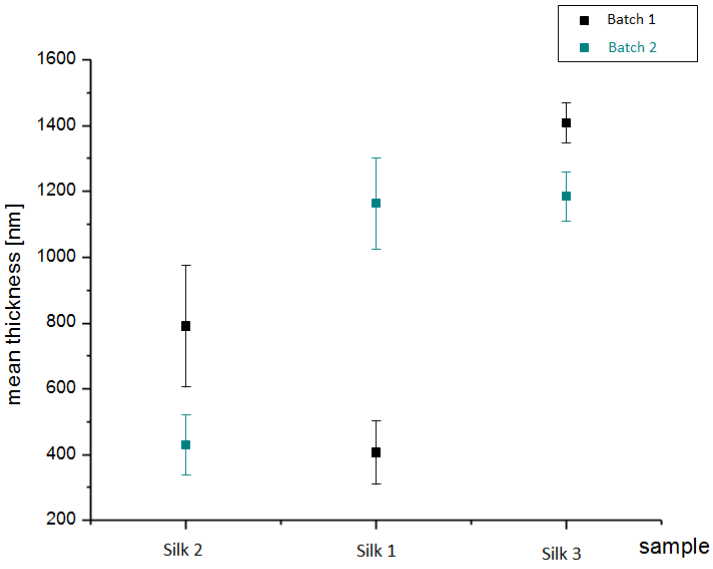

Figure 72: Profilometry of spray-coated PEDOT-PSS on three different silk films

Silk 3 is very flat but very thick, hence being very resistive. Silk 1 shows a huge difference between the two batches, because its highest hydrophilicity makes it very uncomfortable with the deposition of water droplets. Silk 2 has the lowest thickness and a good repeatability inter-samples (even if a mediocre repeatability intra-samples), proving once again to be the optimal choice.

- **Spin coating**: it is a quicker deposition than the spray coating one, and the whole deposition process can be finely tuned and controlled. Details on the spin coating process can be consulted in chapter 3 of this thesis. The big downside of this technique is the initial contact between the silk layer and the PEDOT:PSS solution, a contact that can produce heavy damages to the silk integrity and flatness if the chuck rotation does not start almost immediately. Despite this disadvantage, the spin coating is still the way to go in order to fabricate an high number of devices destined to the implantation in test animals. This is true because of the difference in repeatability between samples that are fabricated within a prolonged time lapse. Also in this case we need to establish a deposition protocol to be repeated for every coating session. This protocol consists in the deposition of PEDOT:PSS on top of the silk bottom layer, performed at 2000 rpm for 1 minute. These numbers were already discussed in the PEDOT literature and they produce the best thickness/conductivity ratio. The thermal annealing process is the same as in the spray coating procedure, that is 5 minutes at 120 °C under normal air atmospheric conditions. Once again it has to be stressed the importance of the limited interval between the pedot deposition and the start of the spin coating, the pedot solution (and particularly its solvent, water) has to be in contact with the silk surface for the shortest possible time.

The characterization for PEDOT:PSS showed that the spray coating technique is well suited in order to preserve the silk integrity during the deposition process. Low conductivity issues and the time consuming nature of the fabrication, hence the low repeatability between samples of the same batch as discussed before, limit its application for a mass-production. Spin coating instead is very repeatable and fast but also very harmful for the silk integrity. The state of the art deposition technique, for this application, would be a combination of the two coatings. A first spray-coating layer, very thin and therefore less time consuming, can be applied in order to prepare the sample for a safer spin coating session. After the initial spray coating, the spin coating is performed with the pedot solution going on top of another pedot layer, already dried, acting as a protecting layer. A typical deposition protocol could be the following one: spray coating at 10 cm of distance, for 10 minutes, at 1,5 bar, followed by a thermal annealing at 120 °C for 5 minutes in air. Then, a spin coating for 1 minute at 2000 rpm, followed by another thermal annealing at the same conditions as before. We have now a pedot layer that is sufficiently flat and conductive. An optical microscopy analysis can show the different effect that the two techniques have on the underlying silk layer:

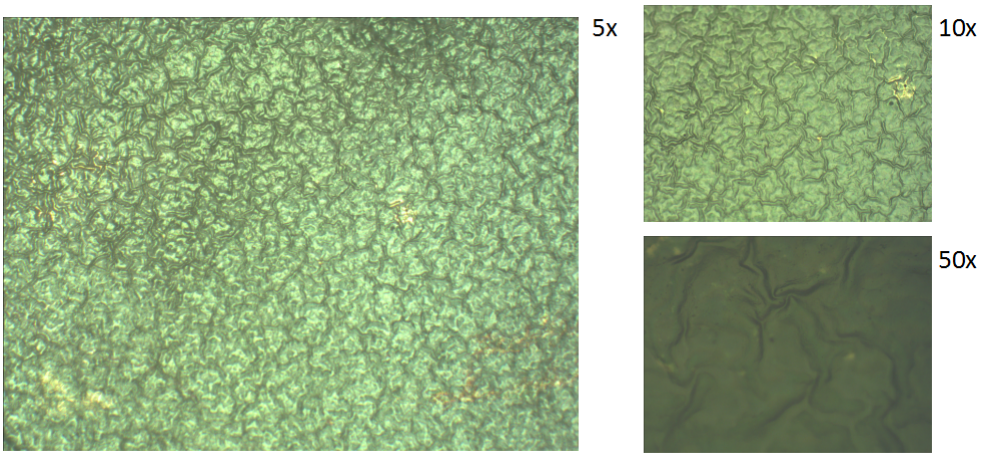

(a) Silk covered with spray and spin-coated PEDOT:PSS

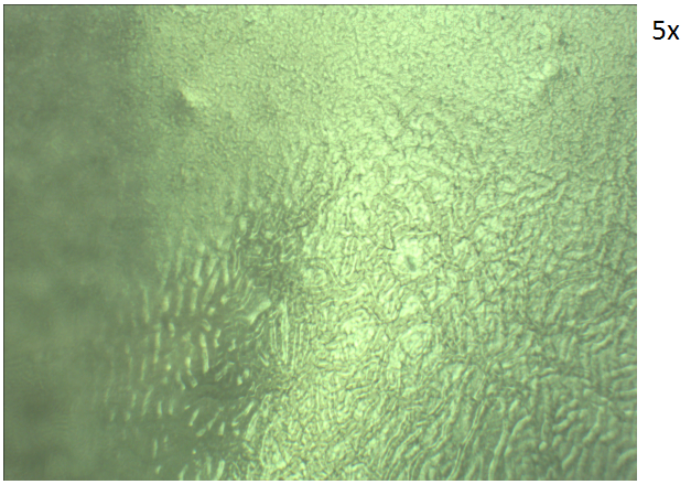

(b) Silk covered with spin-coated PEDOT:PSS

Figure 73: Difference between spray/spin coated silk and spin coated silk

The PEDOT deposed by spray coating shows the typical silk isles domains, that are more or less preserved thanks to the nebulization effect. The spin-coated silk instead shows a reduced isle patterning, and it gives the illusion of an increased flatness for the surface. Instead the flatness is way higher for the spray/spin-coated surface because of the reduced damages it suffers from the contact with water, as the profilometry measurements already demonstrated. Additional proofs of the surface flatness achieved with this technique are supplied by SEM imaging:

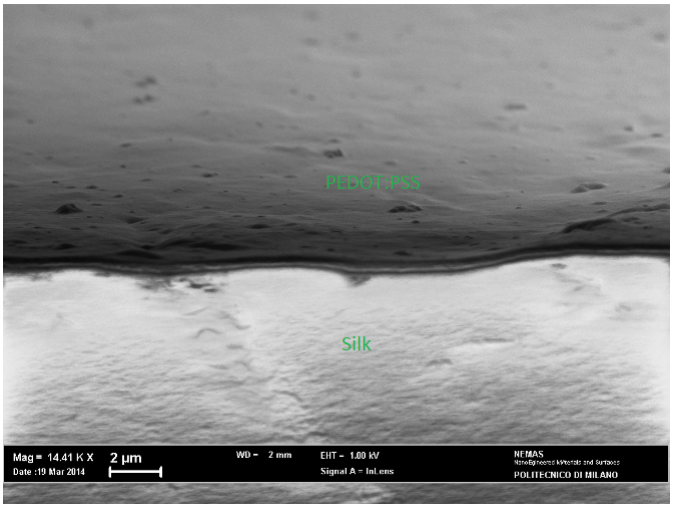

Figure 74: SEM image of a PEDOT:PSS surface spray/spin-coated on silk

4.2.2 P3HT/PCBM Deposition

The Poly-3-hexylthiophene / Phenyl-C61-butyric acid-methyl-ester is the blend responsible for the phototransduction process. Details about its chemical and physical properties can be found in chapter 2 and in the mentioned bibliography. The third layer of our artificial retina is indeed a P3HT/PCBM layer deposited on top of the PEDOT:PSS layer. This particular deposition, and the interface between P3HT/PCBM and PEDOT:PSS in general, is a topic which has been extensively studied in literature. The chosen deposition protocol for this application is actually a widespread solution for many organic solar cell manufacturer. The first process is the preparation of the two P3HT and PCBM solutions, each one dissolved into chlorobenzene in a 30 g/l ratio and sonicated into an ultrasound bath for 30 minutes. The two solutions are then mixed together and sonicated again for 30 minutes. The final solution is the blend of the two polymers and it has a concentration of 15 g/l. Then the deposition is realized with the spin coating technique, being it fast, accurate and very repeatable. The spin coating procedure is composed of two steps, a slow step for 5 seconds at 1200 rpm which spins off the solution to the edges of the substrate, and a fast step for two minutes at 2400 rpm which is responsible for the solvent evaporation (chlorobenzene). During the whole spin coating process the P3HT/PCBM solution is kept on a heating plate at 80 °C in order to dissolve possible lumps. Finally the thermal annealing is carried out for 20 minutes at 120 °C, in a nitrogen-controlled environment (oxygen to about 30 ppm), under an aluminum foil film. The nitrogen-controlled environment is fundamental due to the oxidation processes that are promoted by high temperatures, and the aluminum foil prevents possible photoinduced oxidations.
A way to characterize the P3HT/PCBM layer is the contact angle analysis. The adopted measurement protocol is the same as the one used for silk characterization, with the addition of a baseline contact angle measurement on pristine silk. The following graph shows the mean contact angle for both the complete device and a comparative silk and for both sides of the device. Each contact angle is mediated on five different samples from the same batch:

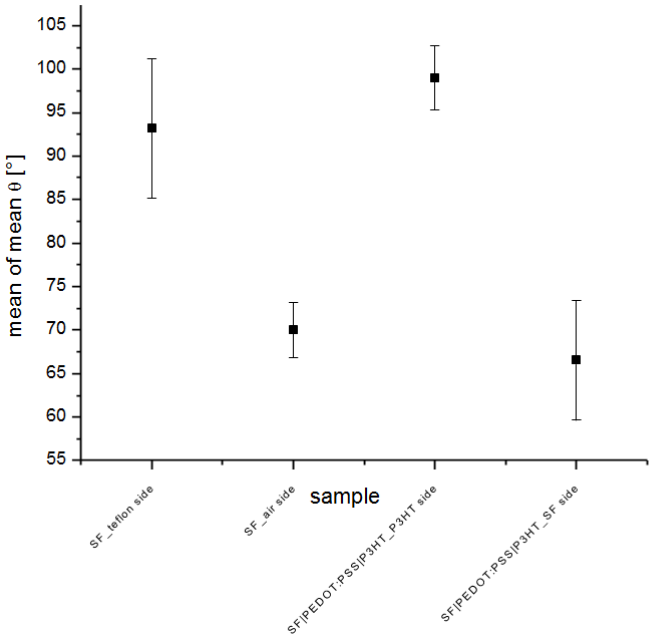

Figure 75: Contact angle analysis for the complete device

The analysis shows the usual behavior for the pristine silk, hydrophilic in its air side and hydrophobic in its teflon side. As far as the entire device is concerned, remembering that the PEDOT:PSS spin coating is always performed on top of the teflon side (or bottom layer), we have that the silk fibroin side is the hydrophilic one (or top layer). The other side is the one with P3HT:PCBM and it is a highly hydrophobic layer, a common feature for many benzene solutions. Its hydrophobicity values are in line with normal ones for blend polymers exposed to oxygen. The contact angles of the top layer for pristine silk and complete device are fairly repeatable, despite the high variability of the measurement due to the intrinsic difference between substrates and to wettability issues. This reasonable repeatability is a good sign of efficiency for the entire fabrication process, and it is

clearly visible in a graph in which are plotted the results for every of the five test samples:

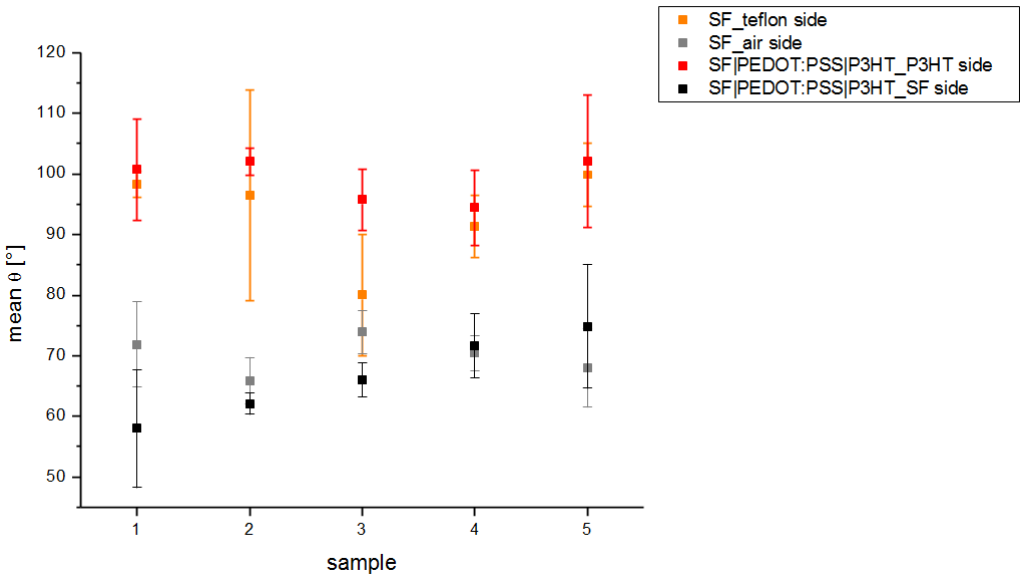

Figure 76: Contact angle analysis for the complete device, splitted for every test sample

4.2.3 Interfaces Characterization

SEM imaging can be used to realize a structural characterization for the entire device and its layers. This kind of imaging is well suited for showing the quality of silk-PEDOT:PSS and PEDOT:PSS-P3HT/PCBM interfaces, and also for the silk-P3HT/PCBM interface which does not ever happen in the device but its analysis can be a good comparative tool. The sample preparation is the same adopted for the pristine silk SEM imaging, that is the application of silver paste and the liquid nitrogen cut. The first interface we are going to analyze is the silk-P3HT/PCBM one. It is a well defined interface, very neat, and there is almost always a good adherence between the two layers:

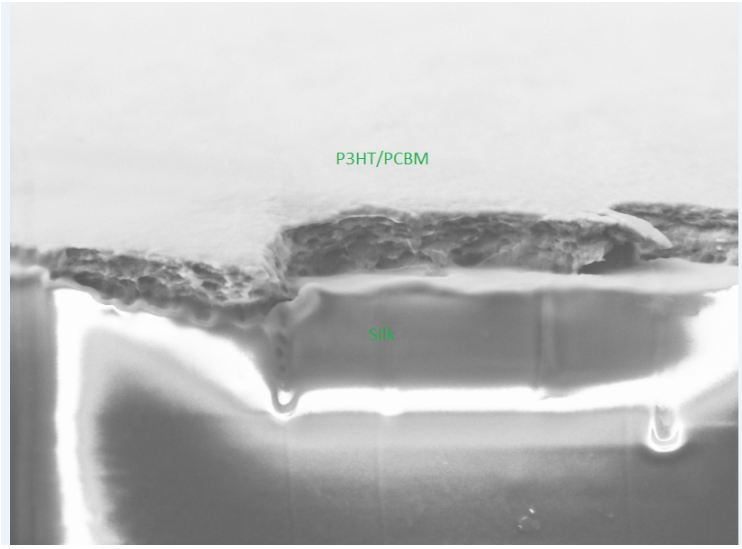

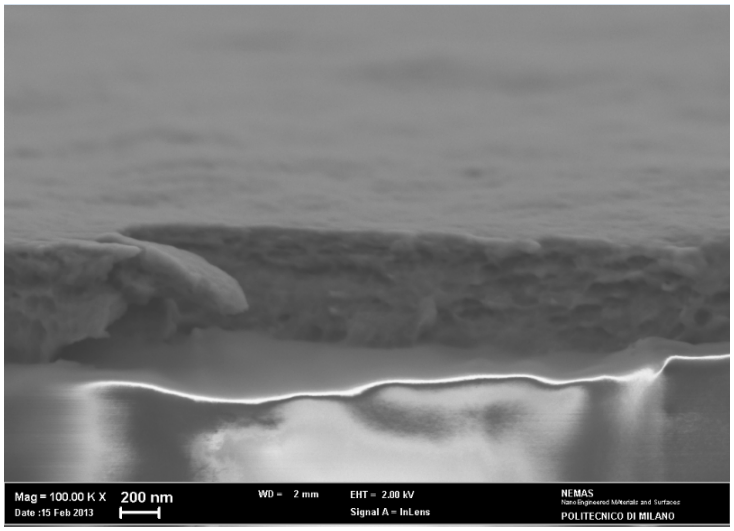

Figure 77: Silk-P3HT/PCBM interface

An unexpected result instead is the creation of a good interface between silk and PEDOT:PSS. The reason behind this behavior is the melting effect that water has on silk, which promotes recrystallization mechanisms and the mixing between the two layers. The SEM image shows also the thickness (384,7 nm) of the PEDOT:PSS film deposed by a single spin coating process:

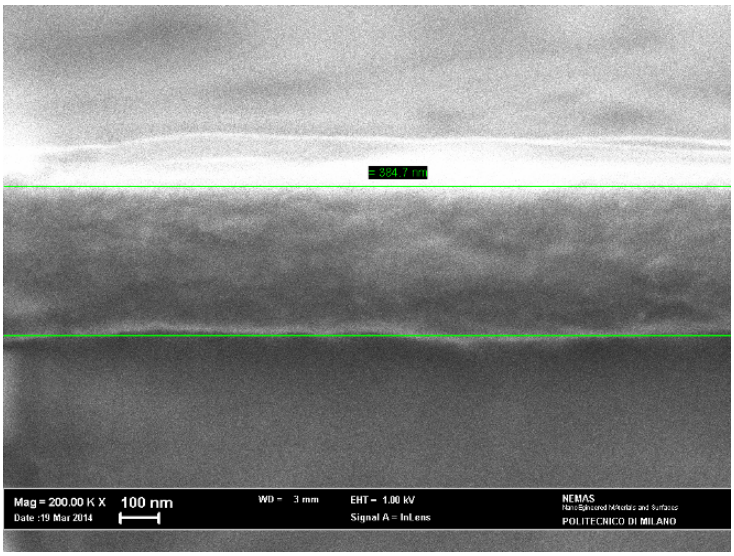

Figure 78: Silk-PEDOT:PSS interface

SEM images of the entire device show every single layer which compose the artificial retina. From these images it can be noticed that P3HT/PCBM does not create a good interface with PEDOT:PSS. This is a know issue for every organic solar cell manufacturer, and it is caused by the different nature of the two polymers. PEDOT:PSS, in fact, uses water as solvent while P3HT/PCBM uses chlorobenzene, and benzene derivatives are not soluble in water. Also, a comparison between all the interfaces clearly shows the melting effect of PEDOT:PSS on silk (especially with respect to the silk-P3HT/PCBM interface which is very neat):

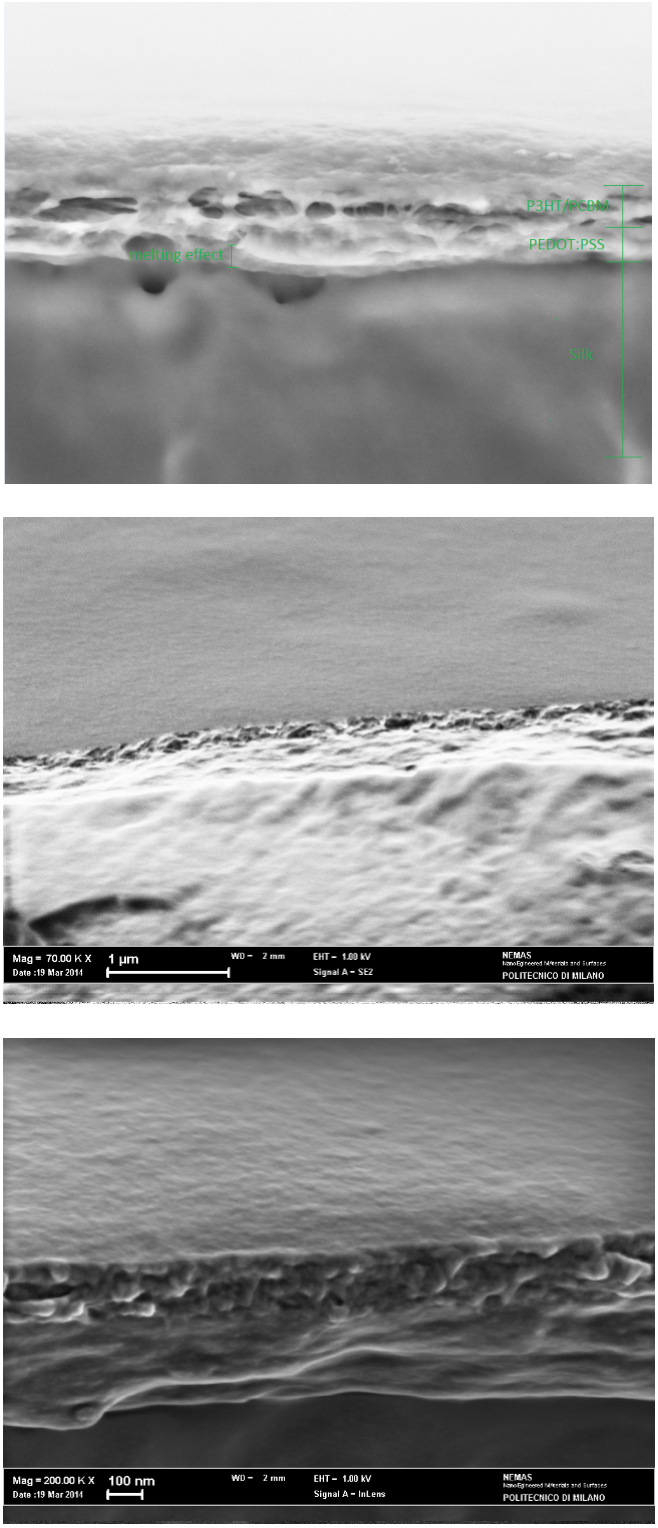

Figure 79: Interfaces for the whole device

The thicknesses for the entire device are shown in the next image. The PEDOT:PSS layer consists in a double step deposition, spray and spin coated, as studied in the deposition protocol before. The thickness here is around 552,3 nm, higher than the thickness achieved with a single spin coating procedure. The thickness of the P3HT/PCBM layer deposed with spin coating is around 215,7 nm. The global thickness of the device is mostly determined by the silk layer thickness, being it in the micron range:

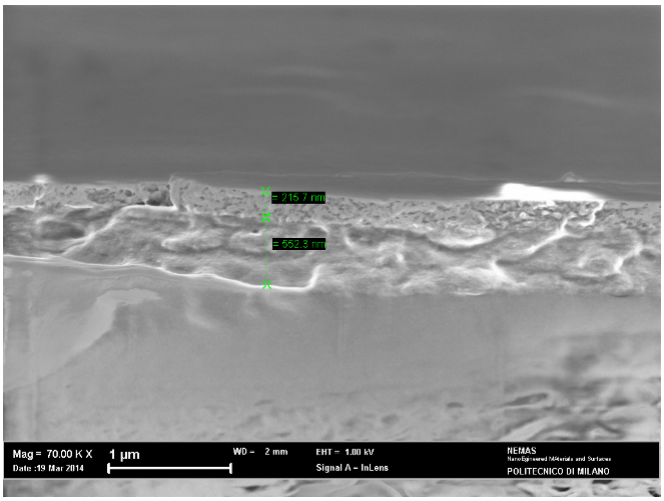

Figure 80: Thicknesses of the polymeric layers with respect to the silk thickness

4.3 Electrical Characterization

The electrical characterization of the organic artificial retina aims to provide an overview of the phototransduction efficiency for the device. The artificial retina works like an organic photodetector whose anode is the PEDOT:PSS layer and cathode is a saline solution, during “in vitro” conditions, or the vitreous humor during “in vivo” conditions. The characterization consists into the recording of the electrical activity of the device in response to an optical stimulus. In order to make a comparison for the photocurrent values, the results are contextualized with respect to a classic organic solar cell based on ITO (indium tin oxide) instead of silk. The experimental setup used for these measurement is described in chapter 3. From a modellistic point of view, the system can be described by the following block diagram:

This simple model uses a black box approach in order to understand the device internal processes responsible for its working principle. The electrical characterization will be performed by feeding the system with a known input and measuring its response. The chosen measurement protocol is the following:

- The samples are irradiated by a LED positioned at a distance of 42 cm. This distance is kept steady for every measurement. The LED power has its power sligthly inferior to its maximum limit, in order to avoid distortions in the optical input;
- The samples are secured inside a cuvette with transparent double side adhesive (optically and electrically inert), and the silk side (top layer) faces the glass of the cuvette. The aim of some experiment is to study the difference between the stimulation side but, if not otherwise specified, the light beam always strikes the sample on top of its polymeric layer;
- The geometry of the samples is rectangular, with dimensions approximately equal to 1 cm x 0,7 cm;
- The saline solution inside the cuvette is NaCl 0,2 mol/l in 2 ml of water;
- The electrode used for the photocurrent measurement is a 2 cm Platinum wire, immersed in the aqueous solution and clamped with a crocodile clip;
- The electrical circuit is closed clamping the upper side of the device with a crocodile clip. When the device has both polymeric layers, the P3HT/PCBM is selectively removed from the upper side using chlorobenzene, in order to leave a free access to PEDOT:PSS (the anode);
- The cuvette holding the device is optically and electrically insulated from the external environment, using a Faraday cage covered by an aluminum foil. The incident light enters the cage through a hole;
- Every measurement session is preceded by the measurement of the LED irradiation power density, realized by an optometer. This is a discrete measurement, the sampling is done for power densities relative to 350 nm, 450 nm, 550 nm, 650 nm, 750 nm, 850 nm;
- Every experiment uses the same setup (lenses, focal distance, photodiode, LED irradiation power density, Faraday cage, chopper, monochromator etc) for the sake of repeatability;
- If not otherwise specified, the optical input signal is a trapezoidal pulse with period equal to 1,012 s and amplitude 0-2 V (white light which contains all the frequencies of the visible spectrum):

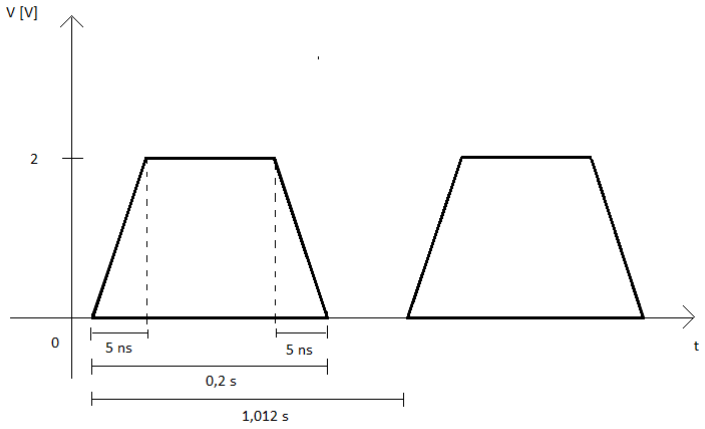

Figure 81: Standard optical input signal (image not in scale)

The first step for an electrical characterization is to acquire a reference signal. The optimal waveform, in terms of quantum efficiency and maximum achievable photocurrent, is produced by an ITO-P3HT/PCBM device. In this device the ITO plays the role of PEDOT:PSS, but in a more efficient way. The reference signal is achieved feeding the ITO-P3HT/PCBM device with a simple optical signal, a light step (light off-light on), using the aforementioned measurement protocol. The output waveform is the following:

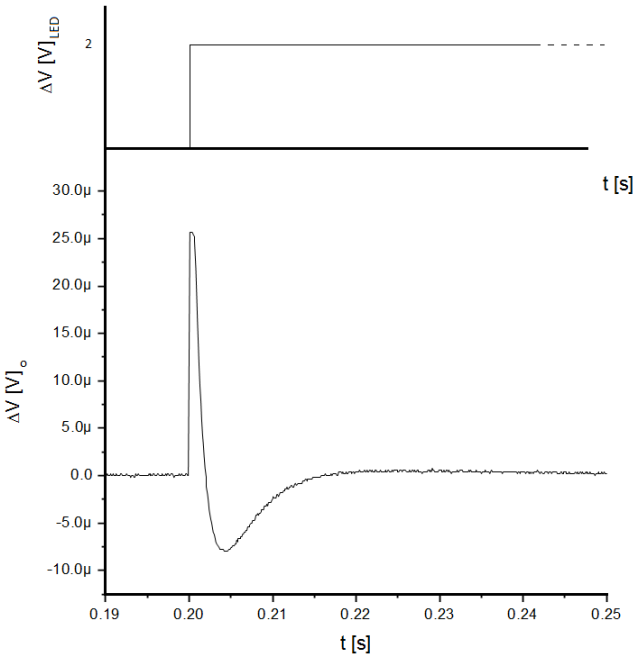

Figure 82: Reference signal from a ITO-P3HT/PCBM device

Before to start studying the response of our artificial retina it is important to understand the output signal of the reference signal. That is true because we expect the behavior of our device to be similar to the reference signal but noisier, being the ITO replaced by silk and PEDOT:PSS. The difference between reference device and final device is in fact only in the passive layer and in the anode, two components that do not introduce distortion in the waveform. The reference signal can be studied using a black box approach and/or a white

box approach. Starting with the black box approach, we realize that the reference signal is very similar to the derivative of an ideal impulse, a signal called *unit doublet*. In order to understand how a physical system can generate such a signal, we can analyze the analogy of a high pass filter which is performing the derivative of an input impulse signal. The analysis is performed in three steps:

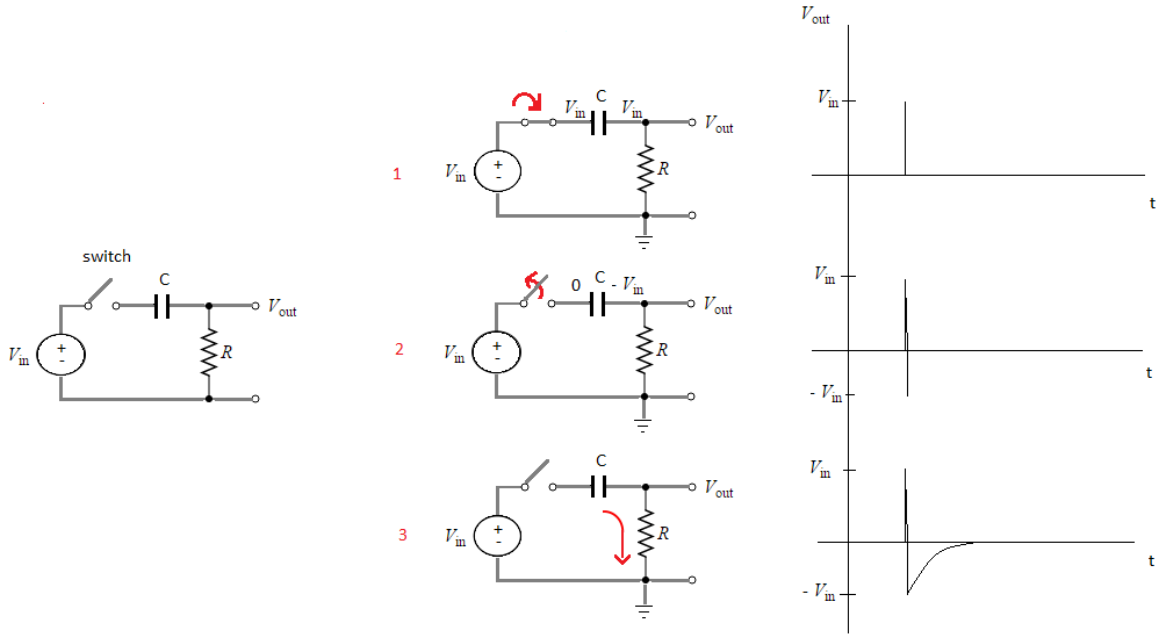

Figure 83: High pass filter derivating an input impulse. This is used as a conceptual tool in order to understand the reference signal

- Step 1: the switch closes and the input signal passes. Since its transition is immediate, the capacitor sees a high frequency signal and it behaves like a short circuit;
- Step 2: the switch opens and the input signal is blocked. At this point, the capacitor is charged with the V_{in} voltage but its left plate is forced to zero. Since the voltage across the capacitor now cannot change instantaneously (there is not charge injection or subtraction), the right plate goes to $-V_{in}$ and the ΔV remains equal to V_{in};
- Step 3: the capacitor is now free to discharge itself on the load resistence R. The rate of discharge depends on the time constant of the circuit;

The reference signal is very similar to the unit doublet we just studied. The only difference is that, according to our general black box model, the input signal to the artificial retina is a step function (the LED lighting) and not an impulse. This means that another derivative operation happens inside our system, hence the step input experiences a cascade of two derivatives. The black box approach therefore showed us a new way to study this hybrid system, because we now understand that two capacitive phenomena have to be searched in order to find a physical demonstration to our conjectures. Also, the waveform of the reference signal suggests us that these two capacitive phenomena have very different time constants, one is fast and almost instantaneous while the other one is very slow. The first derivative mechanism has to be searched in the working principle of an organic solar cell. As we studied in chapter 2, when an incident photon with energy at least equal to the optical gap is absorbed by an organic material like P3HT/PCBM, an exciton is generated. The exciton diffuses for about 10 nm, following Fick's laws, and if it meets a donor/acceptor interface capable to overcome its electronic gap the electron-hole pair splits. Being P3HT a conjugated polymer that in exposure to oxygen and moisture undergoes a p-type doping, a band-bending phenomenon occurs in proximity to the aqueous cathode and it creates a depletion region. This phenomenon is very similar to the build-up of a Schottky barrier in a semiconductor-metal junction. Moreover, it has been studied in literature that the diffusion of ions like Cl^- (from the electrolyte to the polymer) create a surface dipole layer with the same polarity as the Shottky barrier. The depletion layer and the dipole layer act like two capacitance in parallel, generating one complessive capacitance

which is the sum of the previous two. This final capacitance is indeed what we were searching for, that is one of the two responsible for the derivative of the input signal. The value of this capacitance is in the order of magnitude of the nF, and the associated time constants are generally really fast, compatible with the fast behavior shown in the first part of our reference signal. The second derivative effect is, unsurprisingly, the helmholtz layer peculiar of every electrolytic system. The capacitance here is way higher than the previous one and the associated time constants are very slow, compatibly with the slow discharge (in the range of ms) shown in the latest part of the reference signal. The recap of all these mechanism is summarized in the next block diagram , the updated version of our artificial retina-measurement system model:

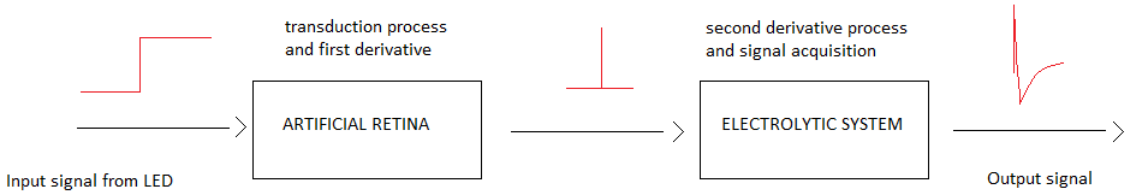

Figure 84: Block diagram of the artificial retina-measurement setup system

A further step toward the study of an effective signal from a real device, is to feed a reference system ITO-P3HT/PCBM with a trapezoidal wave, the signal we chose in the measurement protocol. Under these circumstances our reference signal becomes this:

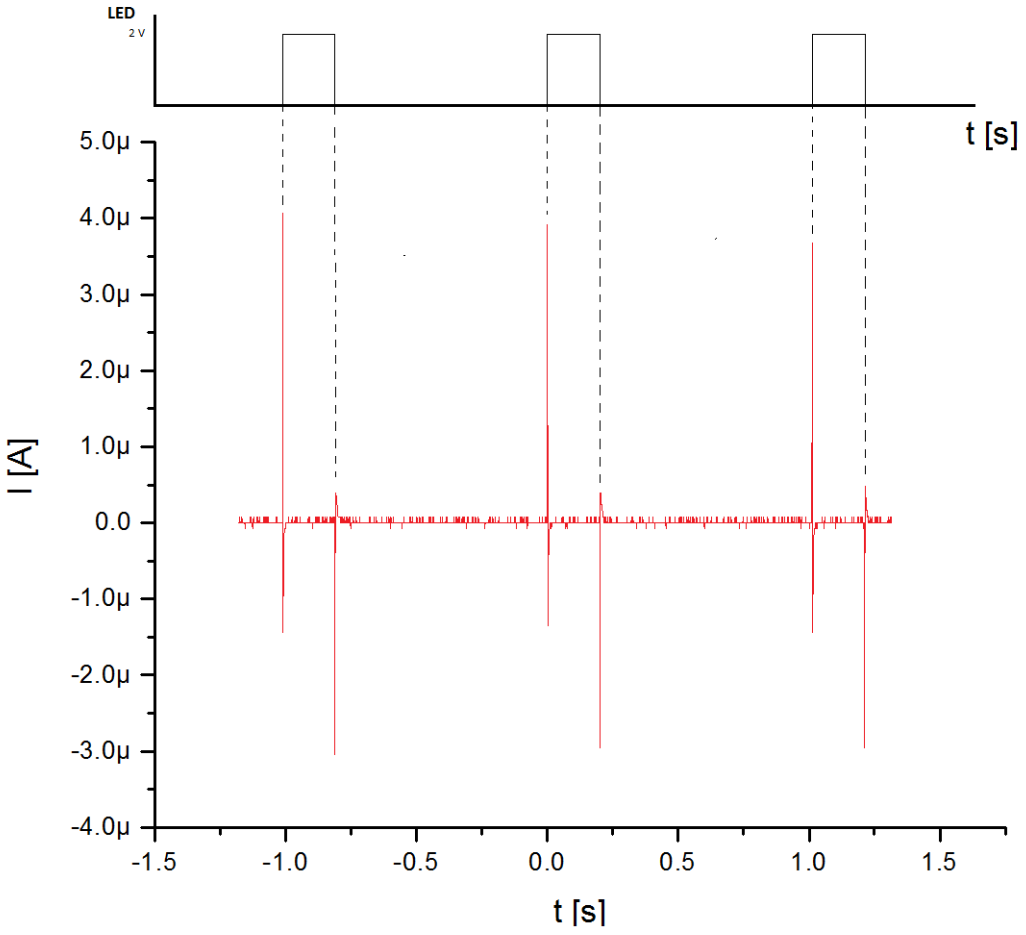

Figure 85: Reference signal for standard measurement protocol conditions. Amplifier gain set to 10^5.

Since the differences between an input step and a trapezoidal wave are the falling edges and the periodicity, we have a periodic response which shows inverted polarities in correspondence of the falling edges.
As discussed before, a signal produced by our artificial retina should preserve this waveform being of course noisier and with a lower amplitude. Following the protocol, the LED power spectrum has to be measured before starting to acquire signals from our device. The acquisitions from optometer show the following power spectrum:

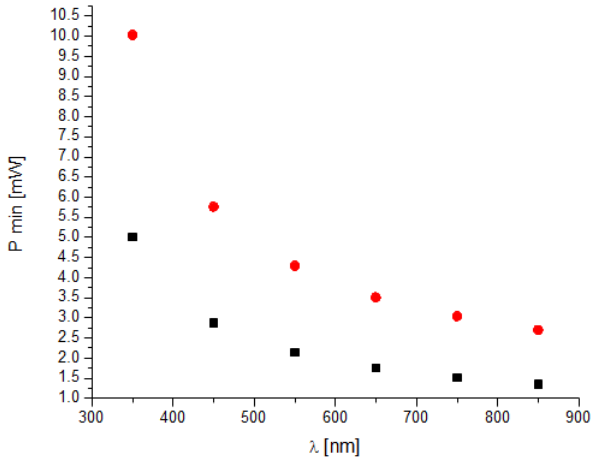

Figure 86: LED power spectrum

Finally, a typical photocurrent signal for our artificial retina (acquired under the aforementioned conditions) confirms all the predictions and shows the following waveform:

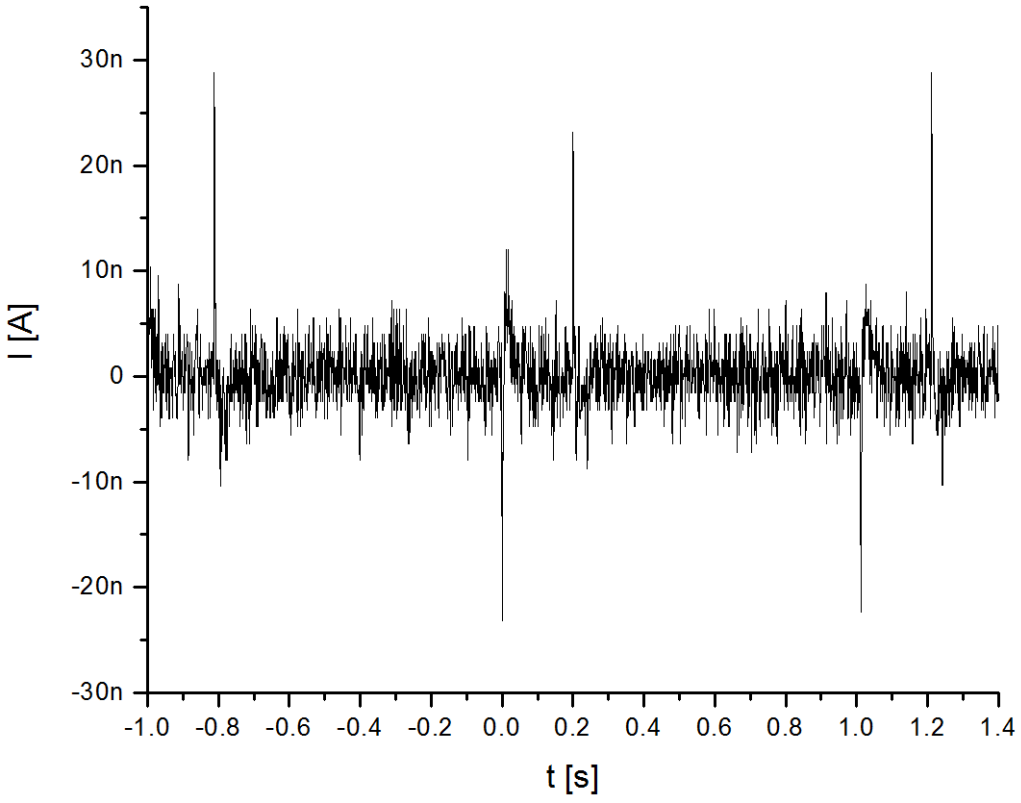

Figure 87: Photocurrent from the artificial retina, measured under standard protocol conditions

Despite the unavoidable noise, the signal clearly shows its "unit doublet" behavior for both rising and falling edges. Also, all the timings are respected being the periodicity equal to the input signal one, and the distance between peaks equal to 0,2 seconds. The amplitude of the peaks is drastically reduced, from the microampere range of the reference signal to tens of nanoamperes. This amplitude, however, is highly variable even under repeatable measurement conditions, since the silk substrate in aqueous environments generates a high variance of mechanical, chemical and physical conditions. The photocurrents were measured different times for several samples from different batches, and a statistic on amplitude peaks gives a mean photocurrent value of 50 ± 30 nA. The time constant of the exponential waveform, relative to the capacitive effect from the electrolyte, can be estimated from the relation $t \approx 5\tau$ where t is the transient response time. A statistic on the aforementioned population of samples produces a time constant mean value of 10 ms with a very low variance, being the preparation of a NaCl solution very repeatable and controllable.

4.4 Degradation Analysis

The last characterization for the organic artificial retina consists in the temporal monitoring of every property we analyzed so far. Contact angles, SEM images, absorption spectroscopy, optical microscopy and photocurrents are monitored four times, once per week, throughout a month. During this time the artificial retinas were stored under aqueous conditions, hence the temporal monitoring of their features works as a characterization of the degradation effect. The work plan is summarized in the next table:

	Sample types	Time points	Size	Multiple samples	Total Required #
Contact angle	S; SPP	0, 4	2x2 cm or less	5 each	10 S 10 SPP
Photocurrent	SPP :P GPP	0, 1, 2, 3, 4 0, 2, 4	1 x 2 cm 1 x 2cm	3 each time point 10	15 SPP:P 10 GPP
SEM	S ; SP; SPP	0, 4	Cm2	2 each	4 S; 4 SP; 4 SPP
Optical Microscopy	S	0, 1	Cm2	1 each time point	2
Absorption spectroscopy	S; SP; SPP	0, 4	Cm2	2 each	4 S; 4 SP; 4 SPP

S = Silk
SP = Silk-PEDOT:PSS
SPP = Silk-PEDOT:PSS-P3HT/PCBM
GPP = ITOglass-PEDOT:PSS-P3HT/PCBM

Time points {
0: First measurement
1: After 1 week
2: After 2 weeks
3: After 3 weeks
4: After 4 weeks

Figure 88: Work plan for the degradation analysis

T_0 measurements are made few hours after the sample fabrication while T_4 measurements are realized one month after the fabrication, hence experiencing one month of degradation in a saline solution environment. T_1, T_2, and $T_3$are intermediate measurements and show significant differences between them only for the photocurrent case. The storage consists in a set of plastic petri capsules with a diameter of 5 cm, ermetically closed and filled with a solution of NaCl(aq) 0,2 mol/l. Samples are kept in a conditioned room at 37 °C under room light, experiencing a lighting condition of a normal day-night cycle. The saline solution is renewed every three days in order to simulate the physiological drainage of the eye. Every artificial retina is labeled in order to acquire both inter-sample and intra-sample variability information:

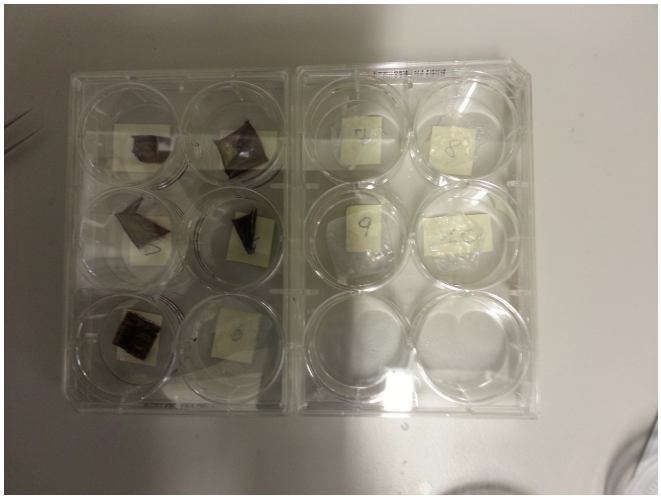

Figure 89: Device storage

Starting from the contact angle, the next figure shows a comparison between T_0 and T_4measurements. The difference in contact angles expresses the changes in wettability, and the degradation degree of silk and polymeric layer after one month of exposure to light and a saline environment:

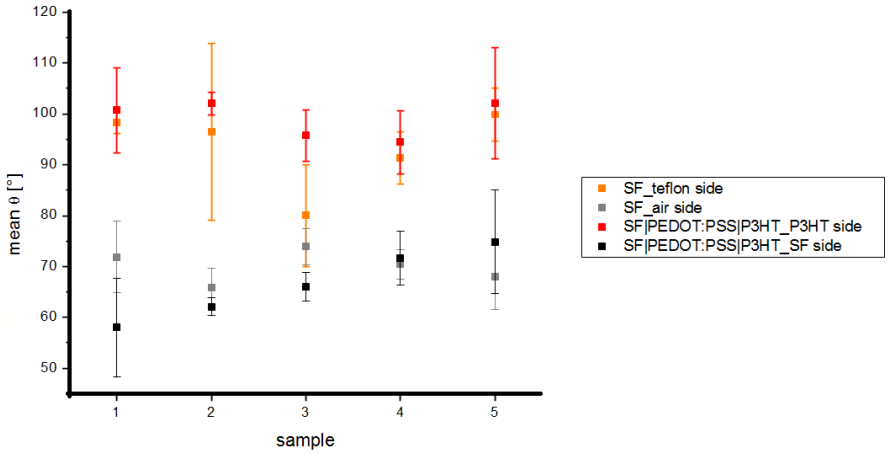

(a) T_0

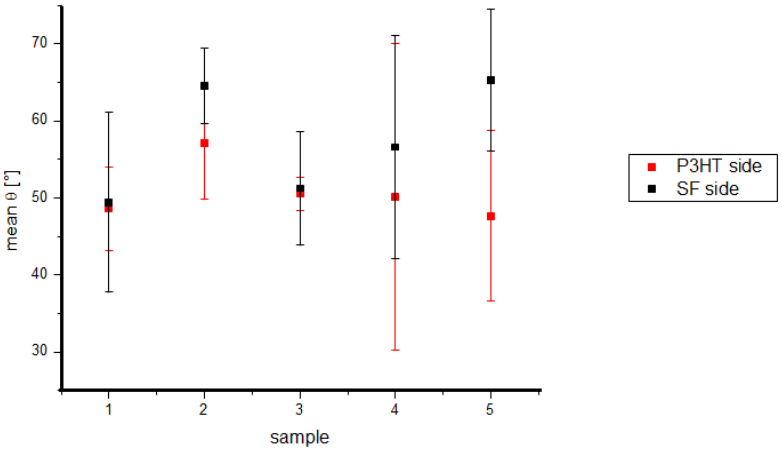

(b) T_4

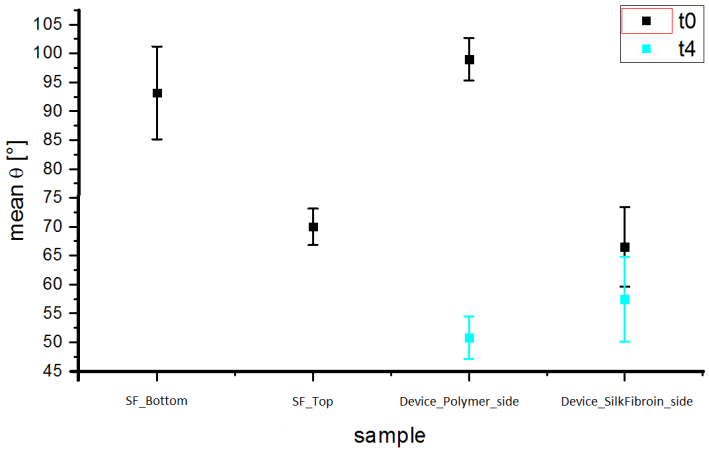

Figure 90: Differences in contact angle after degradation

The plot of T_4contact angles doesn't show values for the silk-fibroin (SF) film but only for the entire device (Silk-PEDOT:PSS-P3HT/PCBM), because as we already mentioned the silk film becomes highly irregular after immersion in water. The melting effect makes the contact angle measurement almost impossible, other than severely damaging the structural integrity of the silk film. The deposition of polymeric layers makes the silk film able to adapt to aqueous conditions, giving him a mechanical backbone that also has hydrophobic properties. This hydrophobicity shows a drastic reduction after the degradation effect, as depicted in the graph, because of prolonged photodoping and oxydation processes promoted by light and oxygen. However the device still shows good mechanical properties after the exposure to corrosion, preserving its integrity and maintaining an optimal flexibility. As far as the silk fibroin side of the device is concerned, it shows contact angles very similar to the values measured at T_0. That is because silk does not experience photodoping or oxidation, and its mechanical integrity is not seriously affected as discussed before. This analysis demonstrates the adaptability of the device in saline solutions like vitreous humor or extracellular liquids, and therefore its suitability for implants in test animals.
It is important now to understand how the hydrophobicity change of the polymeric layer affects the absorption spectrum. An absorption spectroscopy performed at T_0 and T_4 exhibits the following behavior:

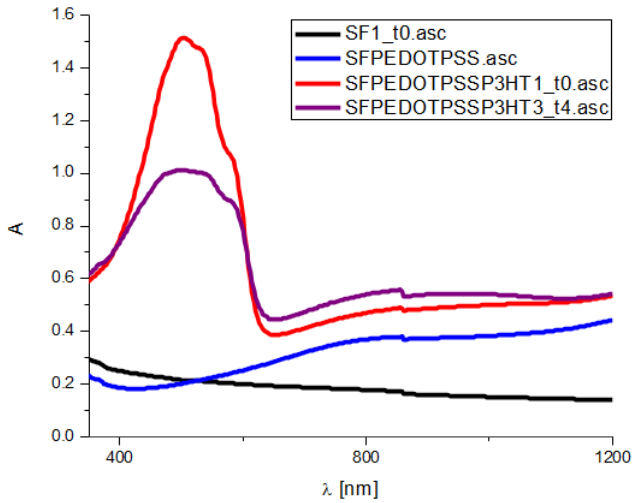

Figure 91: Absorption spectrum for the device at T_0 and T_4. Silk and Silk-PEDOT:PSS are plotted as references. Spectroscope was set to absorption mode, 13 InGaAs gain, 2nm slit width, 100% and 0% correction.

Normal silk and Silk-PEDOT:PSS doesn't show an absorption spectrum since they are not photoactive materials. The spectrum for the artificial retina shows the behavior of P3HT/PCBM, that is an absorption peak around 550 nm with quasi-gaussian shape. Measurements performed at T_4produce a spectrum with lower amplitude but the same waveform. The degradation therefore influences only the absorption coefficient but it does not introduce spectral distortion. This is a very important feature because the absorption spectrum must be limited within the visible range and possibly centered around the green color.
A macroscopic structural analysis of the degradation effect can be performed through optical microscopy, while the repercussions on the device layers can be studied by SEM. T_0optical microscopy images show the peculiar silk patterning, more pronounced for bottom layer than top layer. This can be caused by the solvent casting procedure, and it may be more evident for bottom layer because of the intrinsic microscopic patterning of the Teflon petri which holds the silk solution before its drying. T_1 measurements show instead the presence of big waves and bubbles, hence H_2O infiltrations, and the reduction of the patterning probably due to recrystallization processes. Measurements beyond T_1 are not possible because of the melting effect from saline water:

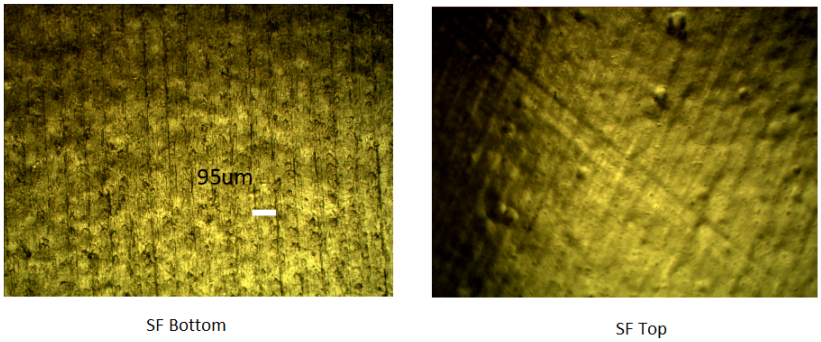

(a) T_0

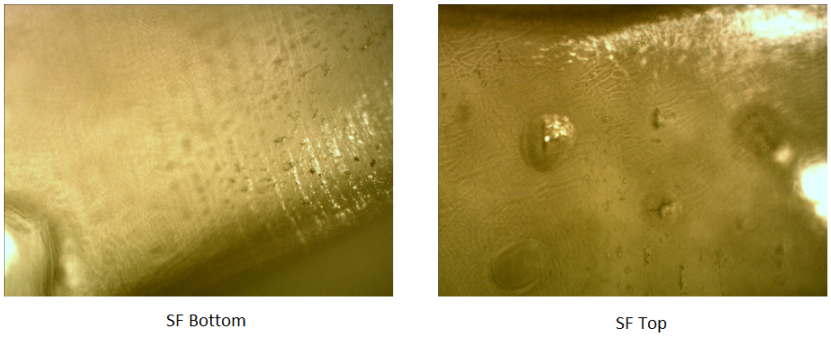

(b) T_1

Figure 92: Optical microscopy for silk at $T_0$and T_1. Silk films were observed after drying with nitrogen gun.

The variation of thicknesses and the quality of layers after degradation and photodoping is addressed by SEM imaging. Images relatively to T_0measurements can be consulted in the previous sections, while SEM images relatively to T_4 are shown below. Starting from silk only, the analysis of thicknesses highlights a huge increase due to water infiltration from both sides of the film:

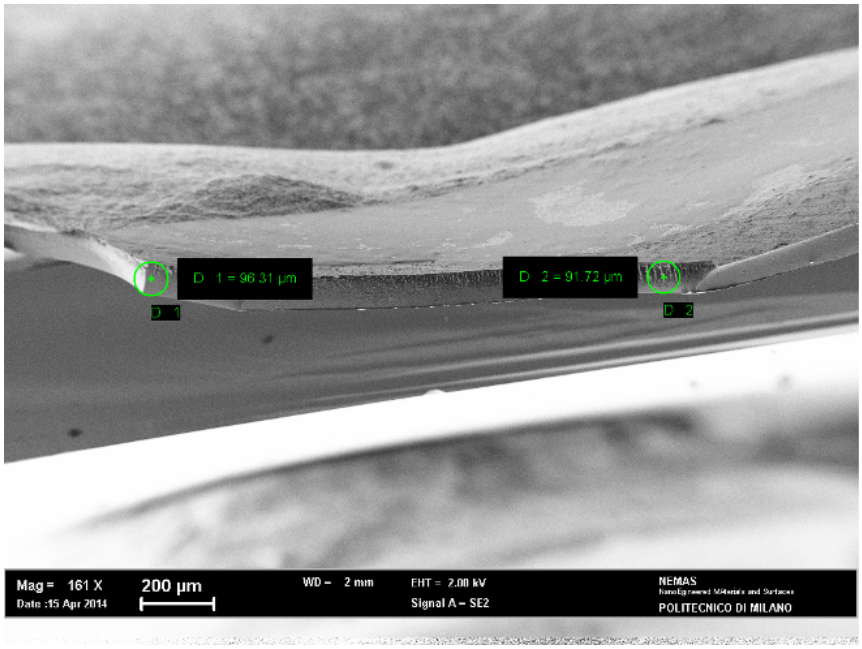

Figure 93: SEM for silk films at T_4

Thicknesses are more than doubled and they became highly space variant, depending from the section. It is also possible to notice the irregularity of the surface and some damaged portion with different texturing. The Silk-PEDOT:PSS device instead shows a little increase in thickness, because PEDOT:PSS is already water-based and the infiltration is limited by osmosis mechanisms. The surface is slightly irregular and shows bubbles and infiltrations:

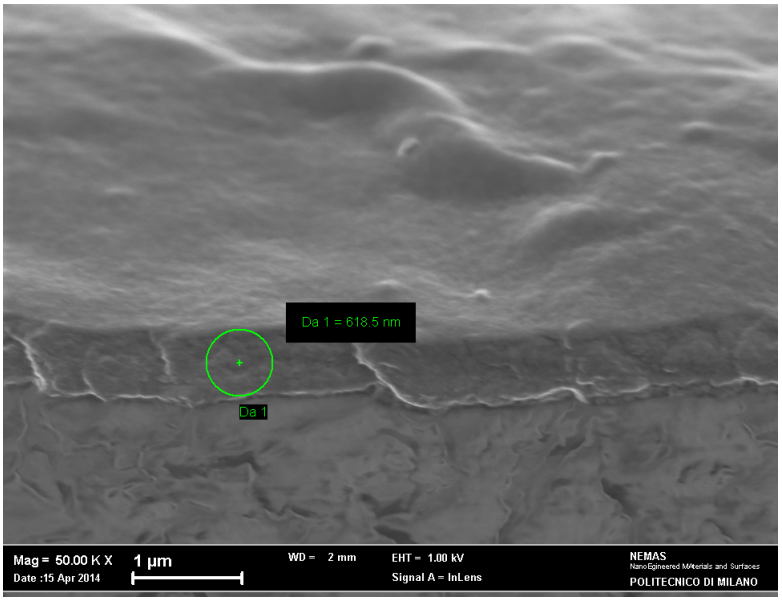

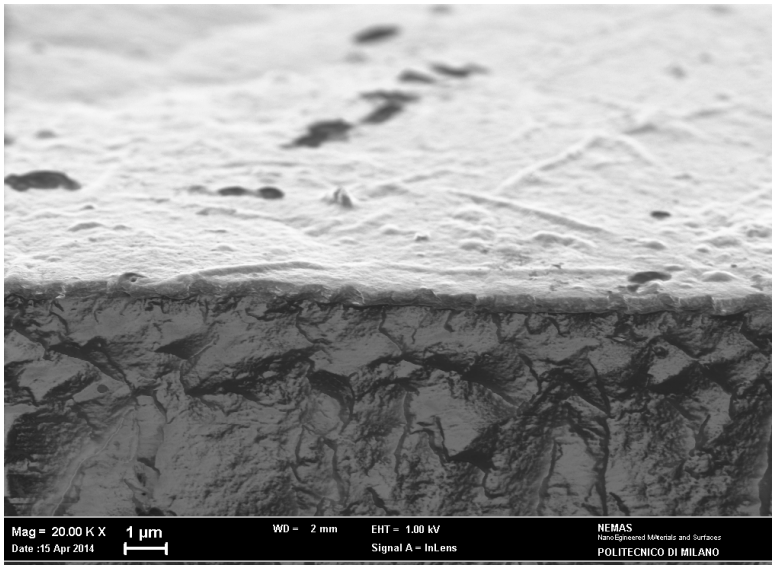

Figure 94: SEM for Silk-PEDOT:PSS at T_4

The Silk-PEDOT:PSS-P3HT/PCBM (the whole device) shows very well defined interfaces even after a month of degradation. Bubbles, infiltrations and swelling effects in general are reduced for the P3HT:PCBM surface being it highly hydrophobic. Thickness are barely afflicted and the surface is still very flat and regular:

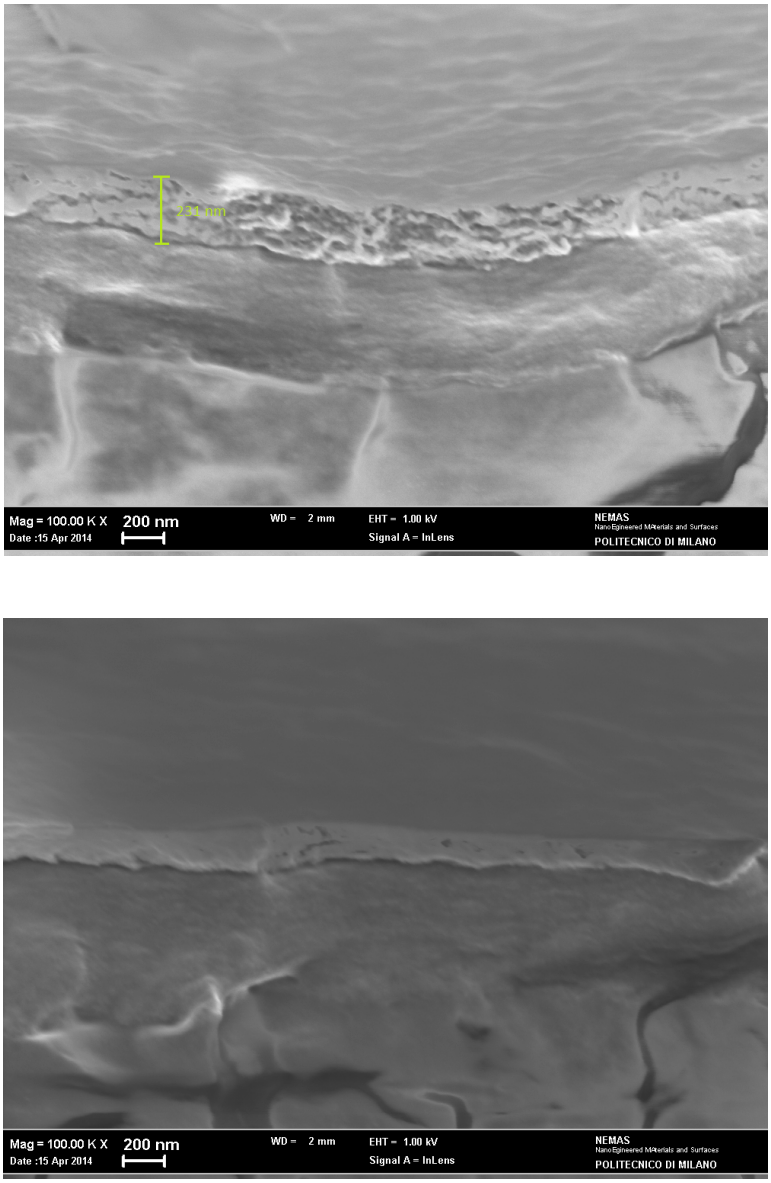

Figure 95: SEM for Silk-PEDOT:PSS-P3HT:PCBM at T_4

We can conclude that the structural integrity of the whole artificial retina is not excessively compromised by the degradation effect, mainly thanks to the hydrophobic P3HT:PCBM layer acting like a protective layer for PEDOT:PSS, which otherwise tends to have superficial water swelling. The silk integrity particularly benefits from the stacking of the polymeric layers, and the overall effect is a flexible device which is able to endure aggressive environments like physiological solutions.

Photocurrents show a noisier behaviour with the increasing degradation time, and a great variability in peak values and waveform. Some samples keep similar peak value to the initial ones, while others show a slight-to-medium decrease in amplitude over time. Photocurrent of GPP samples (ItoGlass-PEDOT:PSS-P3HT:PCBM) are shown for comparison:

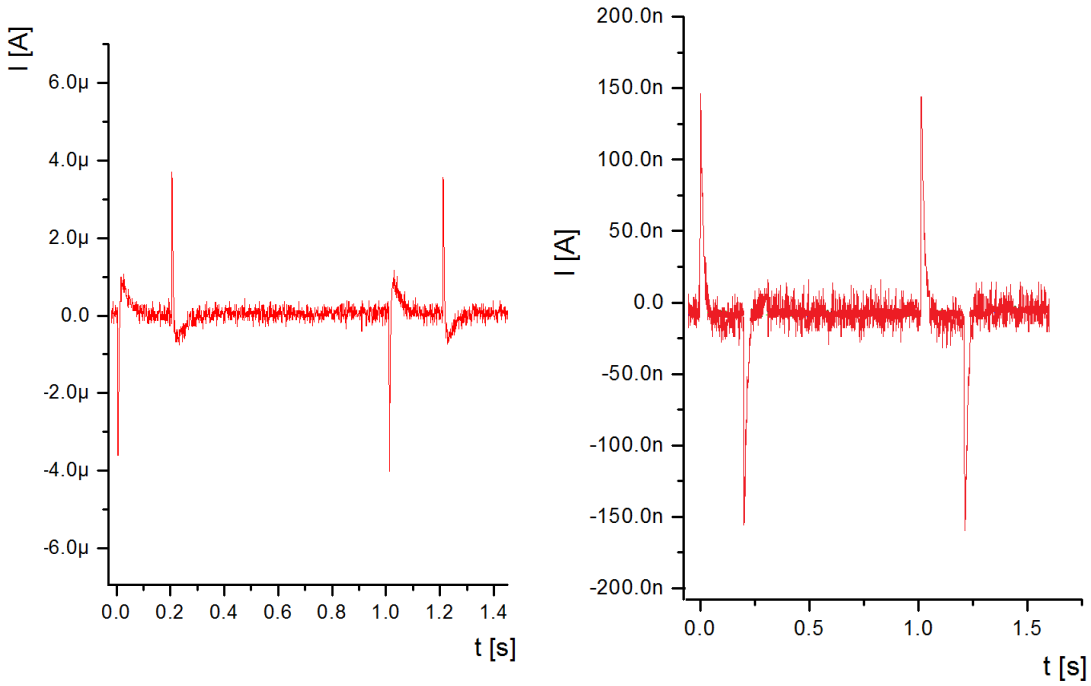

(a) GPP T_0

(b) GPP T_4

Figure 96: GPP photocurrents at T_0 and T_4 (not in scale)

GPP generally produces low noise photocurrent but most samples experience a decrease in the second peak of the unit doublet. That may be caused by the photodoping process, which introduces a p-type superficial doped layer acting like an ulterior capacitance for the system. This capacitance has opposite polarity with respect to the double helmholtz layer, hence opposing the charge transfer process. The time constant of the process instead remains around 10 ms, probably because the decrease in capacitance is compensated by an increase in series resistance due to the p-doping. The decrease in peak amplitude is about one order of magnitude (from µA to hundreds of nA). SPP (Silk-PEDOT:PSS-P3HT:PCBM) samples show again a similar behaviour with respect to the reference device,with a noisier photocurrent but variable peak values. Out of the 15 monitored samples, almost half had a really low signal, possibly confusable with the noise. The noisy behaviour is due to a mixed effect of photodoping, gradual loss of structural integrity for the device, and intrinsic noise of the process (already high for T_0 measurements). A statistic on the collected data is shown in the following table:

Sample	1	2	3	4	5	6	7	8	9	10	11	12	13	14	15
T_0	64,8 nA	40,3 nA	75,2 nA	50,4 nA	19,8 nA	37 nA	19,3 nA	62,0 nA	80,1 nA	58,7 nA	40,4 nA	61,1 nA	93,4 nA	67,5 nA	10,2 nA
T_4	52,9 nA	noisy	31,1 nA	noisy	noisy	8,3 nA	9,1 nA	noisy	noisy	43,7 nA	noisy	noisy	75,5 nA	52,6 nA	1,55 nA

Figure 97: Analysis of peak values

Two examples of photocurrent signals, one for T_0 and the other for T_4 are shown below:

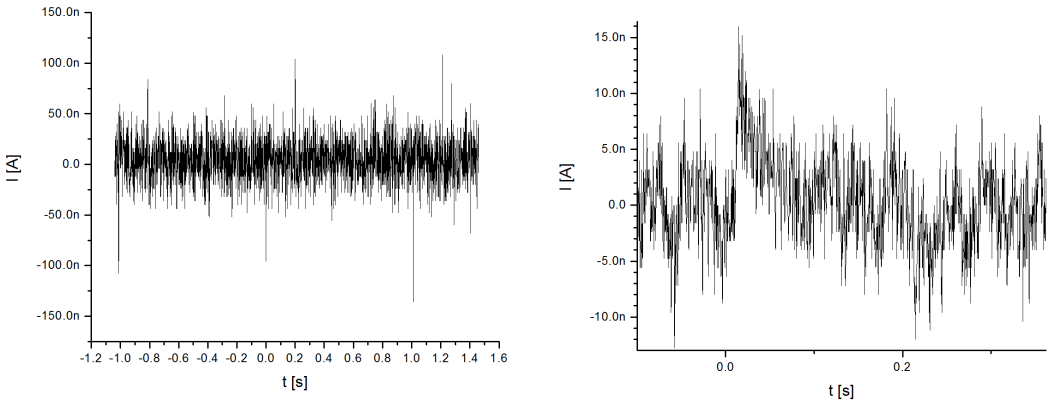

(a) SPP T_0

(b) SPP T_4 (zoomed, not in scale)

Figure 98: SPP photocurrents at T_0 and T_4

Also for the SPP device the amplitude reduction of the second peak happens. It is difficult to see with naked eyes, but it is demonstrated by an accurate analysis of the numbers in the photocurrent signal. The supposed mechanics of the amplitude peak reduction are the same of the GPP case, being the only difference between GPP and SPP a passive layer replacement. Two examples of a noisy response are shown in the next figure:

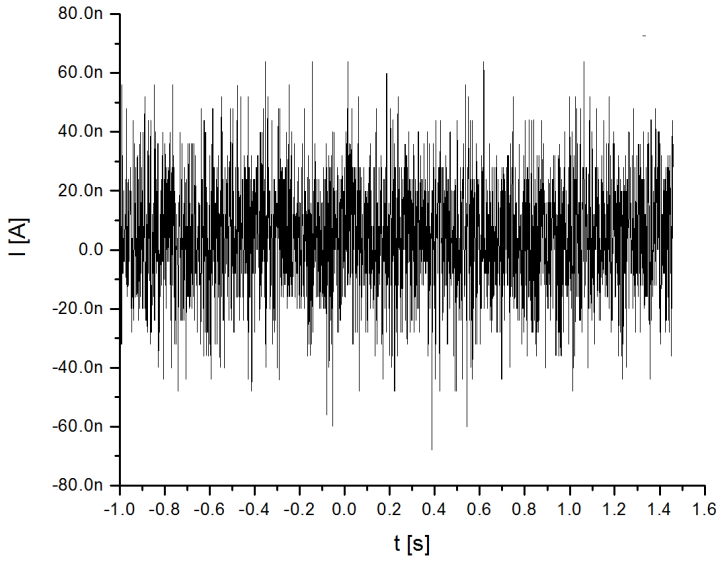

Figure 99: SPP noisy response at T_4

As depicted in the previous figure, the noisy signal has peaks very confusable with the noise peaks. Signal filtering is a very complex process here. A low pass filter would be very well suited for the application, but the problem is the determination of its cut frequency. The cut frequency should be almost 10 times higher than the maximum frequency of the signal, the latter being settled by the quick mechanism inside the polymer. The current literature of organic polymers has not yet converged towards a unique model for the physical representation of this systems, hence it is difficult to determinate a RC model from which estimating a time constant and a maximum frequency.
A final comparison can be made between T_4 responses with relatively low noise, in order to show the peak variability:

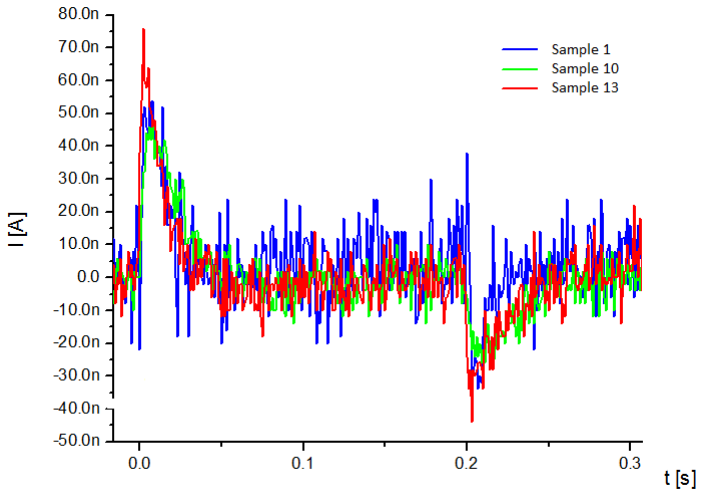

Figure 100: T_4 samples comparison, only 3 samples chosen for the sake of readability

Summarizing, the photocurrent analysis for the degradation study showed a variable behaviour for the peak amplitude and the noise, while the time constants kept their mean value around 10 ms with a good repeatability. Low noise responses had a mean peak value of 50 nA and the waveform tended to lower its second peak, the one related to the slow charge/discharge of Helmholtz capacitance.

Chapter 5

Validation and Conclusions

The organic artificial retina studied in this work is validated through its implantation in the eyes of RCS rats. The RCS (Royal College of Surgeons) rat is an animal which genetically inherits a retinal degeneration. In particular, its retinal pigment epithelium loses the ability to phagocyte the photoreceptors outer segment (see chapter 1). RCS rats are the perfect test animals in order to study retinal degenerations and the effect of an implanted artificial retina.
The complete implantation protocol is described below. Firstly, after the fabrication process, the artificial retinas are cut and shaped using a femtosecond laser. The advantages of a laser cut rather than a mechanical cut are discussed in chapter 3. The shape of the cut has to be asymmetric in order to distinguish the silk side from the polymer side. This is a relevant information for the oculists that are going to perform the implantation procedure, because the device has to be positioned with its correct orientation. Particularly, we want the silk side to face the pigment epithelium and the polymer side to face the incident photons, in order to avoid absorption phenomena from silk or PEDOT:PSS. The geometry of the cut is a rectangle trapezoid in which the rounded edge on the right identifies the silk side:

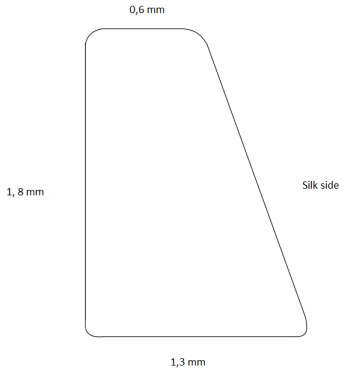

Figure 101: Geometry of laser cut

In every cutting session the incident photons strike the device from the silk side, because of possible photodoping processes or local melting effects to P3HT/PCBM. The laser parameters were 22,5 mA (amplificator), 260 mW, green coherent monochromatic light on stage. Optical microscopy performed on artificial retinas cut under this protocol shows the smoothness of the edges:

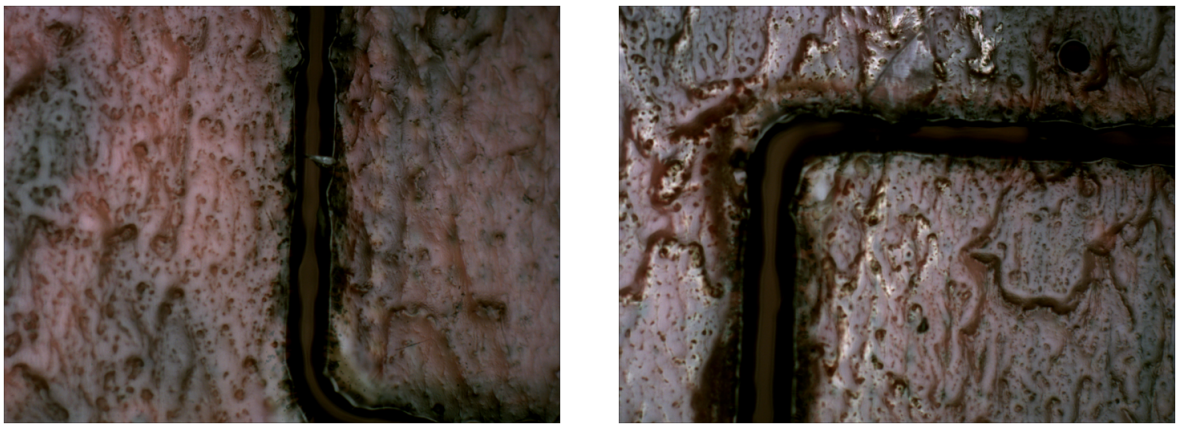

Figure 102: Optical microscopy showing the quality of the cut

The rectangle trapezoid geometry of the cut, instead, is highlighted in the next figure:

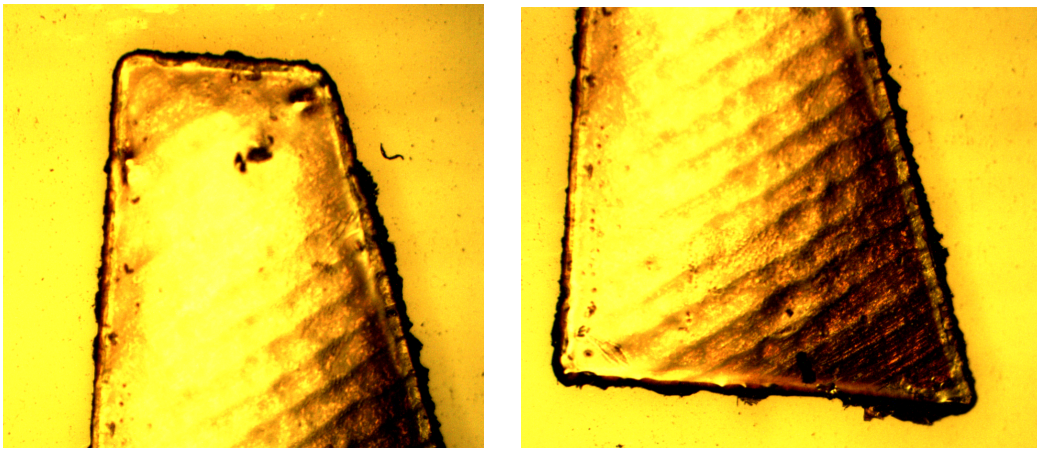

Figure 103: Optical microscopy showing the rectangle trapezoid geometry

Some validation experiments were aimed to analyze the immunochemistry of the implant. In order to create a healthy environment for both the device and the implanted eye, a good fluid recycle around the artificial retina must be guaranteed. The best way to accomplish this purpose is to create pinholes on the device surface. Pinholes, in fact, promote an healthy flow of vitreous humor and the pigment epithelium can be fed by its nutrients. The pinhole diameter is about 3 μm and their spatial period is about 20 μm:

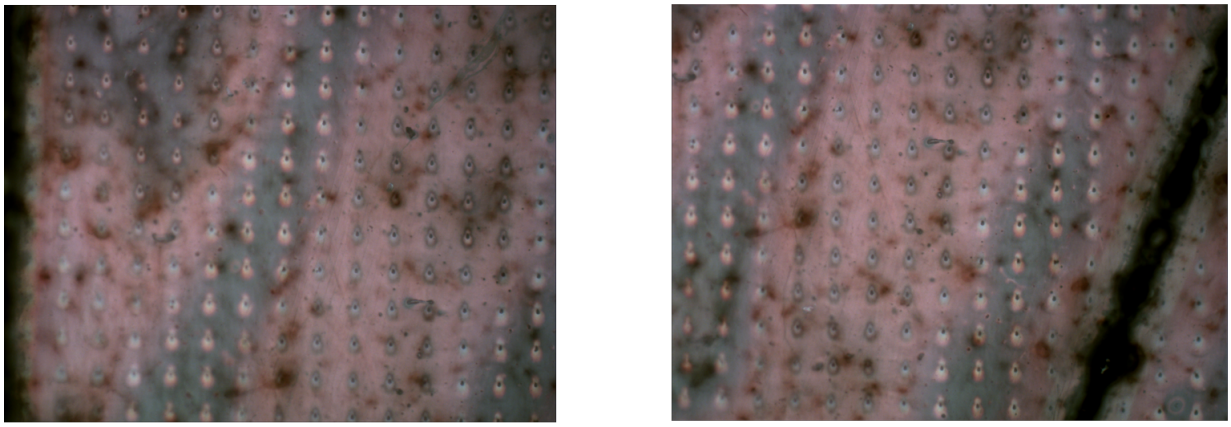

Figure 104: Optical microscopy of pinholes

After the laser cut, the device are sterilized through an ethylene oxyde treatment. Then, the last step before the implantation is to put them under water in order to enhance their flexibility. The surgery is realized at the Ospedale Sacro Cuore Don Calabria (Verona), at the Ophthalmology operating unit. The insertion procedure is aided by two surgical tools based on PET (Polyethylene terephthalate). These tools are shaped through a laser cut, they have a thickness of 20 μm and the following aspect:

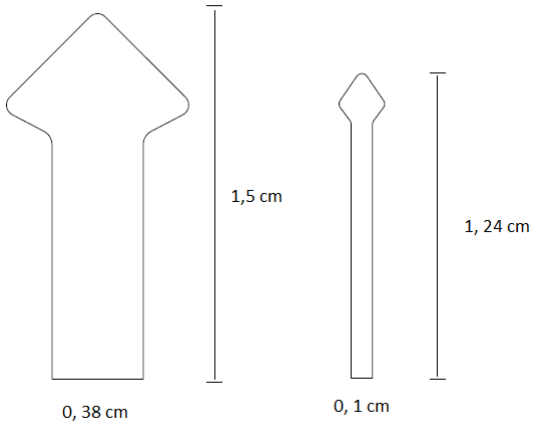

Figure 105: Surgical tools used during the implantation

The chosen type of implant is a subretinal one, involving the retinal detachment and the placement of the device on top of the pigment epithelium. Some implant sessions were designed with the insertion of one device per eye, while other with more than one. A summary of all the implant sessions is shown in the next table:

Days	Details about implants
3-4/06/2013	Bilateral implants, about 60 artificial retinas, half of them with pinholes
27-28/06/2013	Bilateral implants, about 60 artificial retinas, half of them with pinholes
5-7/08/2013	Bilateral implants on 40 rats, half of them with pinholes.
3-4/10/2013	Bilateral implants on 25 rats, 100 artificial retinas, all with pinholes
21-22/10/2013	Bilateral implants on 18 rats, 72 artificial retinas, all with pinholes
4-5/11/2013	Bilateral implants on 28 rats, 112 artificial retinas, all with pinholes
16-17/11/2013	Bilateral implants on 26 rats, 104 artificial retinas, all with pinholes

Table 1: Implant sessions

All implant sessions last 2-3 days. About 7-10 days after the implantation it is possible to evaluate the positioning of the device through OCT (Optical Coherence Tomography) imaging, due to the decrease of the inflammatory reaction. Usually the OCT checks are made after 15, 30 and 60 days after implantation. After 15 days the implants appear quite rigid, and almost all of them do not follow the curvature of the eye. After 30 and 60 days, about half of the implants adapt their shape to the fundus oculi. The other 50% is considered to be a failed implant, mainly due to the artificial retina being still too rigid, or because of retinal detachments. Further details about the implantation process, OCT and immunochemistry are still subjected to copyright restrictions, at the time of the drafting of this thesis. The available information, however, are evoked potentials and psychophysical experiments on implanted rats. These measurements were performed at the IIT headquarters in Genova. Visual Evoked Potentials (VEP) are measured before and after the artificial retina insertion. The measurement on blind rats, without artificial retina (labeled RCS), provides a comparative baseline for the analysis on implanted animals. Also, some measures were performed on RCS rats without retinal degeneration (labeled RCS - rdy), again as comparative tools. Finally, blind rats implanted with artificial retinas (labeled RCS + Silk:Pedot:P3HT) show higher signal latencies and lower amplitudes with respect to RCS - rdy ones (the healty rats). Results are shown below:

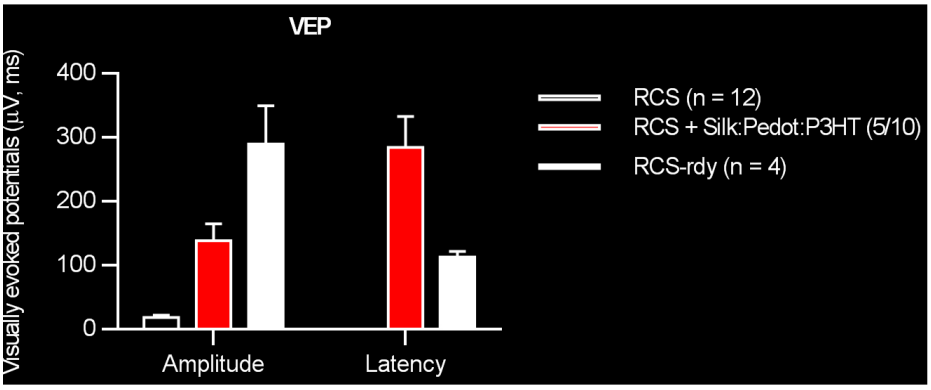

Figure 106: VEP blind rats (RCS), healthy rats (RCS-rdy) and blind implanted rats (RCS + Silk:Pedot:P3HT)

These results demonstrate a clear difference between implanted rats and blind rats. With these evidences, we can be sure that the artificial retina is capable of delivering a signal to the visual cortex, while before the implantation the VEP is almost zero. This is an objective test which guarantees the correct "hardware functioning" of the device, but it cannot give information on "how the rat sees" or "what the rat sees".
The last validation consists of a psychophysical assessment on healthy animals and implanted animals. The following protocol was chosen for this experiment:

- Healthy rats and implanted rats are placed inside a box for a relatively long period of time. Every rat is placed in its own box, in order to avoid the development of social behaviours which can possibly influence the experiment;
- The box is divided into two areas separated by a septum. One chamber is dark, while the other has a light inside it;

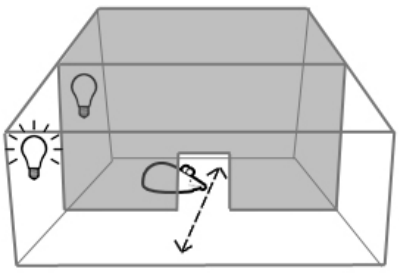

Figure 107: Psychophysical test for RCS rats

- The experiment for implanted rats starts a reasonable time after the implantation process itself;
- During the entire permanence of the rat into the box, it is monitored the time he spends into each chamber;

It is already known that the rat is a nocturnal animal. An healthy rat always chooses to live in a dark environment. However, several behavioural studies on rats demonstrated that it is a fairly inquiring animal. Hence, even if a healthy rat prefers darkness over light, he will pass a little part of his time in a bright environment in order to explore his surroundings. The box-test for an healthy rat should demonstrate that most of his time is spent in the dark chamber, but also that a significant time is spent in the bright chamber. A blind animal should show instead a quasi-random choice. There is also the possibility that the rat spends most of its time in one chamber because he is frightened of his new life condition inside the box, or because he received some

neuromuscular damage after the anesthesia or the implantation process itself. In order to exclude this possibility it has to be performed a cross-check. A smart cross-check could be to count the number of transitions between light to dark and viceversa, within a certain time lapse. If the animal is healthy (both his sight and its neuromuscular system), he generally shows a certain number of transitions due to its inquiring nature mixed to its good physical conditions. If the animal is damaged, this number of transitions drastically decreases. The results of this psychophysical test are shown in the next figure:

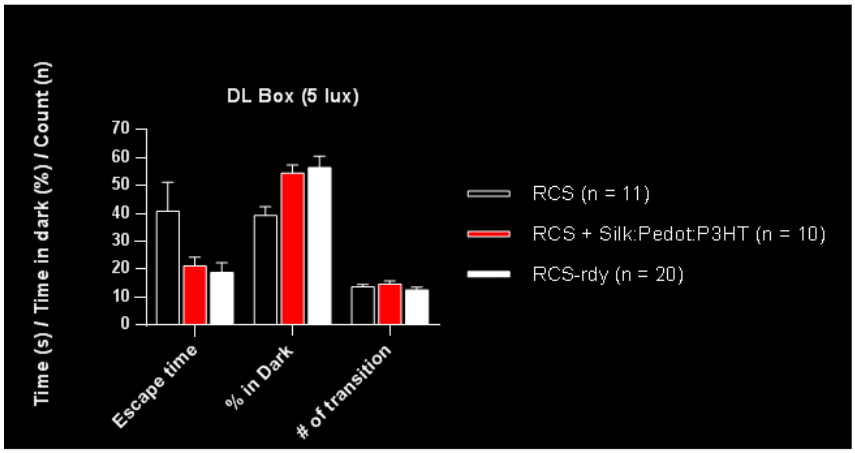

Figure 108: Results of the psychophysical test for RCS rats

We notice that the blind rat has a dark percentage time around 40% , hence he spends more time in the bright chamber. Healthy rats and implanted rats show, instead, a very similar behaviour which is very different to the blind rat one. Their dark percentage is almost 60%, slightly higher for the healthy rat of course. The number of transitions are similar for all the rats, but this information only demonstates that no damaged animals were used for the test.

These are promising results, demonstrating the efficiency of the organic artificial retina approach discussed in this thesis work. But much has yet to be done. A first future perspective could be a precise modeling of the enire system. Not only the electrical model of the artificial retina, but also a model capable of correlating the measurements on rats to the fabrication parameters. For example, if the thicknesses of silk, PEDOT:PSS and/or P3HT/PCBM are changed, what is the repercussion on the validation measurements? The same question could be done for the silk fabrication formula, the polymeric deposition parameters, change in conductivity and/or absorption spectrum for the polymeric layer etc.

Another interesting development could be the implementation of a different animal model, one possibily similar to the human being. The pig seems to be a good candidate here, since its visual system is not too different from our own.

Furthermore, the same artificial retina structure could be studied with different materials. A different choice for the substrate, like for example cellulose, polycaprolactone or PMMA. Also, a photoactive layer consisting of a multi-polymeric blend, possibly one with a good absorption for red and another for blue, could recreate the typical trichromatic visual system of human beings.

Last, but not least, improvements in the knowledge of the organic photodetector field, a gradual increase of quantum efficiencies, and a general refinement of the fabrication processes could definitely bring better results and new excellence standards.